

การจำลองพลวัตโมเลกุลควอนตัมกับไอออนไฮโดรเนียม  
และไอออนทริฟเลตในสารละลายน้ำ

นายเจริญศักดิ์ เถางาม



วิทยานิพนธ์นี้เป็นส่วนหนึ่งของการศึกษาตามหลักสูตรปริญญาวิทยาศาสตรดุษฎีบัณฑิต  
สาขาวิชาเคมี  
มหาวิทยาลัยเทคโนโลยีสุรนารี  
ปีการศึกษา 2554

**QUANTUM MOLECULAR DYNAMICS SIMULATIONS  
ON HYDRONIUM AND TRIFLATE IONS  
IN AQUEOUS SOLUTIONS**

**Charoensak Lao-ngam**



**A Thesis Submitted in Partial Fulfillment of the Requirements for  
the Degree of Doctor of Philosophy in Chemistry**

**Suranaree University of Technology**

**Academic Year 2011**

**QUANTUM MOLECULAR DYNAMICS SIMULATIONS ON  
HYDRONIUM AND TRIFLATE IONS  
IN AQUEOUS SOLUTIONS**

Suranaree University of Technology has approved this thesis submitted in partial fulfillment of the requirements for the Degree of Doctor of Philosophy.

Thesis Examining Committee

\_\_\_\_\_  
(Asst. Prof. Dr. Kunwadee Rangsiwatananon)

Chairperson

\_\_\_\_\_  
(Prof. Dr. Kritsana Sagarik)

Member (Thesis Advisor)

\_\_\_\_\_  
(Assoc. Prof. Dr. Anan Tongraar)

Member

\_\_\_\_\_  
(Asst. Prof. Dr. Viwat Vchirawongkwin)

Member

\_\_\_\_\_  
(Asst. Prof. Dr. Visit Vao-Soongnern)

Member

\_\_\_\_\_  
(Prof. Dr. Sukit Limpijumnong)

Vice Rector for Academic Affairs

\_\_\_\_\_  
(Assoc. Prof. Dr. Prapun Manyum)

Dean of Institute of Science

เจริญศักดิ์ เลางาม : การจำลองพลวัตโมเลกุลควอนตัมกับไอออนไฮโดรเนียมและไอออนทริฟเลตในสารละลายน้ำ (QUANTUM MOLECULAR DYNAMICS SIMULATIONS ON HYDRONIUM AND TRIFLATE IONS IN AQUEOUS SOLUTIONS) อาจารย์ที่ปรึกษา: ศาสตราจารย์ ดร.กฤษณะ ศาคริก, 165 หน้า.

วิทยานิพนธ์เรื่องนี้ศึกษากลไกการเกิดปฏิกิริยาและพลวัตของปฏิกิริยาการถ่ายโอนโปรตอน โดยใช้แบบจำลองเป็นกลุ่มโมเลกุลไอออนไฮโดรเนียมและไอออนทริฟเลตในสารละลายน้ำและระเบียบวิธีทางทฤษฎีกลศาสตร์ควอนตัมและกลศาสตร์สถิติ ผลการคำนวณ โครงสร้างพลังงาน และอินฟราเรดสเปกตรัม (IR spectra) ของกลุ่มโมเลกุลไฮโดรเนียมในสารละลายน้ำ (protonated water clusters) โดยวิธี Density Functional Theory (DFT) ที่ระดับ B3LYP/TZVP แสดงว่า threshold asymmetric O-H stretching frequency ( $\nu^{\text{OH}^*}$ ) สำหรับการเกิดปฏิกิริยาการถ่ายโอนโปรตอนในสารประกอบซุนเดล (Zundel complex,  $\text{H}_5\text{O}_2^+$ ) ในสถานะแก๊สและสารละลายน้ำ มีค่าเท่ากับ 1984 และ 1881  $\text{cm}^{-1}$  ตามลำดับ ในขณะที่ Born-Oppenheimer Molecular Dynamic (BOMD) simulations ที่ 350 K ( $\nu_{\text{A}}^{\text{OH}^*, \text{MD}}$ ) มีค่าเท่ากับ 1917 และ 1736  $\text{cm}^{-1}$  ในสถานะแก๊สและสารละลายตามลำดับ ซึ่งต่ำกว่าค่าที่ทำนายด้วยวิธี DFT เล็กน้อย นอกจาก BOMD simulations จะแสดง asymmetric O-H stretching band ที่ความถี่ต่ำ ( $\nu_{\text{A}}^{\text{OH}, \text{MD}}$ ) แล้ว ยังแสดงที่ความถี่สูงขึ้นในช่วง 1650 ถึง 2592  $\text{cm}^{-1}$  ( $\nu_{\text{B}}^{\text{OH}, \text{MD}}$ ) ด้วย ซึ่งความถี่ทั้งสองสอดคล้องกับรูปแบบการสั่นของ O-H แบบอสมมาตรสองรูปแบบ กล่าวคือความถี่ต่ำสอดคล้องกับรูปแบบการสั่นกลับไปกลับมาของโปรตอนตรงกึ่งกลางของพันธะไฮโดรเจนที่เรียกว่า oscillatory shuttling ซึ่งในกรณีศึกษาที่สอดคล้องกับสารประกอบที่มีโครงสร้างแบบใช้โปรตอนร่วมกัน (shared-proton structure,  $\text{O}\cdots\text{H}^+\cdots\text{O}$ ) ส่วนแถบที่มีความถี่สูงกว่าสอดคล้องกับรูปแบบการสั่นที่โปรตอนมีจุดศูนย์กลางการสั่นเคลื่อนไปยังออกซิเจนอะตอมข้างใดข้างหนึ่ง เรียกการสั่นเช่นนี้ว่า structural diffusion โดยพันธะไฮโดรเจนมีโครงสร้างแบบประชิดกัน (contact structure,  $\text{O}-\text{H}^+\cdots\text{O}$ ) ทั้งนี้ได้คำนวณพลังงานการสั่นสำหรับการเปลี่ยนแปลงจากการสั่นแบบ oscillatory shuttling ไปเป็นการสั่นแบบ structural diffusion ( $\Delta\nu_{\text{BA}}^{\text{OH}, \text{MD}}$ ) โดยประมาณเท่ากับค่าผลต่างของตำแหน่งของแถบความถี่ต่ำและตำแหน่งของแถบความถี่สูง ในกรณีของไอออนไฮโดรเนียมในสารละลายน้ำ ค่าผลต่างนี้มีค่าเท่ากับ 473  $\text{cm}^{-1}$  หรือประมาณ 5.7 kJ/mol นอกจากนี้ อินฟราเรดสเปกตรัมที่ได้จาก BOMD simulations ที่ 350 K ยังสามารถทำนายประสิทธิภาพสูงสุดในการเปลี่ยนแปลงสถานะการสั่นของโปรตอนจาก oscillatory shuttling ไปเป็น structural diffusion ได้อีกด้วย

ผลการศึกษากลไกการถ่ายโอนโปรตอนในกลุ่มโมเลกุลทริฟเลตและน้ำ ( $\text{CF}_3\text{SO}_3^- - \text{H}_3\text{O}^+ - n\text{H}_2\text{O}$ ) โดยใช้วิธีคำนวณเดียวกัน แสดงว่ากลไกการถ่ายโอนโปรตอนในกลุ่มโมเลกุลทริฟเลตในสารละลายน้ำเป็นไปได้สองรูปแบบ ได้แก่การถ่ายโอนโปรตอนผ่านหมู่ซัลโฟเนต ( $-\text{SO}_3^-$ ) โดยมีการให้และรับโปรตอนที่ออกซิเจนอะตอมของหมู่ซัลโฟเนต เรียกกลไกแบบนี้ว่ากลไกการถ่ายโอนแบบพาส-ทรู (pass-through mechanism) ในขณะที่แบบที่สองโปรตอนถ่ายโอนผ่านพันธะไฮโดรเจน ( $\text{O}\dots\text{H}^+\dots\text{O}$ ) ในสารประกอบซุนเดลที่อยู่ในบริเวณใกล้เคียงโดยไม่มีการให้หรือรับโปรตอนที่หมู่  $-\text{SO}_3^-$  เรียกว่ากลไกแบบพาส-บาย (pass-by mechanism) จากการวิเคราะห์อินฟราเรดสเปกตรัมที่ได้จากการคำนวณด้วยวิธี DFT ทั้งในสถานะแก๊สและสารละลาย พบว่า  $\nu^{\text{OH}^*}$  มีค่าอยู่ในช่วง 1921 ถึง 2239  $\text{cm}^{-1}$  ในขณะที่ BOMD simulations ที่ 350 K แสดงค่า  $\nu_{\text{A}}^{\text{OH}^*, \text{MD}}$  อยู่ในช่วง 1736 ถึง 1917  $\text{cm}^{-1}$  เมื่อเปรียบเทียบผลการศึกษาที่ได้จากระบบทริฟเลตในสารละลายน้ำกับระบบไฮโดรเนียมในสารละลายน้ำพบว่าหมู่  $-\text{SO}_3^-$  มีบทบาทสำคัญในการสนับสนุนการเกิดปฏิกิริยาการถ่ายโอนโปรตอนคือ สามารถทำให้  $\Delta\nu_{\text{BA}}^{\text{OH}, \text{MD}}$  ในสารประกอบซุนเดลลดลง ส่งผลให้มีโปรตอนมีศักยภาพการเคลื่อนที่แบบ structural diffusion มากขึ้น สรุปได้ว่าหมู่  $-\text{SO}_3^-$  ในกลุ่มโมเลกุลทริฟเลตในสารละลายน้ำทำหน้าที่เป็นตำแหน่งที่ไวต่อปฏิกิริยา (active binding site) โดยสามารถสร้างสถานะที่เหมาะสมทั้งเชิงโครงสร้าง พลังงานและพลวัตเพื่อส่งเสริมให้ประสิทธิภาพการส่งผ่านโปรตอนในสารละลายน้ำดีขึ้น

สาขาวิชาเคมี

ปีการศึกษา 2554

ลายมือชื่อนักศึกษา \_\_\_\_\_

ลายมือชื่ออาจารย์ที่ปรึกษา \_\_\_\_\_

CHAROENSAK LAO-NGAM : QUANTUM MOLECULAR DYNAMICS  
SIMULATIONS ON HYDRONIUM AND TRIFLATE IONS IN AQUEOUS  
SOLUTIONS. THESIS ADVISOR : PROF. KRITSANA SAGARIK,  
Ph.D. 165 PP.

PROTON TRANSFER REACTIONS/ PROTONATED WATER CLUSTERS/  
NAFION<sup>®</sup>/ TRIFLATE ION/ BOMD SIMULATIONS/ VIBRATIONAL SPECTRA

Proton transfer reactions and dynamics were theoretically studied using the protonated water clusters and the hydrogen-bond (H-bond) complexes formed from  $\text{CF}_3\text{SO}_3^-$ ,  $\text{H}_3\text{O}^+$  and  $n\text{H}_2\text{O}$ ,  $n = 1 - 4$ , as model systems. For the protonated water clusters, Density Functional Theory (DFT) method at the B3LYP/TZVP level revealed the threshold asymmetric O-H stretching frequencies ( $\nu^{\text{OH}^*}$ ) for the proton transfer in the Zundel complex ( $\text{H}_5\text{O}_2^+$ ) in the gas phase and continuum aqueous solution at 1984 and 1881  $\text{cm}^{-1}$ , respectively. Born-Oppenheimer Molecular Dynamics (BOMD) simulations at 350 K suggested lower threshold frequencies ( $\nu_{\text{A}}^{\text{OH}^*, \text{MD}} = 1917$  and  $1736 \text{ cm}^{-1}$ , respectively), with two characteristic  $\nu^{\text{OH}, \text{MD}}$  being the IR spectral signatures of the transferring protons. The low-frequency band ( $\nu_{\text{A}}^{\text{OH}, \text{MD}}$ ) could be associated with the “oscillatory shuttling motion” and the high-frequency band ( $\nu_{\text{B}}^{\text{OH}, \text{MD}}$ ) with the “structural diffusion motion”. These can be regarded as the spectroscopic evidences of the formations of the shared-proton ( $\text{O}\cdots\text{H}^+\cdots\text{O}$ ) and  $\text{H}_3\text{O}^+ - \text{H}_2\text{O}$  contact ( $\text{O}-\text{H}^+\cdots\text{O}$ ) structures, respectively. The vibrational energy for the interconversion between the two dynamic states ( $\Delta\nu_{\text{BA}}^{\text{OH}, \text{MD}}$ ) can be approximated

from the difference between  $\nu_B^{\text{OH, MD}}$  and  $\nu_A^{\text{OH, MD}}$ ; for the protonated water clusters,

$$\Delta\nu_{\text{BA}}^{\text{OH, MD}} = 473 \text{ cm}^{-1} \text{ or } 5.7 \text{ kJ/mol.}$$

For proton transfer reactions in the  $\text{CF}_3\text{SO}_3^- - \text{H}_3\text{O}^+ - n\text{H}_2\text{O}$  complexes,  $n = 1 - 4$ , the equilibrium structures obtained from DFT calculations suggested at least two structural diffusion pathways at the  $-\text{SO}_3^-$  group namely, the “pass-through” and “pass-by” mechanisms. The former involves the protonation and deprotonation at the  $-\text{SO}_3^-$  group, whereas the latter the proton transfer in the adjacent Zundel complex. Analyses of  $\nu^{\text{OH}}$  of the H-bond protons showed  $\nu^{\text{OH*}}$  in the range of 1921 to 2239  $\text{cm}^{-1}$ . BOMD simulations at 350 K anticipated slightly lower threshold frequencies ( $\nu_A^{\text{OH*, MD}}$ ), with  $\nu_A^{\text{OH, MD}}$  and  $\nu_B^{\text{OH, MD}}$  being the spectral signatures of proton transfer in the H-bond complexes. Comparison of the results on the  $\text{CF}_3\text{SO}_3^- - \text{H}_3\text{O}^+ - n\text{H}_2\text{O}$  complexes,  $n = 1 - 4$ , with the protonated water clusters indicated that the  $-\text{SO}_3^-$  group facilitates proton transfer by reducing  $\Delta\nu_{\text{BA}}^{\text{OH, MD}}$ , resulting in a higher population of the H-bonds with the structural diffusion motion. One could therefore conclude that the  $-\text{SO}_3^-$  group acts as active binding site, which provides appropriate structural, energetic and dynamic conditions for effective structural diffusion processes.

School of Chemistry

Student's Signature\_\_\_\_\_

Academic Year 2011

Advisor's Signature\_\_\_\_\_

## ACKNOWLEDGEMENTS

I would like to express my sincere gratitude to Prof. Dr. Kritsana Sagarik for his exceptional generous support, academic guidance, advice and encouragement during my graduate career. I would like to thank Assoc. Prof. Dr. Anan Tongraar for his encouragement and help. I would like to thank committee members for their time and useful suggestions. I would also like to express my great gratitude to all lecturers at the School of Chemistry, Suranaree University of Technology and Department of Chemistry, Faculty of Science, Ramkhamhaeng University for their good attitude and advices.

I would also like to acknowledge the financial support from the Thailand Research Fund (TRF) through the Royal Golden Jubilee (RGJ) Ph.D. program (Grant No. PHD/0121/2549). Special thanks should go to the School of Chemistry and the School of Mathematics, Institute of Science, Suranaree University of Technology (SUT), as well as the National Electronics and Computer Technology Center (NECTEC) and the National Nanotechnology Center (NANOTEC), for providing computer facilities.

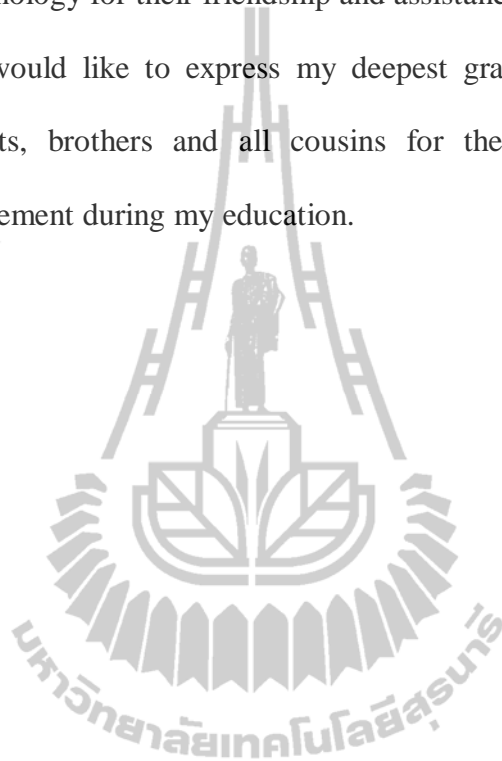
I would like to express my sincere thanks to Prof. Dr. Yoshiyuki Kawazoe at Institute of Materials Research (IMR), Tohoku University, Japan, who provides me valuable advices and suggestions with respect to my work.



I would like to take this opportunity to express my deepest gratitude to all of the teachers at Ban Nongkok and Phibunmangsaan schools for their kindness giving a valuable knowledge and chances. Thanks to all of my friends at Suranaree University of Technology for their friendship and assistance.

Finally, I would like to express my deepest gratitude to my grandmother, grandfather, parents, brothers and all cousins for their unconditional love and continual encouragement during my education.

Charoensak Lao-ngam



# CONTENTS

	<b>Page</b>
ABSTRACT IN THAI.....	I
ABSTRACT IN ENGLISH.....	III
ACKNOWLEDGEMENTS.....	V
CONTENTS.....	VII
LIST OF TABLES.....	X
LIST OF FIGURES.....	XIII
LIST OF ABBREVIATIONS.....	XX
<b>CHAPTER</b>	
<b>I INTRODUCTION.....</b>	<b>1</b>
<b>II RESEARCH METHODOLOGY.....</b>	<b>12</b>
2.1 Static calculations.....	15
2.1.1 Searching for potential precursors and transition state complexes.....	15
2.1.2 Structural refinements.....	17
2.1.3 Interaction energies and asymmetric stretching coordinates.....	18
2.1.4 Infrared spectra and normal mode analyses.....	21

## CONTENTS (Continued)

	<b>Page</b>
2.2 Dynamic calculations.....	22
2.2.1 Born-Oppenheimer MD simulations.....	22
2.2.2 Infrared spectra and diffusion coefficients.....	26
<b>III RESULTS AND DISCUSSIONS.....</b>	<b>28</b>
3.1 The $\text{H}_3\text{O}^+ - n\text{H}_2\text{O}$ complexes, $n = 1 - 4$ .....	28
3.1.1 Static results.....	28
Structures and energetic of the shared-proton complexes.....	28
Asymmetric stretching coordinates and infrared spectra of transferring protons.....	35
3.1.2 Dynamic results.....	44
Average H-bond structures and IR spectra.....	44
Threshold frequencies and relative probability of proton transfer.....	47
Vibration energy for proton transfer reaction.....	58
Dynamics of proton transfer and diffusion coefficients.....	64
Kinetics of proton transfer in protonated water clusters.....	65

## CONTENTS (Continued)

	<b>Page</b>
3.2 The $\text{CF}_3\text{SO}_3^- - \text{H}_3\text{O}^+ - n\text{H}_2\text{O}$ complexes, $n = 1 - 4$ .....	71
3.2.1 Static results.....	71
Structures and energetic of the shared-proton complexes.....	71
Asymmetric stretching coordinates and IR spectra of transferring proton.....	82
3.2.2 Dynamic results.....	99
Average H-bond structures and IR spectra.....	99
Dynamics of proton transfer and diffusion coefficients.....	113
<b>IV CONCLUSION</b> .....	116
REFERENCES.....	121
APPENDICES.....	135
APPENDIX A SUPPLEMENTARY RESULTS FOR THE $\text{CF}_3\text{SO}_3^- - \text{H}_3\text{O}^+ - n\text{H}_2\text{O}$ COMPLEXES, $n = 1 - 4$ .....	136
APPENDIX B PUBLICATIONS.....	149
CURRICULUM VITAE.....	165

## LIST OF TABLES

<b>Table</b>	<b>Page</b>
3.1 H-bond distances and energies of the protonated water cluster obtained from B3LYP/TZVP calculations, both in the gas phase and continuum aqueous solution (values in parenthesis). They are in Å and kJ/mol, respectively.....	31
3.2 Asymmetric stretching coordinates ( $\Delta d_{DA}$ ) and asymmetric O-H stretching frequencies ( $\nu^{OH}$ ) of the protonated water cluster obtained from B3LYP/TZVP calculations, both in the gas phase and continuum aqueous solution (values in parenthesis). They are in Å and $\text{cm}^{-1}$ , respectively.....	40
3.3 Average H-bond distances ( $\langle R_{O-O} \rangle$ and $\langle R_{O-H} \rangle$ ) and asymmetric stretching coordinates ( $\langle \Delta d_{DA} \rangle$ ) of the shared-proton complexes, derived from BOMD simulations at 350 K, both in the gas phase and continuum aqueous solution (values in parenthesis). Distances are in Å	51
3.4 IR frequencies ( $\text{cm}^{-1}$ ) of the shared-proton complexes obtained from BOMD simulations at 350 K, both in the gas phase and continuum aqueous solution (values in parenthesis).....	52

## LIST OF TABLES (Continued)

Table	Page
3.5 The vibrational energy for the interconversion between the oscillatory shuttling and structural diffusion motions ( $\Delta v_{BA}^{OH, MD}$ ), the probability of finding the structural diffusion motion relative to the oscillatory shuttling motion ( $P_B/P_A$ ) and the proton diffusion coefficient ( $D$ ) obtained from BOMD simulations at 350 K, both in the gas phase and continuum aqueous solution (values in parenthesis).....	61
3.6 H-bond distances and energies of the $CF_3SO_3^- - H_3O^+ - nH_2O$ complexes, $n = 1 - 4$ , obtained from B3LYP/TZVP calculations, both in the gas phase and continuum aqueous solution. They are in Å and kJ/mol, respectively.....	74
3.7 Asymmetric stretching coordinate ( $\Delta d_{DA}$ ) and O-H stretching frequency ( $\nu^{OH}$ ) of the $CF_3SO_3^- - H_3O^+ - nH_2O$ complexes, $n = 1 - 4$ , obtained from B3LYP/TZVP calculations, both in the gas phase and continuum aqueous solution. They are in Å and $cm^{-1}$ , respectively.....	83
3.8 Dynamic results of the $CF_3SO_3^- - H_3O^+ - nH_2O$ complexes, $n = 1 - 4$ , obtained from BOMD simulation at 350 K in continuum aqueous solution. Distances and IR frequencies are in Å and $cm^{-1}$ , respectively.....	102

## LIST OF TABLES (Continued)

<b>Table</b>	<b>Page</b>
A.1 Static results of the $\text{CF}_3\text{SO}_3^- - \text{H}_3\text{O}^+ - n\text{H}_2\text{O}$ complexes, $n = 1 - 4$ , obtained from B3LYP/TZVP calculations, both in the gas phase and continuum aqueous solution. Distances and energies are in Å and kJ/mol, respectively .....	136
A.2 Asymmetric stretching coordinate ( $\Delta d_{\text{DA}}$ ) and O-H stretching frequency ( $\nu^{\text{OH}}$ ) of the $\text{CF}_3\text{SO}_3^- - \text{H}_3\text{O}^+ - n\text{H}_2\text{O}$ complexes, $n = 1 - 4$ , obtained from B3LYP/TZVP calculations, both in the gas phase and continuum aqueous solution. They are in Å and $\text{cm}^{-1}$ , respectively.	141
A.3 Dynamic results of the $\text{CF}_3\text{SO}_3^- - \text{H}_3\text{O}^+ - n\text{H}_2\text{O}$ complexes, $n = 1 - 4$ , obtained from B3LYP/TZVP calculations, both in the gas phase and continuum aqueous solution (the values in parenthesis). Distances and energies are in Å and kJ/mol, respectively .....	146

## LIST OF FIGURES

Figure		Page
1.1	Example structure of sulfonated fluoroethylene .....	2
1.2	An example of hydration structure of Nafion <sup>®</sup> . Hydrated regions are shown around the sulfonate side chains.....	3
2.1	Basic steps employed in investigation of elementary reactions and dynamics of proton transfer in H-bond.....	14
2.2	Construction of T-model potentials.....	16
2.3	Basic steps in MD simulations of N-particle system.....	25
2.4	Definitions of the symmetric and asymmetric O-H stretching modes, as well as the O-O vibration.....	27
3.1	Trends of the interaction ( $\Delta E$ ) and solvation energies ( $\Delta E^{\text{sol}}$ ) with respect to the number of water molecules, obtained from B3LYP/TZVP calculations: -▲- = $\Delta E$ in the gas phase; -Δ- = $\Delta E$ in continuum aqueous solution; -■- = $\Delta E^{\text{sol}}$ .....	33



## LIST OF FIGURES (Continued)

Figure	Page
<p>3.2 Trends of the interaction energies between the central charged species and water molecules (<math>\Delta E^X</math>, <math>X = H_3O^+</math> or <math>H_5O_2^+</math>) with respect to the number of water molecules, obtained from B3LYP/TZVP calculations:            -▲- = <math>H_3O^+</math> in the gas phase; -Δ- = <math>H_3O^+</math> in continuum aqueous solution; -■- = <math>H_5O_2^+</math> in the gas phase; -□- = <math>H_5O_2^+</math> in continuum aqueous solution. — = calculations without the counterpoise correction. ----- = calculations with the counterpoise correction. ....</p>	34
<p>3.3 a) Plot of the asymmetric stretching coordinates (<math>\Delta d_{DA}</math>) and the O-H..O H-bond distances (<math>R_{O-O}</math>), obtained from B3LYP/TZVP calculations. b) Plot of the asymmetric O-H stretching frequencies (<math>\nu^{OH}</math>) and the O-H..O H-bond distances (<math>R_{O-O}</math>), obtained from B3LYP/TZVP calculations. c) Plot of the asymmetric O-H stretching frequencies (<math>\nu^{OH}</math>) and the asymmetric stretching coordinates (<math>\Delta d_{DA}</math>), obtained from B3LYP/TZVP calculations. ....</p>	42

## LIST OF FIGURES (Continued)

Figure	Page
3.4 Symmetric and asymmetric O-H stretching bands of the transferring protons in the shared-proton complexes, together with the O-O vibration band, obtained from BOMD simulations at 350 K. a) The Zundel complex (structure <b>a</b> ) in the gas phase; b) The Zundel complex (structure <b>a</b> ) in continuum aqueous solution, c) The $\text{H}_3\text{O}^+ - \text{H}_2\text{O}$ 1 : 4 complex (structure <b>f</b> ) in the gas phase; d) The $\text{H}_3\text{O}^+ - \text{H}_2\text{O}$ 1 : 4 complex (structure <b>f</b> ) in continuum aqueous solution.....	53
3.5 a) Plot of the average asymmetric stretching coordinates ( $\langle \Delta d_{\text{DA}} \rangle$ ) and the average O-H..O H-bond distances ( $\langle R_{\text{O..O}} \rangle$ ), obtained from BOMD simulations at 350 K. b). Plot of the asymmetric O-H stretching frequencies ( $\nu^{\text{OH,MD}}$ ) and the average O-H..O H-bond distances ( $\langle R_{\text{O..O}} \rangle$ ), obtained from BOMD simulations at 350 K. c) Plot of the asymmetric O-H stretching frequencies ( $\nu^{\text{OH,MD}}$ ) and the asymmetric stretching coordinates ( $\langle \Delta d_{\text{DA}} \rangle$ ), obtained from BOMD simulations at 350 K. ....	56

## LIST OF FIGURES (Continued)

Figure	Page
3.6 a) Plot of standard deviations of the O-H distances ( $\sigma_{\text{R}_{\text{O-H}}}$ ) and the asymmetric stretching coordinates ( $\langle \Delta d_{\text{DA}} \rangle$ ), obtained from BOMD simulations at 350 K. b) Plot of the vibrational energy for the interconversion between the oscillatory shuttling and structural diffusion motions ( $\Delta v_{\text{BA}}^{\text{OH, MD}}$ ) and the asymmetric stretching coordinates ( $\langle \Delta d_{\text{DA}} \rangle$ ), obtained from BOMD simulations at 350 K. c) Plot of probability of finding the structural diffusion motion relative to the oscillatory shuttling motion ( $\mathbf{P}_B/\mathbf{P}_A$ ) and the asymmetric stretching coordinates ( $\langle \Delta d_{\text{DA}} \rangle$ ), obtained from BOMD simulations at 350K.....	62
3.7 Examples of velocity autocorrelation functions (VACF) of the O-O vibrations in the shared-proton structures, obtained from BOMD simulations at 350 K. a) the Zundel complex in the gas phase; b) the Zundel complex in continuum aqueous solution. c) the $\text{H}_3\text{O}^+ - \text{H}_2\text{O}$ 1 : 4 complex (structure <b>f</b> ) in the gas phase. d) the $\text{H}_3\text{O}^+ - \text{H}_2\text{O}$ 1 : 4 complex (structure <b>f</b> ) in continuum aqueous solution.....	67
3.8 Symmetric and asymmetric O-H stretching bands of the transferring protons in Zundel complex (structure <b>a</b> ) in the gas phase, together with the O-O vibration band, obtained from BOMD simulations at 350 K with the simulation length of 2.4 and 4.8 ps.....	70

## LIST OF FIGURES (Continued)

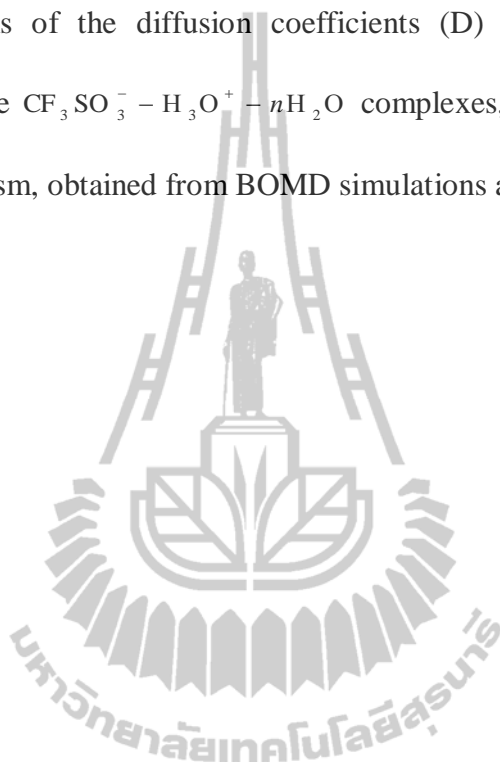
Figure	Page
3.9 Trends of the interaction ( $\Delta E$ ) and solvation energies ( $\Delta E^{\text{sol}}$ ) with respect to the number of water molecules, obtained from B3LYP/TZVP calculations: $\blacktriangle$ = $\Delta E$ in the gas phase; $\blacktriangle$ = $\Delta E$ in continuum aqueous solution; $\blacksquare$ = $\Delta E^{\text{sol}}$ .....	80
3.10 Static results of the $\text{CF}_3\text{SO}_3^- - \text{H}_3\text{O}^+ - n\text{H}_2\text{O}$ complexes, $n = 1 - 4$ , obtained from B3LYP/TZVP calculations a) Plot of the asymmetric stretching coordinates ( $\Delta d_{\text{DA}}$ ) and the O-H..O H-bond distances ( $R_{\text{O-O}}$ ) for the pass-through mechanism. b) Plot of the asymmetric O-H stretching frequencies ( $\nu^{\text{OH}}$ ) and the O-H..O H-bond distances ( $R_{\text{O-O}}$ ) for the pass-through mechanism. c) Plot of the asymmetric O-H stretching frequencies ( $\nu^{\text{OH}}$ ) and the asymmetric stretching coordinates ( $\Delta d_{\text{DA}}$ ) for the pass-through mechanism. d) Plot of the asymmetric stretching coordinates ( $\Delta d_{\text{DA}}$ ) and the O-H..O H-bond distances ( $R_{\text{O-O}}$ ) for the pass-by mechanism. e) Plot of the asymmetric O-H stretching frequencies ( $\nu^{\text{OH}}$ ) and the O-H..O H-bond distances ( $R_{\text{O-O}}$ ) for the pass-by mechanism. f) Plot of the asymmetric O-H stretching frequencies ( $\nu^{\text{OH}}$ ) and the asymmetric stretching coordinates ( $\Delta d_{\text{DA}}$ ) for the pass-by mechanism.....	92

## LIST OF FIGURES (Continued)

Figure	Page
3.11 The domains of $\nu^{\text{OH}}$ for the H-bond protons in <b>Group 1</b> and <b>2</b> , as well as Subgroup (I) to (IV). a) in the gas phase. b) in continuum aqueous solution. ....	98
3.12 The results of the $\text{CF}_3\text{SO}_3^- - \text{H}_3\text{O}^+ - n\text{H}_2\text{O}$ complexes, $n = 1 - 4$ , in continuum aqueous solution for the pass-by mechanism, obtained from BOMD simulations at 350 K. a) Plot of the average asymmetric stretching coordinates ( $\langle \Delta d_{\text{DA}} \rangle$ ) and the average O-H..O H-bond distances ( $\langle R_{\text{O-O}} \rangle$ ). b) Plot of the asymmetric O-H stretching frequencies ( $\nu^{\text{OH, MD}}$ ) and the average O-H..O H-bond distances ( $\langle R_{\text{O-O}} \rangle$ ). c) Plot of the asymmetric O-H stretching frequencies ( $\nu^{\text{OH, MD}}$ ) and the asymmetric stretching coordinates ( $\langle \Delta d_{\text{DA}} \rangle$ ). d) Symmetric, asymmetric O-H stretching and O-O vibration bands of the $\text{CF}_3\text{SO}_3^- - \text{H}_3\text{O}^+ - \text{H}_2\text{O}$ 1 : 1 : 4 complex (structure <b>k</b> ). e) Plot of standard deviations of the O-H distances ( $\sigma_{R_{\text{O-H}}}$ ) and the asymmetric stretching coordinates ( $\langle \Delta d_{\text{DA}} \rangle$ ). f) Plot of $\Delta \nu_{\text{BA}}^{\text{OH, MD}}$ and the asymmetric stretching coordinates ( $\langle \Delta d_{\text{DA}} \rangle$ ). g) Plot of probability of finding the structural diffusion motion relative to the oscillatory shuttling motion ( $\mathbf{P}_B/\mathbf{P}_A$ ) and the asymmetric stretching coordinates ( $\langle \Delta d_{\text{DA}} \rangle$ ).....	109

**LIST OF FIGURES (Continued)**

<b>Figure</b>		<b>Page</b>
3.13	Distributions of the diffusion coefficients (D) of the transferring proton in the $\text{CF}_3\text{SO}_3^- - \text{H}_3\text{O}^+ - n\text{H}_2\text{O}$ complexes, $n = 1 - 4$ , for pass-by mechanism, obtained from BOMD simulations at 350 K. ....	115



## LIST OF ABBREVIATIONS

Å	=	Angström
au	=	Atomic unit
cm <sup>-1</sup>	=	Wavenumber
fs	=	Femtosecond
K	=	Kelvin
kJ/mol	=	Kilo joule per mole
ps	=	Picosecond
A-H..B	=	Hydrogen-bond between the proton donor A and acceptor B
CF <sub>3</sub> SO <sub>3</sub> H	=	Trifluoromethanesulfonic (triflic) acid
CF <sub>3</sub> SO <sub>3</sub> <sup>-</sup>	=	Trifluoromethanesulfonate (triflate) anion
g(R)	=	Atom-atom pair correlation function
H-bond	=	Hydrogen bond
H <sub>2</sub> O	=	Water
H <sub>3</sub> O <sup>+</sup>	=	Hydronium ion
H <sub>9</sub> O <sub>4</sub> <sup>+</sup>	=	Eigen complex
H <sub>5</sub> O <sub>2</sub> <sup>+</sup>	=	Zundel complex
-SO <sub>3</sub> H	=	Sulfonic acid group
-SO <sub>3</sub> <sup>-</sup>	=	Sulfonate group

## LIST OF ABBREVIATIONS (Continued)

$I_A$	=	IR intensity at $\nu_A^{\text{OH, MD}}$
$I_B$	=	IR intensity at $\nu_B^{\text{OH, MD}}$
$I_{\text{O-O}}$	=	IR intensity of the O-O vibration
$k$	=	Classical first-order rate constant
$\Delta H$	=	Enthalpy change
$E_0$	=	Ground-state electronic energy
$\rho_0$	=	Ground-state electron density
$\tau_p$	=	Proton hopping time
$\tau$	=	Lifetime of shared-proton complex
$\varepsilon$	=	Relative permittivity or dielectric constant
$\sigma_{\text{R}_{\text{O-H}}}$	=	Standard deviations of the O-H distances
$P_B/P_A$	=	Probability of finding the structural diffusion motion relative to the oscillatory shuttling motion
$R_{\text{O-O}}$	=	O-O distance
$R_{\text{O-H}}$	=	O-H distance
$\Delta d_{\text{DA}}$	=	Asymmetric stretching coordinate
$\Delta d_{\text{DA}}^*$	=	Threshold asymmetric stretching coordinate
$\nu^{\text{OH}}$	=	Asymmetric O-H stretching frequency
$\nu^{\text{OH}*}$	=	Threshold asymmetric O-H stretching frequency



## LIST OF ABBREVIATIONS (Continued)

$\nu^{\text{OH, MD}}$	=	Characteristic asymmetric O-H stretching frequency from MD simulations
$\nu_{\text{A}}^{\text{OH, MD}}$	=	Characteristic asymmetric O-H stretching frequency associated with the oscillatory shuttling motion
$\nu_{\text{A}}^{\text{OH*}, \text{MD}}$	=	Threshold asymmetric O-H stretching frequency obtained from MD simulations
$\nu_{\text{B}}^{\text{OH, MD}}$	=	Characteristic asymmetric O-H stretching frequencies associated with the structural diffusion motion
$\Delta E$	=	Interaction energy
$\Delta E^{\text{X}}$	=	Interaction energy between the central charged species ( $\text{X} = \text{H}_3\text{O}^+$ or $\text{H}_5\text{O}_2^+$ ) and the surrounding water molecules
$\Delta E^{\text{sol}}$	=	Solvation energy
$\Delta \text{PA}$	=	Proton affinity of a donor-acceptor pair
$\Delta \nu^{\text{OH}}$	=	Frequency shifts due to continuum aqueous solvent
$\Delta \nu_{\text{BA}}^{\text{OH, MD}}$	=	Vibrational energy for the interconversion between the oscillatory shuttling and structural diffusion motions
$\langle \Delta d_{\text{DA}} \rangle$	=	Average asymmetric stretching coordinate
$\langle R_{\text{O-O}} \rangle$	=	Average O-O distance
$\langle R_{\text{O-H}} \rangle$	=	Average O-H distance

**LIST OF ABBREVIATIONS (Continued)**

B3LYP	=	Becke three-parameters hybrid functional combined with Lee-Yang-Parr correlation function
BO	=	Born-Oppenheimer
BOMD	=	Born-Oppenheimer molecular dynamics
BSSE	=	Basis set superposition error
COSMO	=	Conductor-like screening model
D	=	Diffusion coefficient
DFT	=	Density functional theory
FT-IR	=	Fourier transform infrared spectroscopy
HF	=	Hartree-Fock
IR	=	Infrared
IRMPD	=	IR multiple photon dissociation
MC	=	Monte Carlo
MCTDH	=	Multiconfiguration time-dependent Hartree
MD	=	Molecular dynamics
MO	=	Molecular orbital
MP2	=	Second-order Møller-Plesset
MSD	=	Mean-square displacement
MS-EVB	=	Multistate empirical valence-bond
ND	=	Neutron diffraction
NMR	=	Nuclear magnetic resonance
NVE	=	Microcanonical ensemble

**LIST OF ABBREVIATIONS (Continued)**

NVT	=	Canonical ensemble
PEM	=	Polymer electrolyte membrane
PEMFC	=	Polymer electrolyte membrane fuel cells
PT	=	Proton transfer
QM	=	Quantum mechanics
QM/MM	=	Combined quantum mechanical and molecular mechanical calculations
SCF	=	Self-consistent field
SCRf	=	Self-consistent reaction field
SDF	=	Spatial distribution function
T-model	=	Test-particle model
TZVP	=	Triple zeta valence plus polarization
VACF	=	Velocity autocorrelation function
XANES	=	X-ray absorption near edge structure

# CHAPTER I

## INTRODUCTION

Energy crisis and environmental concerns about global warming, as well as to reduce CO<sub>2</sub> emissions, have provided strong motivation to seek ways of improving energy conversion technology. The proton exchange membrane fuel cell (PEMFC) has received much attention as one of the most promising energy suppliers for the future world (Gierke, Munn, and Wilson, 1981; Kreuer, 1996; Kreuer, Paddison, Spohr, and Schuster, 2004; Larminie and Dicks, 2001; Mauritz and Moore, 2004; Paddison, 2003; Smitha, Sridhar, and Khan, 2005). Polymer electrolyte membrane which has been widely used in PEMFCs is Nafion<sup>®</sup>, introduced by Dupont in 1967 (Gierke, Munn, and Wilson, 1981; Larminie and Dicks, 2001). The main features of Nafion<sup>®</sup> are highly chemical resistance and mechanical strength. Moreover, Nafion<sup>®</sup> is acidic polymer materials; it is able to absorb large quantity of water and conduct protons (Gierke, Munn, and Wilson, 1981). This type of PEM has become an industrial standard for PEMFC, and has been developed and used until today (Mauritz and Moore, 2004).

Nafion<sup>®</sup> is a perfluorinated polymer, which consists of the high hydrophobicity of Teflon<sup>®</sup> backbone, with the side chains terminated by trifluoromethanesulfonic (triflic) acid (CF<sub>3</sub>SO<sub>3</sub>H) (Kreuer, 1996; Kreuer, Paddison, Spohr, and Schuster, 2004). A possible structure of sulfonated fluoroethylene is shown in Figure 1.1.

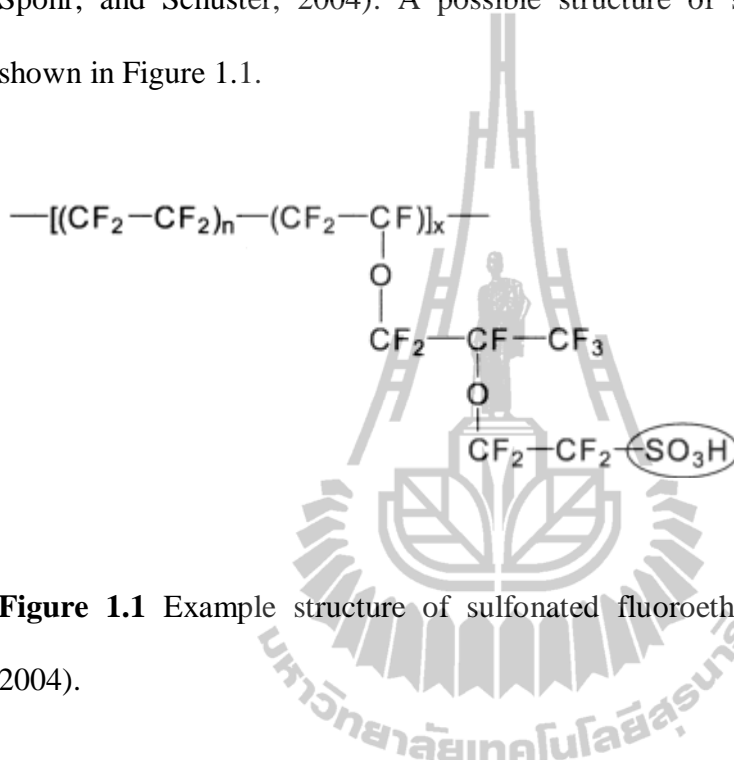


**Figure 1.1** Example structure of sulfonated fluoroethylene (Mauritz and Moore, 2004).

Owing to the  $-\text{SO}_3\text{H}$  groups at the end of the side chains, Nafion<sup>®</sup> is very polar and highly hydrophilic; the ionization of the  $-\text{SO}_3\text{H}$  group in aqueous solution produces  $-\text{SO}_3^-$  and  $\text{H}_3\text{O}^+$  or proton (Gierke, Munn, and Wilson, 1981; Larminie and Dicks, 2001; Mauritz and Moore, 2004). The most important consequence is that the water molecules at the side chains form clusters within Nafion<sup>®</sup>, with the shortest distance between the adjacent  $-\text{SO}_3^-$  groups of about 6 – 8 Å (Mauritz and Moore, 2004). Most importantly, within these hydrated regions, protons are relatively weakly attracted to the  $-\text{SO}_3\text{H}$  and  $-\text{SO}_3^-$  groups and, therefore, ready to move (Larminie

and Dicks, 2001). Figure 1.2 shows a possible hydration structure of Nafion<sup>®</sup> type membrane materials.

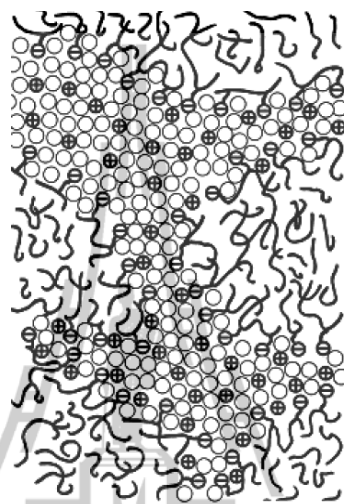


**Figure 1.2** An example of hydration structure of Nafion<sup>®</sup>. Hydrated regions are shown around the sulfonate side chains (Mauritz and Moore, 2004).

As the basic knowledge at the molecular level is important for the improvement of the efficiency of PEMFC and experimental approaches are rather restricted due to the amorphous structures in PEM (Kreuer, Paddison, Spohr, and Schuster, 2004; Larminie and Dicks, 2001; Mauritz and Moore, 2004), theoretical methods could provide deeper insights into various aspects of the proton conduction in Nafion<sup>®</sup>. To establish molecular scale information necessary for molecular modeling of structures, thermodynamics and dynamics of proton in Nafion<sup>®</sup>, basic knowledge of the hydration structures and dynamic behavior of proton in liquid water and at the side chains in Nafion<sup>®</sup> represents important information (Gierke, Munn,

and Wilson, 1981; Kreuer, 1996; Kreuer, Paddison, Spohr, and Schuster, 2004; Larminie and Dicks, 2001; Mauritz and Moore, 2004).

Proton transfer reaction in water has been of interest especially in connection with the understanding of elementary reactions in electrochemical and biological systems (Kreuer, 1996; Larminie and Dicks, 2001; Tuckerman, Laasonen, Sprik, and Parrinello, 1995). The unusually high mobility of proton relative to other cations such as sodium ( $\text{Na}^+$ ) and potassium ( $\text{K}^+$ ) cations (Agmon, 1995; Han, Zhou, and Liu, 2006; Kornyshev, Kuznetsov, Spohr, and Ulstrup, 2003) has motivated the investigation of transport mechanisms both in aqueous solutions and condensed phases. It has been proposed based on experimental and theoretical studies (Cappa, Smith, Messer, Cohen, and Saykally, 2005; Marx, Tuckerman, Hutter, and Parrinello, 1999) that there are three basic structures involved in proton transfer reactions in aqueous solution namely, the hydronium ion ( $\text{H}_3\text{O}^+$ ), the Eigen complex ( $\text{H}_9\text{O}_4^+$ ), in which the  $\text{H}_3\text{O}^+$  core is strongly H-bonded to three water molecules and the dihydrated cation known as the Zundel ( $\text{H}_5\text{O}_2^+$ ) complex. The latter is represented by an excess proton equally shared between two neutral water molecules. The mobility of proton depends upon the size of its solvated structure, indicating that the transport involves a mechanism rather than ionic diffusion (Agmon, 1995; Tuckerman, Laasonen, Sprik, and Parrinello, 1995). Explanations for the anomalously high mobility of protons in liquid water began with Grotthus's idea of "structural diffusion", the diffusion of the H-bond structure in which an excess proton is shuttling back and forth, represents an important elementary reaction in proton transfer processes (Agmon, 1995; Cappa, Smith, Messer, Cohen, and Saykally, 2005; Han,

Zhou, and Liu, 2006; Kornyshev, Kuznetsov, Spohr, and Ulstrup, 2003; Marx, Tuckerman, Hutter, and Parrinello, 1999). Subsequent explanation has refined this concept by invoking thermal hopping, proton tunneling and solvation effects (Bernal and Fowler, 1933; Han, Zhou, and Liu, 2006; Stearn and Eyring, 1937).

Based on a combination of neutron diffraction experiment with hydrogen isotope substitutions and MC simulations (Botti, Bruni, Imberti, Ricci, and Soper, 2005), it was found that the first hydration shell of  $\text{H}_3\text{O}^+$  consists of four water molecules; three of them H-bond directly to the hydrogen atoms and one of them locates in the vicinity of the oxygen atom of  $\text{H}_3\text{O}^+$ . Moreover, the analyses of atom-atom pair correlation functions ( $g(R)$ ) and spatial distribution functions (SDF) of  $\text{H}_3\text{O}^+$  in water, obtained from MC simulations, revealed that water molecules in the vicinity of the oxygen atom shows strong orientational correlation with respect to  $\text{H}_3\text{O}^+$ . The hydration structures of  $\text{H}_3\text{O}^+$  were confirmed by combined quantum mechanical and molecular mechanical (QM/MM) calculations with polarizable potentials (Hermida-Ramón and Karlström, 2004), which suggested that the hydrated excess proton in the forms of  $\text{H}_5\text{O}_2^+$  and  $\text{H}_9\text{O}_4^+$  is a part of the H-bond networks in the first hydration shell of  $\text{H}_3\text{O}^+$  (Hermida-Ramón and Karlström, 2004).

There has been a debate on the nature of hydration structures of proton and the extent to which species containing an excess proton,  $\text{H}_5\text{O}_2^+$  or  $\text{H}_9\text{O}_4^+$  (Kreuer, Paddison, Spohr, and Schuster, 2004), in acidic aqueous solutions. The controversy was partly resolved by *ab initio* molecular dynamics (MD) simulations (Tuckerman, Laasonen, Sprik, and Parrinello, 1995; Tuckerman, Marx, Klein, and Parrinello, 1997). According to the results of MD simulations, a single proton in H-bond



network, regarded as “proton defect”, could belong to  $\text{H}_5\text{O}_2^+$  or  $\text{H}_9\text{O}_4^+$ , with the center of the area with the excess proton coincides with the center of symmetry of the H-bond structure. It was demonstrated that, changes in these H-bond structures and those in the vicinities through H-bond breaking and forming processes displace the center of symmetry in space and also the center of the excess charge (Tuckerman, Laasonen, Sprik, and Parrinello, 1995; Tuckerman, Marx, Klein, and Parrinello, 1997). In this way,  $\text{H}_5\text{O}_2^+$  can be converted to  $\text{H}_9\text{O}_4^+$  and, therefore, termed “structural diffusion”. The proposed mechanism for the diffusion of an excess proton in water was supported by NMR data (Agmon, 1995).

One of the most powerful experimental techniques in H-bond research is vibrational spectroscopy. The most evident effects of H-bond formations in aqueous solution are the red shift of the high-frequency hydroxyl (O-H) stretching mode, accompanied by its intensity increase and band broadening (Asbury, Steinel, and Fayer, 2004; Jiang, Chaudhuri, Lee, and Chang, 2002; Wu, Chaudhuri, Jiang, Lee, and Chang, 2003). The broad and intense IR absorption bands ranging from 1000 to 3000  $\text{cm}^{-1}$  were interpreted as spectral signatures of protonated water networks (Iftimie, Thomas, Plessis, Marchand, and Ayotte, 2008). The correlation between the O-H stretching frequency and the probability of proton transfer in H-bond has been discussed in details (Buzzoni, Bordiga, Ricchiardi, Spoto, and Zecchina, 1995; Iftimie, Thomas, Plessis, Marchand, and Ayotte, 2008; Wu, Chaudhuri, Jiang, Lee, and Chang, 2003); the probability of proton transfer could be related to a strong red shift of the asymmetric O-H stretching frequency ( $\nu^{\text{OH}}$ ), compared with the corresponding “free” or “non-H-bonded” one (Wu, Chaudhuri, Jiang, Lee, and Chang, 2003). The red shift cannot be detected easily in experiment due to the coupling and

overlapping of various vibrational modes, as well as the detection limit of IR equipment (Okumura, Yeh, Myers, and Lee, 1990; Termath and Sauer, 1997; Wu, Jiang, Boo, Lin, Lee, and Chang, 2000); whereas, the harmonic approximation employed in conventional *ab initio* calculations seems to be inadequate to predict accurately the asymmetric O-H stretching frequency of the active proton in  $\text{H}_5\text{O}_2^+$  (Asmis, Pivonka, Santambrogio, Brummer, Kaposta, Neumark, and Woste, 2003; Termath and Sauer, 1997; Wu, Jiang, Boo, Lin, Lee, and Chang, 2000).

Theories (Cheng and Krause, 1997) and experiments (Fridgen, McMahon, MacAleese, Lemaire, and Maitre, 2004; Okumura, Yeh, Myers, and Lee, 1990) proposed that IR spectra of protonated water clusters in the gas phase and aqueous solution could be divided into three distinct regions. Born-Oppenheimer MD (BOMD) simulations at 225 and 360 K (Cheng and Krause, 1997) proposed that the vibrational frequencies above  $3000\text{ cm}^{-1}$  are associated with the symmetric and asymmetric O-H stretching modes of individual water molecules, whereas those between  $1000$  and  $2000\text{ cm}^{-1}$  are the characteristic vibrational frequencies of the transferring proton (Schmitt and Voth, 1999). The IR multiple photon dissociation (IRMPD) spectra of the  $\text{H}_5\text{O}_2^+$  ion were measured in the gas-phase (Asmis, Pivonka, Santambrogio, Brummer, Kaposta, Neumark, and Woste, 2003; Fridgen, McMahon, MacAleese, Lemaire, and Maitre, 2004), from which two possible assignments of the observed IR bands were discussed. The IRMPD spectra suggested a characteristic asymmetric O-H stretching frequency at  $990\text{ cm}^{-1}$ , which is in good agreement with B3LYP/6-31+G\*\* calculations based on harmonic approximation (Fridgen, McMahon, MacAleese, Lemaire, and Maitre, 2004). Moreover, an additional IR band

was observed at  $1756\text{ cm}^{-1}$ . It was assigned to the  $\text{H}_2\text{O}$  bending mode (Asmis, Pivonka, Santambrogio, Brummer, Kaposta, Neumark, and Woste, 2003).

Since water and proton are confined in hydrophilic domains of Nafion<sup>®</sup> (Mauritz and Moore, 2004), its structure and dynamical properties are quite different from bulk water, and the dynamics of water seem to have direct effects on the transport properties of protons within the membrane. *Ab initio* calculation at Hartree-Fock (HF) and second-order Møller-Plesset perturbation (MP2) (Gejji, Hermansson, and Lindgren, 1994) and Density Functional Theory (DFT) at B3LYP/6-31G (d,p) (Paddison, 2003) reported that three water molecules are sufficient to yield a lowest energy structure, in which proton resides on the water cluster side of the complex creating a contact ion pair between  $-\text{CF}_2\text{SO}_3^-$  group and the solvated  $\text{H}_3\text{O}^+$ . Interesting results were obtained when six water molecules were added namely, a complete separation of  $\text{H}_3\text{O}^+$  from  $\text{CF}_3\text{SO}_3^-$  was observed. This suggested that with sufficient water, the proton is shielded from direct electrostatic interaction with the  $-\text{SO}_3^-$  anion by an intermediate layer of water molecules (Paddison, 2003). Thus the first hydration shell of the  $-\text{SO}_3^-$  anions in these membranes consists of five water molecules.

Extensive calculations on proton mobility in Nafion<sup>®</sup> were presented (Spohr, Commer, and Kornyshev, 2002), in which MD simulations were applied in the calculations of the diffusion coefficients of water and all important solvated proton. The results indicated that the diffusion coefficient increases with increasing hydration level. The mobility of the side chains of the model Nafion<sup>®</sup> membrane was also taken into accounts in MD simulations (Spohr, Commer, and Kornyshev, 2002). The

authors concluded that proton mobility increases with the increase of the delocalization of the counter charges, which are distributed on the polymer side chains. And with the increasing charge delocalization, protons are less-strongly located in the vicinity of the charge center. Decreasing spatial localization was attributed to a higher propensity for symmetric Zundel ion-like configurations. Furthermore, the authors also added that the motion of the  $-\text{SO}_3^-$  groups could lead to a higher mobility of proton (Spohr, Commer, and Kornyshev, 2002).

*Ab initio* MD simulations (Eikerling, Paddison, Pratt, and Zawodzinski, 2003) showed that proton transfer in the minimally hydrated Nafion<sup>®</sup> involves formation of the Zundel complex and the reorganization of the neighboring  $-\text{SO}_3^-$  groups. On the other hand, *ab initio* DFT calculations showed that the proton transfer accompanied by a water molecule occurs via the formation of  $\text{H}_3\text{O}^+$  (Tsuda, Arboleda Jr, and Kasai, 2006).

In order to understand proton transfer processes in condensed phase, MD simulations on triflic acid monohydrate solid  $((\text{CF}_3\text{SO}_3^- - \text{H}_3\text{O}^+)_4)$  (Eikerling, Paddison, Pratt, and Zawodzinski, 2003) were performed at 300 K, using DFT method at PW91 level of accuracy. The results suggested a relay-type mechanism, in which a proton defect represents an intermediate state; the defect involves formation of the Zundel complex ( $\text{H}_5\text{O}_2^+$ ) and the reorganization of the neighboring  $-\text{CF}_2\text{SO}_3^-$  groups, which share a proton between the oxygen atoms of the anionic sites. The proposed mechanism also revealed a possibility for proton conduction along the hydrophilic head groups,  $-\text{CF}_2\text{SO}_3\text{H}$  and  $-\text{CF}_2\text{SO}_3^-$ . The results are in good agreement with the

activation energy for proton transfer in minimally hydrated Nafion<sup>®</sup>, obtained from impedance spectroscopy study (Cappadonia, Erning, Niaki, and Stimming, 1995).

From the above literature survey, an important remark could be made on the theoretical treatments of proton transport in PEM. Previous theoretical investigations (Cui, Liu, Selvan, Keffer, Edwards, and Steele, 2007; Glezakou, Dupuis, and Mundy, 2007; Kreuer, Paddison, Spohr, and Schuster, 2004; Paddison and Elliott, 2005, 2006; Paddison, Pratt, Zawodzinski, and Reagor, 1998; Vishnyakov and Neimark, 2001) focused on conditions and mechanisms of proton dissociation from  $-\text{CF}_2\text{SO}_3\text{H}$ , as well as proton conduction from the dissociated species ( $-\text{CF}_2\text{SO}_3^-$ ), and seem to pay little attention on the detail information on the intermediate state of proton transfer, especially in the first hydration shell of the side chain  $-\text{SO}_3^-$ .

Recently, proton transfer reactions at a hydrophilic group of Nafion<sup>®</sup> were studied using the H-bond complexes formed from triflic acid ( $\text{CF}_3\text{SO}_3\text{H}$ ),  $\text{H}_3\text{O}^+$  and  $\text{H}_2\text{O}$  (Phonyiem, Chaiwongwattana, Lao-ngam, and Sagarik, 2011; Sagarik, Phonyiem, Lao-ngam, and Chaiwongwattana, 2008), as model systems. For the most basic unit in aqueous solution, the  $\text{H}_3\text{O}^+ - \text{H}_2\text{O}$  complexes, BOMD simulations at 350 K revealed that a quasi-dynamic equilibrium is established between the Eigen and Zundel complexes and considered to be the most important elementary reaction in proton transfer process (Sagarik, Phonyiem, Lao-ngam, and Chaiwongwattana, 2008). It was demonstrated that proton transfer reactions are not concerted due to the thermal energy fluctuations and dynamics. The BOMD results and IR spectra of the transferring protons revealed that, for the protonated  $\text{CF}_3\text{SOH} - \text{H}_2\text{O}$  clusters, the  $-\text{SO}_3\text{H}$  group could be directly and indirectly involved in proton transfer reactions,

through the formation of proton defects, as well as  $-\text{SO}_3^-$  and  $-\text{SO}_3\text{H}^+$  (Sagarik, Phonyiem, Lao-ngam, and Chaiwongwattana, 2008). It was concluded that, due to the coupling among various modes of vibrations, the discussions on proton transfer reactions cannot be made based only on static proton transfer potentials and it is necessary to incorporate thermal energy fluctuation and dynamics in the model calculations (Sagarik, Chaiwongwattana, Vchirawongkwin, and Prueksaaron, 2010; Sagarik, Phonyiem, Lao-ngam, and Chaiwongwattana, 2008).

In order to provide additional fundamental information for further investigations on the proton transfer reactions at a hydrophilic group of Nafion<sup>®</sup>, characteristics of the transferring protons in protonated water and the  $\text{CF}_3\text{SO}_3^- - \text{H}_3\text{O}^+ - \text{H}_2\text{O}$  (triflate-hydronium-water) clusters were studied in the present work. The investigations began with searching for the equilibrium structures of the shared-proton structures which could be important in the proton transfer pathways using pair potentials. The computed equilibrium structures were refined using the DFT method, and employed as starting configurations in BOMD simulations at 350 K, the optimal operation temperature in PEMFC. As proton transfer reactions are governed by various modes of vibrations, IR spectra of the H-bond protons susceptible to proton transfers were computed from DFT calculations and BOMD simulations. Characteristic IR frequencies and dynamics of the transferring protons in the gas phase and continuum aqueous solutions, obtained from BOMD simulations, were analyzed, discussed and compared with available theoretical and experimental data.

## CHAPTER II

### RESEARCH METHODOLOGY

The present theoretical study concentrated on elementary reactions and dynamics of proton transfer in the protonated water clusters (the  $\text{H}_3\text{O}^+ - n\text{H}_2\text{O}$  complexes) and the complexes formed from  $\text{CF}_3\text{SO}_3^-$ ,  $\text{H}_3\text{O}^+$  and  $n\text{H}_2\text{O}$ ,  $n = 1 - 4$ . These model systems represent H-bond complexes at low hydration levels. In this work, attention was focused on the H-bond structures, which could be precursors or transition states in the proton transfer pathways. Three basic steps (Sagarik, Chaiwongwattana, Vchirawongkwin, and Prueksaaron, 2010; Sagarik, Phonyiem, Lao-ngam, and Chaiwongwattana, 2008) were employed in investigation of elementary reactions and dynamics of proton transfer in H-bond; (1) searching for the H-bond structures which could be intermediate states in the dynamic proton transfer pathways using pair potentials; (2) refining the computed structures using an accurate quantum chemical method; (3) BOMD simulations using the refined structures as the starting configurations. These basic steps are shown in Figure 2.1.

Since proton transfer reactions involve formation and cleavage of covalent bonds, inclusion of too many water molecules in the model systems could lead to difficulties in the analyses of the elementary reactions and dynamics (Sagarik, Chaiwongwattana, Vchirawongkwin, and Prueksaaron, 2010; Sagarik, Phonyiem, Lao-ngam, and Chaiwongwattana, 2008; Termath and Sauer, 1997). Therefore, the strategy of the present work was to restrict the number of water molecules. For the  $\text{H}_3\text{O}^+ - \text{H}_2\text{O}$  and  $\text{CF}_3\text{SO}_3^- - \text{H}_3\text{O}^+ - \text{H}_2\text{O}$  complexes, the maximum number of water molecules were four; according to a neutron diffraction experiment with hydrogen isotope substitutions and Monte Carlo (MC) simulations (Botti, Bruni, Imberti, Ricci, and Soper, 2005), the first hydration shell of  $\text{H}_3\text{O}^+$  consists of four water molecules and only three of them strongly H-bond to the hydrogen atoms of  $\text{H}_3\text{O}^+$ .

As the electric field introduced by polar solvent could determine the potential energy surface, on which the transferring proton in H-bond moves (Chen, McAllister, Lee, and Houk, 1998; Rospenk, Fritsch, and Zundel, 1984; Sagarik, Chaiwongwattana, Vchirawongkwin, and Prueksaaron, 2010; Zundel and Fritsch, 1984), a continuum solvent model had to be included in the model calculations. To approximate the solvent effects, a conductor-like screening model (COSMO) was proved to be applicable on similar H-bond systems (Rejnek, Hanus, Kabelac, Ryjacek, and Hobza, 2005; Sagarik, Chaiwongwattana, Vchirawongkwin, and Prueksaaron, 2010). Therefore, to partially account for the effects of the extended H-bond networks of water, COSMO with the dielectric constant ( $\epsilon$ ) of 78 was employed in the present quantum chemical calculations and BOMD simulations.



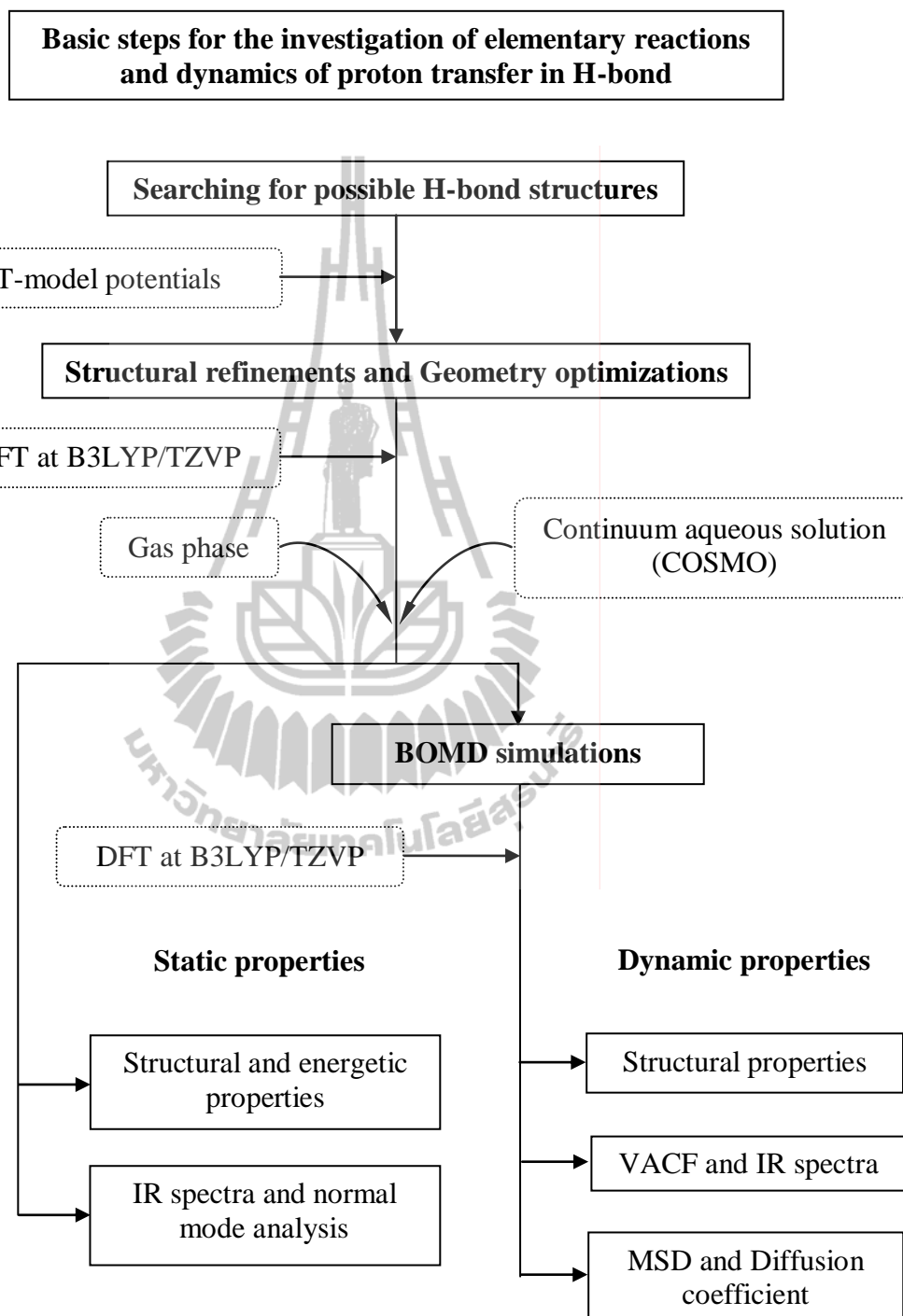


**Figure 2.1** Basic steps employed the investigation of elementary reactions and dynamics of proton transfer in H-bond.

## 2.1 Static calculations

### 2.1.1 Searching for potential precursors and transition state complexes

In the present investigation, attention was focused on the H-bond structures which could be involved in proton transfer processes. The T-model potentials for  $\text{CF}_3\text{SO}_3^-$ ,  $\text{H}_3\text{O}^+$ , and  $\text{H}_2\text{O}$  were taken from (Sagarik, Phonyiem, Lao-ngam and Chaiwongwattana 2008) and employed in the calculations of the equilibrium structures of the  $\text{H}_3\text{O}^+ - n\text{H}_2\text{O}$  complexes, and  $\text{CF}_3\text{SO}_3^- - \text{H}_3\text{O}^+ - n\text{H}_2\text{O}$  complexes,  $n = 1 - 4$ .

The T-model had been discussed in details in the previous studies (Sagarik, 1999; Sagarik and Asawakun, 1997; Sagarik, Chaiwongwattana, and Sisot, 2004; Sagarik and Chaiyapongs, 2005; Sagarik and Rode, 2000; Sagarik and Spohr, 1995; Sagarik and Ahlrichs, 1987; Sagarik, Pongpituk, Chaiyapongs, and Sisot, 1991). Some important aspects relevant to the geometry optimizations will be briefly summarized using the Eigen complex as an example. Experimental geometries (Giguere, 1979) of  $\text{H}_3\text{O}^+$  and  $\text{H}_2\text{O}$  were kept constant in the T-model geometry optimizations. For the Eigen complex, a rigid  $\text{H}_3\text{O}^+$  was placed at the origin of the Cartesian coordinate system. The coordinates of  $\text{H}_2\text{O}$  molecules were randomly generated in the vicinities of  $\text{H}_3\text{O}^+$ . Based on the T-model potentials, equilibrium structures of the Eigen complex were searched using a minimization technique. For each H-bond complex, fifty configurations were generated randomly and employed as starting configurations in the T-model geometry optimizations. The derivation of the T-model potential is shown schematically in Figure 2.2.

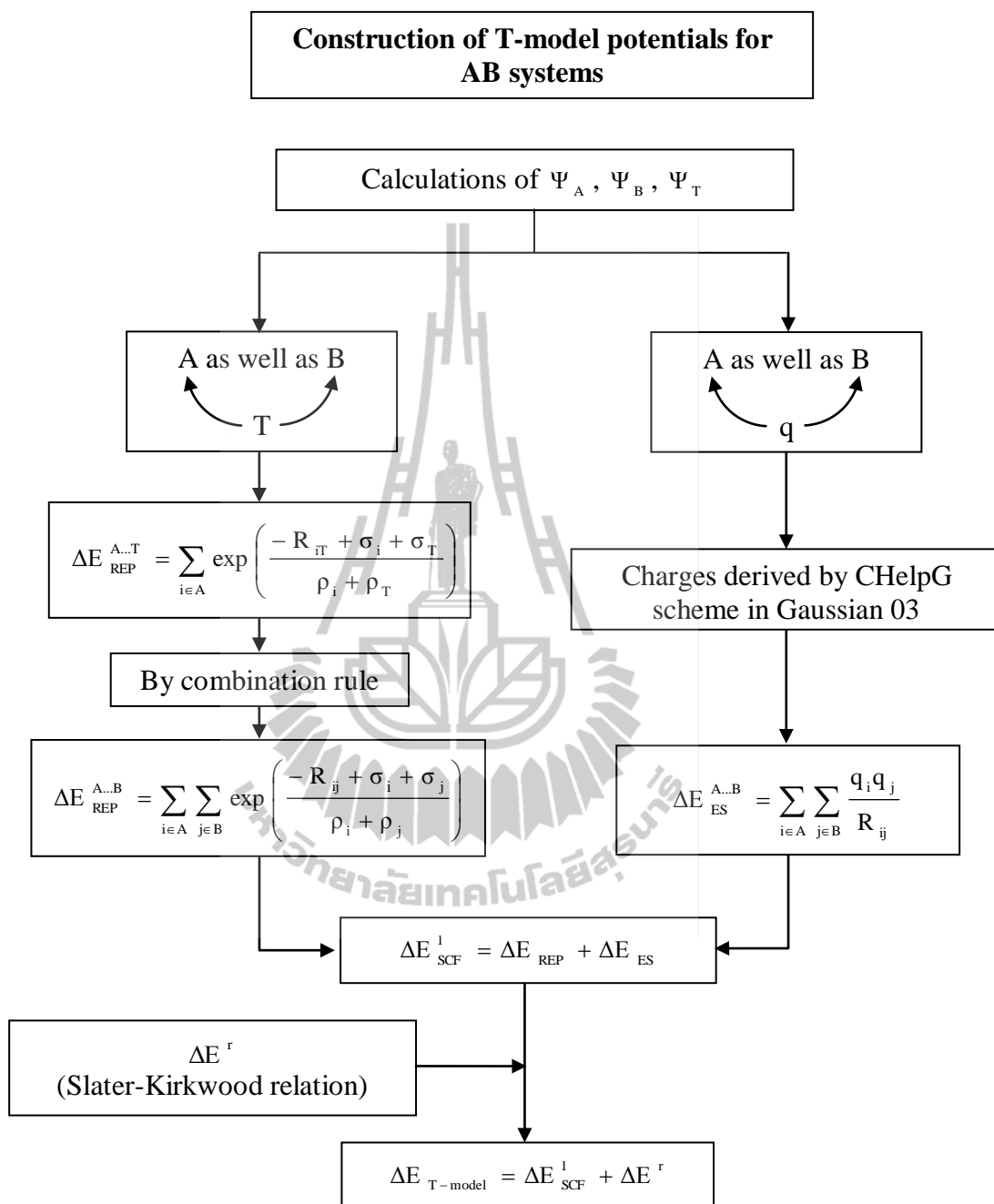


**Figure 2.2** Construction of T-model potentials (Deeing, 2005).

### 2.1.2 Structural refinements

Because the T-model is based on rigid molecules, in which the cooperative effects are neglected, further structural refinements had to be made using an appropriate quantum chemical method. For H-bond system, literature survey showed that, the DFT methods have been frequently chosen due to the ability to treat molecules of relatively large sizes with reasonable accuracies compared to other nonempirical methods (Paddison, 2001; Paddison and Elliott, 2005; Paddison, Pratt, and Zawodzinski, 1999; Paddison, Pratt, and Zawodzinski, 2001; Paddison and Zawodzinski, 1998). Especially, in the present case, calculations of IR spectra and BOMD simulations with thousands of time steps had to be made, it was necessary to compromise between the accuracy of theoretical methods and available computer resources. According to the DFT methods, the ground-state electronic energy ( $E_0$ ) and other ground-state molecular properties are determined by the ground-state electron density ( $\rho_0$ ). In order to achieve all the objectives, DFT calculations were made using the B3LYP hybrid functional (Becke, 1993; Lee, Yang, and Parr, 1988), with the triple-zeta valence basis sets augmented by polarization functions (TZVP). The TZVP basis sets were developed and tested by Ahlrichs and coworkers (Schafer, Huber, and Ahlrichs, 1994). The applicability of the TZVP basis sets in DFT calculations of H-bond structures and IR spectra was discussed in details (Santambrogio, Brummer, Woste, Dobler, Sierka, Sauer, Meijer, and Asmis, 2008). It was concluded that the TZVP basis sets are sufficient for the systems with and without occupied d-states, and could be applied in the calculations of equilibrium structures and interaction energies, as well as IR spectra, of such systems (Santambrogio, Brummer, Woste, Dobler, Sierka, Sauer, Meijer, and Asmis, 2008). The applicability of B3LYP calculations on

protonated water clusters was also systematically analyzed and discussed in details (Termath and Sauer, 1997).

The absolute and local minimum energy geometries of the protonated water clusters obtained from the T-model potentials were employed as starting configurations in the B3LYP/TZVP geometry optimizations. In order to ensure that the optimized structures were at the stationary points and to obtain reasonable IR frequencies, a tight SCF energy convergence criterion (less than  $10^{-8}$  au), with the maximum norm of Cartesian gradients less than  $10^{-4}$  au, was employed in the B3LYP/TZVP geometry optimizations. All quantum chemical calculations were made using TURBOMOLE 6.0 (Ahlich, Bär, Häser, Horn, and Kölmel, 1989; Treutler and Ahlich, 1995).

### 2.1.3 Interaction energies and asymmetric stretching coordinates

The interaction energies ( $\Delta E$ ) of the equilibrium structures of the  $\text{H}_3\text{O}^+ - n\text{H}_2\text{O}$  complexes,  $n = 1 - 4$ , were computed as

$$\Delta E = E(\text{H}_3\text{O}^+ - n\text{H}_2\text{O}) - [E(\text{H}_3\text{O}^+) + nE(\text{H}_2\text{O})] \quad (2.1)$$

where  $E(\text{H}_3\text{O}^+ - n\text{H}_2\text{O})$  is the total energy of the optimized structures of the  $\text{H}_3\text{O}^+ - n\text{H}_2\text{O}$  complexes;  $E(\text{H}_3\text{O}^+)$  and  $E(\text{H}_2\text{O})$  are the total energies of the isolated  $\text{H}_3\text{O}^+$  and  $\text{H}_2\text{O}$  at their optimized structures, respectively. The energetic effects due to the continuum aqueous solvent (COSMO with  $\epsilon = 78$ ) were estimated from the solvation energy ( $\Delta E^{\text{sol}}$ ), approximate as

$$\Delta E^{\text{sol}} = E(\text{H}_3\text{O}^+ - n\text{H}_2\text{O})^{\text{COSMO}} - E(\text{H}_3\text{O}^+ - n\text{H}_2\text{O}) \quad (2.2)$$

$E(\text{H}_3\text{O}^+ - n\text{H}_2\text{O})^{\text{COSMO}}$  and  $E(\text{H}_3\text{O}^+ - n\text{H}_2\text{O})$  are the total energies of the optimized structures, obtained from B3LYP/TZVP calculations with and without COSMO, respectively. The interaction energies between the central charged species and the surrounding water molecules ( $\Delta E^{\text{X}}$ ,  $\text{X} = \text{H}_3\text{O}^+$  or  $\text{H}_5\text{O}_2^+$ ) were computed with and without the continuum aqueous solvent as

$$\Delta E^{\text{X}} = E(\text{X} - n\text{H}_2\text{O}) - [E(\text{X}) + E(n\text{H}_2\text{O})] \quad (2.3)$$

$E(\text{X} - n\text{H}_2\text{O})$  is the total energy of the optimized structures;  $E(\text{X})$  and  $E(n\text{H}_2\text{O})$  are the total energies obtained by removing water molecules and the central charged species from the optimized structures, respectively. In order to test the reliability of the energetic results obtained from B3LYP/TZVP calculations, the basis set superposition errors (BSSE) were estimated for  $\Delta E^{\text{X}}$  using the counterpoise correction (Boys and Bernardi, 1970). For  $\text{CF}_3\text{SO}_3^- - \text{H}_3\text{O}^+ - n\text{H}_2\text{O}$  complexes,  $n = 1 - 4$ , the interaction energies ( $\Delta E$ ) of the H-bond complexes were computed from

$$\Delta E = E(\text{CF}_3\text{SO}_3^- - \text{H}_3\text{O}^+ - n\text{H}_2\text{O}) - [E(\text{CF}_3\text{SO}_3^-) + E(\text{H}_3\text{O}^+) + nE(\text{H}_2\text{O})] \quad (2.4)$$

where  $E(\text{CF}_3\text{SO}_3^- - \text{H}_3\text{O}^+ - n\text{H}_2\text{O})$  are the total energies of the H-bond complexes;  $E(\text{CF}_3\text{SO}_3^-)$ ,  $E(\text{H}_3\text{O}^+)$  and  $E(\text{H}_2\text{O})$  the total energies of the isolated molecules at their optimized structures. The solvation energy ( $\Delta E^{\text{sol}}$ ) is calculated from;

$$\Delta E^{\text{sol}} = E(\text{CF}_3\text{SO}_3^- - \text{H}_3\text{O}^+ - n\text{H}_2\text{O})^{\text{COSMO}} - E(\text{CF}_3\text{SO}_3^- - \text{H}_3\text{O}^+ - n\text{H}_2\text{O}) \quad (2.5)$$

where  $E(\text{CF}_3\text{SO}_3^- - \text{H}_3\text{O}^+ - n\text{H}_2\text{O})^{\text{COSMO}}$  and  $E(\text{CF}_3\text{SO}_3^- - \text{H}_3\text{O}^+ - n\text{H}_2\text{O})$  are the total energies of the H-bond complexes, obtained from B3LYP/TZVP calculations with and without COSMO, respectively.

Attempt was made to anticipate tendency of proton transfer in H-bond using the asymmetric stretching coordinate ( $\Delta d_{\text{DA}}$ ) (Benoit and Marx, 2005; Sagarik, Chaiwongwattana, Vchirawongkwin, and Prueksaaron, 2010), for which a concept of the “most active” H-bond (Marx, Tuckerman, Hutter, and Parrinello, 1999) was employed in the discussion of the Grotthuss mechanism. Within the framework of the most active H-bond,  $\Delta d_{\text{DA}}$  of a H-bond donor (D) - acceptor (A) pair is defined by

$$\Delta d_{\text{DA}} = |d_{\text{A-H}} - d_{\text{B..H}}| \quad (2.6)$$

where  $d_{\text{A-H}}$  and  $d_{\text{B..H}}$  are the A-H and B..H distances in the A-H..B H-bond, respectively. The H-bond with small  $\Delta d_{\text{DA}}$  is considered to be susceptible to proton transfer (Sagarik, Chaiwongwattana, Vchirawongkwin, and Prueksaaron, 2010); “active” with respect to proton transfer when  $\Delta d_{\text{DA}} < 0.1 \text{ \AA}$ , and “inactive” when  $\Delta d_{\text{DA}} > 0.4 \text{ \AA}$  (Morrone, Haslinger, and Tuckerman, 2006).

#### 2.1.4 Infrared spectra and normal mode analyses

Being associated with the dynamics of proton transfer in H-bonds, asymmetric O-H stretching frequencies ( $\nu^{\text{OH}}$ ) were of primary interest. Based on the optimized H-bond structures obtained in the previous subsection, harmonic IR frequencies were computed from the numerical second derivatives of the B3LYP/TZVP total energies. The calculations of the second derivatives and the analyses of the normal modes in terms of internal coordinates were performed using NUMFORCE and AOFORCE programs, respectively. They were incorporated in TURBOMOLE 6.0 software package (Ahlich, Bär, Häser, Horn, and Kölmel, 1989; Treutler and Ahlich, 1995).  $\nu^{\text{OH}}$  derived from the static proton transfer potentials (B3LYP/TZVP calculations) were used to estimate the tendencies of proton transfers in the protonated water clusters.

It should be mentioned that the vibrational frequencies derived from quantum chemical calculations are in general larger than those from experiments. Therefore, a scaling factor, which partially accounts for the anharmonicities and systematic errors, is required. Although in the present study, only the changes in the O-H stretching frequencies due to different H-bond environments were of interest, a scaling factor was used throughout; a scaling factor of 0.9614 (Scott and Radom, 1996) was proved to be appropriate for B3LYP/TZVP calculations with comparable basis sets (Scott and Radom, 1996; Xenides, Randolph, and Rode, 2005).



## 2.2 Dynamic calculations

### 2.2.1 Born-Oppenheimer MD simulations

Dynamics of rapid covalent and H-bond formations and cleavages could be studied reasonably well using quantum MD simulations (Balbuena and Seminario, 1999), among which BOMD simulations have been widely used in recent years (Barnett and Landman, 1993; Cramer, 2002; Huisken, Mohammad-Pooran, and Werhahn, 1998; Hunter and Lias, 1998; Jing, Troullier, Dean, Binggeli, Chelikowsky, Wu, and Saad, 1994; Lobaugh and Voth, 1995). Within the framework of BOMD simulations, classical equations of motions of nuclei on the Born-Oppenheimer (BO) surfaces are integrated, whereas forces on nuclei are calculated in each MD step from quantum energy gradients, with the molecular orbitals (MO) updated by solving Schrödinger equations in the BO approximation; the nuclei thus undergo classical Newtonian dynamics on quantum potential hypersurface. BOMD simulations are therefore more accurate, as well as considerably CPU time consuming, compared to classical MD simulations, in which forces on nuclei are determined from predefined empirical or quantum pair potentials. It should be mentioned that, although the high mobility of excess proton was initially attributed to quantum mechanical (QM) tunneling (Leach, 1996), the results of BOMD simulations (Schmitt and Voth, 1999) and conductivity measurements (Conway, Bockris, and Linton, 1956) indicated that mechanisms of proton transfers could be explained reasonably well without assuming the proton tunneling as an important pathway. As proton transfers in aqueous solution involve dynamic processes with different timescales (Agmon, 1995; Giguere, 1979; Kreuer, 2000), the complexity of proton transfer reactions could be reduced using various approaches. The observation that the actual proton transfer occurs in

femtosecond (fs) timescale (Giguere, 1979), which is faster than solvent structure reorganization (Agmon, 1995), made it possible to perform BOMD simulations by focusing on short-lived phenomena taking place before the H-bond structure reorganization.

In order to obtain insights into the dynamic behavior of H-bonds in  $\text{H}_3\text{O}^+ - n\text{H}_2\text{O}$  complexes,  $n = 1 - 4$ , BOMD simulation was performed in a canonical (NVT) ensemble at 350 K. The temperature was kept constant by applying the Nosé-Hoover chain thermostat to each degree of freedom in the system. In order to ensure that all important dynamics in the gas phase and continuum aqueous solution (COSMO) were taken into account, the shared-proton complexes predicted in the previous subsection were used as the starting configurations. Since in aqueous solution, the rapid interconversion between the Zundel and Eigen complexes takes place within 100 fs ( $10^{-13}$  s) (Kreuer, 2000), the time step used in solving dynamic equations was set to 0.24 fs. In each BOMD simulation, 2000 steps were devoted to equilibration, after which 10,000 steps to property calculations, corresponding to about 2.4 ps.

For the  $\text{CF}_3\text{SO}_3^- - \text{H}_3\text{O}^+ - n\text{H}_2\text{O}$  complexes,  $n = 1 - 4$ , the BOMD simulations were also performed with canonical (NVT) ensemble at 350 K, by applying a Nosé-Hoover chain thermostat to each degree of freedom in the system. Only the H-bond structures which could be susceptible to proton transfer,  $\Delta d_{\text{DA}} < 0.4 \text{ \AA}$ , were chosen as starting configuration in BOMD simulations. In this case, the size of time step was set to 0.96 fs. The system was initially equilibrated for 2000 time steps, after which the simulations were continued for 10,000 steps for properties

calculations. All BOMD simulations were performed using FROG program, included in TURBOMOLE 6.0 (Ahlrichs, Bär, Häser, Horn, and Kölmel, 1989; Treutler and Ahlrichs, 1995); the MD program employs the Leapfrog Verlet algorithm to turn the electronic potential energy gradients into new atomic positions and velocities. The basics steps in MD simulations are illustrated in Figure 2.3.

Remarks should be made on the ensemble and simulation length chosen in the present study. The applicability and performance of NVE and NVT BOMD simulations on small H-bond chains were investigated and discussed in details (Sadeghi and Cheng, 1999). For NVE BOMD simulations, it was demonstrated that the potential energy of the system decreases quite rapidly in the course of BOMD simulations. Once the proton stays at the center of the H-bond, the potential energy is at the lowest point and the proton is trapped in the minimum; no proton transfer can be observed in the later timesteps. Since NVE BOMD simulations are conducted at constant energy, a decrease in the potential energy is accompanied by an increase in the kinetic energy, as well as temperature, leading to the H-bond structure reorganization and fragmentation. For NVT BOMD simulations, the energy released during the proton transfer processes can be absorbed by the thermostat bath, allowing the H-bond structure and local temperature to be maintained for a longer time (2 – 5 ps), depending upon the size and the complexity of the H-bond structure. Thus, NVT BOMD simulations are more appropriate for the present investigations.

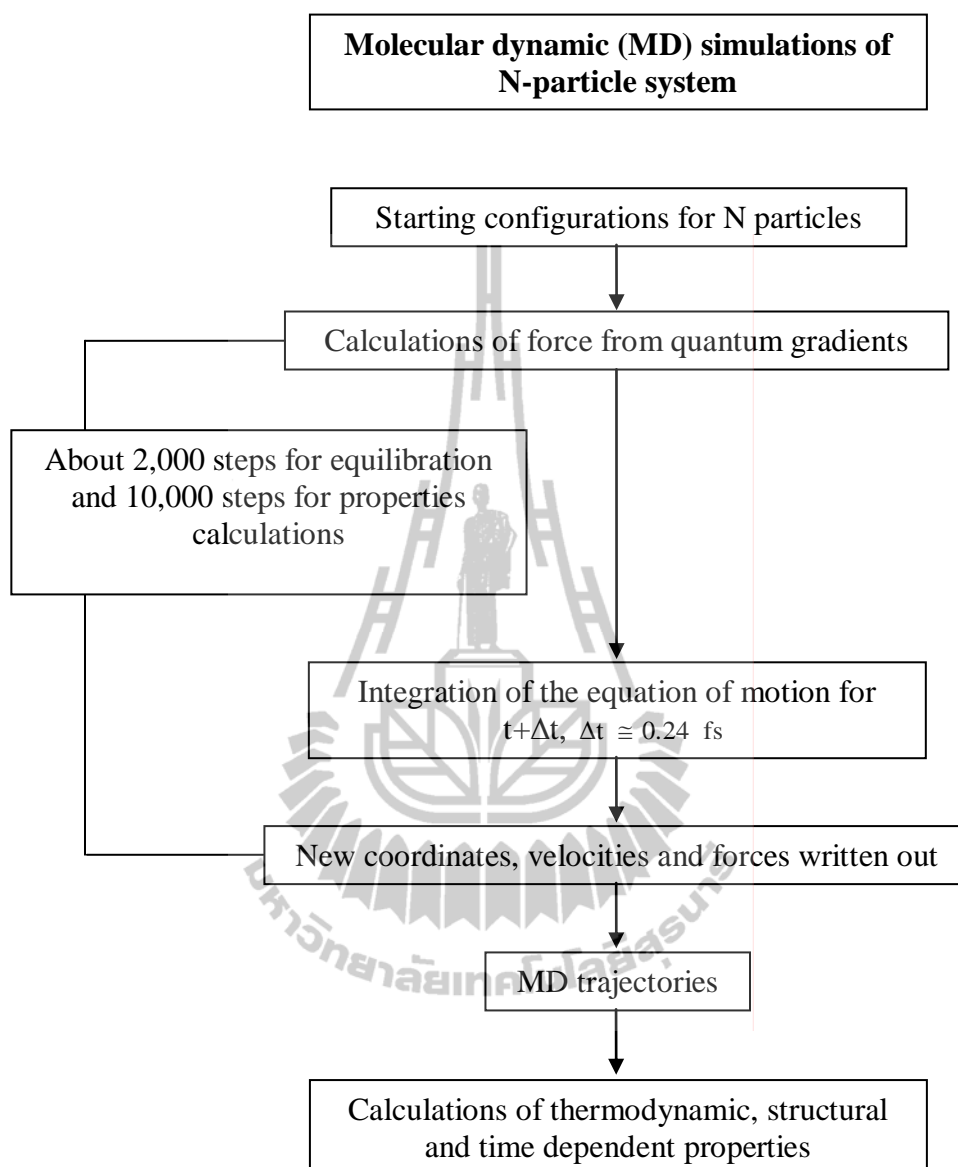


**Figure 2.3** Basic steps in MD simulations of N-particle system (Deeying, 2005).

### 2.2.2 Infrared spectra and diffusion coefficients

Since proton transfer reactions in H-bonds are strongly coupled with various degrees of freedom, especially the O-O vibration (Cheng and Krause, 1997; Kreuer, 1996; Sagarik, Chaiwongwattana, Vchirawongkwin, and Prueksaaron, 2010), attention was focused on the symmetric and asymmetric O-H stretching modes, as well as the O-O vibrations. Definitions of the symmetric and asymmetric O-H stretching modes, as well as the O-O vibration are shown in Figure 2.4. In the present work, the IR spectra of the transferring protons were computed from BOMD simulations by Fourier transformations of the velocity autocorrelation function (VACF) (Bopp, 1986). This approach is appropriate as it allows the coupled vibrations to be distinguished, characterized and analyzed separately. Fourier transformations of VACF were made within a short time limit of 100 fs. This choice is justified by the observation that the average lifetime of the most important shared-proton complex, the Zundel complex, is about 100 fs (Kreuer, 2000; Tuckerman, Laasonen, Sprik, and Parrinello, 1995). The diffusion coefficients ( $D$ ) of the transferring protons were computed from BOMD simulations using the Einstein relation (Allen and Tildesley, 1987; Haile, 1997), by which  $D$  were determined from the slopes of the mean-square displacements (MSD). Because the transferring proton is confined in a short H-bond distance, care must be exercised in selecting the time interval in which MSD is computed (Rapaport, 1995). The previous (Sagarik, Chaiwongwattana, Vchirawongkwin, and Prueksaaron, 2010) and present experience showed that, linear relationship between MSD and simulation time could be obtained when the time intervals are not larger than 0.5 ps.

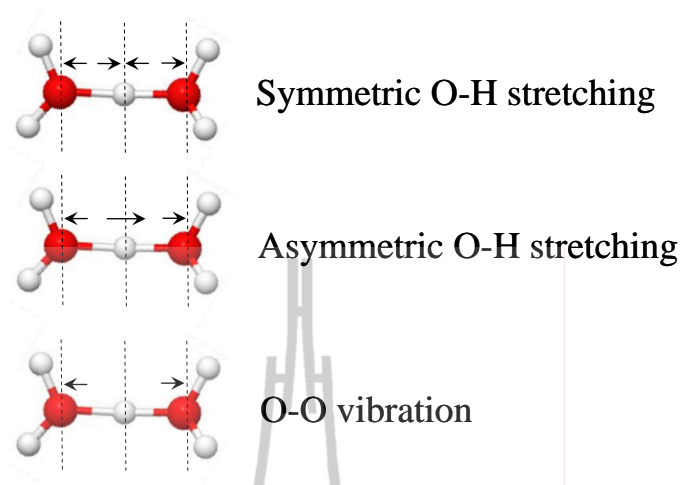


**Figure 2.4** Definitions of the symmetric and asymmetric O-H stretching modes, as well as the O-O vibration (Sagarik, Chaiwongwattana, Vchirawongkwin, and Prueksaaron, 2010).



## CHAPTER III

### RESULTS AND DISCUSSION

In this chapter, all important results are presented, with the emphasis on the H-bonds in the shared-proton complexes. The discussions are made primarily on the static results obtained from B3LYP/TZVP calculations, both in the gas phase and continuum aqueous solution. Then, the BOMD results are analyzed and discussed in comparison with the B3LYP/TZVP results, with special emphases on the relationships among the H-bond structures, characteristic IR frequencies and dynamics in connection with the mechanisms of proton transfer reactions.

#### 3.1 The $\text{H}_3\text{O}^+ - n\text{H}_2\text{O}$ complexes, $n = 1 - 4$

##### 3.1.1 Static results

###### Structures and energetic of the shared-proton complexes

Table 3.1 shows the refined equilibrium structures, interaction energies ( $\Delta E$  and  $\Delta E^X$ ,  $X = \text{H}_3\text{O}^+$  or  $\text{H}_5\text{O}_2^+$ ) and solvation energies ( $\Delta E^{\text{sol}}$ ) of the  $\text{H}_3\text{O}^+ - n\text{H}_2\text{O}$  complexes,  $n = 1 - 4$ , in the gas phase and continuum aqueous solution, together with characteristic H-bond distances ( $R_{\text{O}-\text{O}}$  and  $R_{\text{O}-\text{H}}$ ). In order to simplify the discussion, the H-bonds in Table 3.1 are labeled with numbers in parentheses. The trends of  $\Delta E$ ,  $\Delta E^{\text{sol}}$  and  $\Delta E^X$  with respect to the number of water molecules are compared in Figures 3.1 and 3.2.

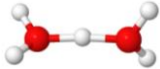
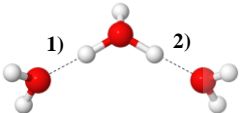
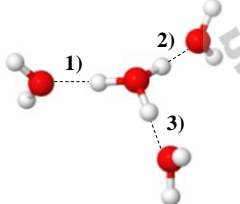
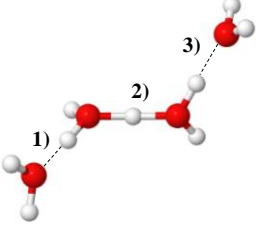
The equilibrium structures,  $\Delta E$  and  $\Delta E^X$  obtained from B3LYP/TZVP calculations agree in general with the results in literatures (Fridgen, McMahon, MacAleese, Lemaire, and Maitre, 2004; Park, Shin, Singh, and Kim, 2007; Parthasarathi, Subramanian, and Sathyamurthy, 2007; Termath and Sauer, 1997; Wu, Chen, Wang, Paesani, and Voth, 2007). The Zundel complex with  $C_2$  symmetry (structure **a** in Table 3.1) represents the absolute minimum energy geometry of the  $H_3O^+ - H_2O$  1 : 1 complex, both in the gas phase and continuum aqueous solution. The equilibrium structure of the  $H_3O^+ - H_2O$  1 : 2 complex (structure **b** in Table 3.1) consists of two symmetric O-H...O H-bonds at  $H_3O^+$ , with  $R_{O-O}$  about 0.2 Å shorter than the Zundel complex. For the  $H_3O^+ - H_2O$  1 : 3 complex, three equilibrium structures were predicted by B3LYP/TZVP calculations (structures **c**, **d** and **e** in Table 3.1). With a complete water coordination at  $H_3O^+$ ,  $\Delta E$  of the Eigen complex (structure **c**) is about 13 kJ/mol more stable than the structures with the Zundel complex as the central charged species (structures **d** and **e**). Structures **f**, **g** and **h** are three important equilibrium structures of the  $H_3O^+ - H_2O$  1 : 4 complex. Having the Eigen complex as the central charged species, structure **g** in the gas phase is about 14 kJ/mol more stable than structures **f** and **h**, whereas in the continuum aqueous solvent (COSMO), structure **h** is about 2 kJ/mol more stable than structure **g**. The stabilization effects at the central charged species can be confirmed by the values of  $\Delta E^X$ ,  $X = H_3O^+$  or  $H_5O_2^+$ . It appeared that, for the same number of water coordination,  $H_3O^+$  can be more effectively stabilized by water molecules compared to the Zundel complex; as an example,  $\Delta E^{H_3O^+}$  of structure **b** in the gas phase is -290.7 kJ/mol, whereas  $\Delta E^{H_5O_2^+}$  of structures **d** and **e** are -191.7 kJ/mol.



The environmental effects on the stabilities of charged H-bonds were investigated using *ab initio* SCRF (self-consistent reaction field) calculations at the Hartree-Fock level, from which the dependence of  $\Delta E$  on a wide range of dielectric constant ( $\epsilon$ ) was established (Chen, McAllister, Lee, and Houk, 1998). It was reported that small increases in  $\epsilon$  from the gas-phase value ( $\epsilon = 1$ ) rapidly reduce the stabilities of the charged H-bonds. In the present work, although the equilibrium structures in the gas phase and continuum aqueous solution are almost the same,  $\Delta E$  and  $\Delta E^x$  are considerably higher (less negative) in continuum aqueous solution (see Figures 3.1 and 3.2).

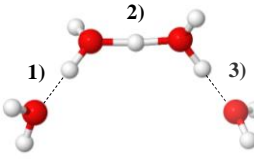
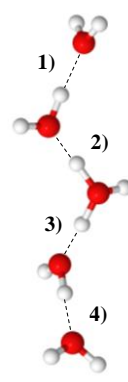
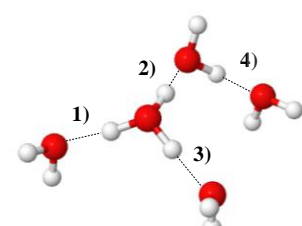
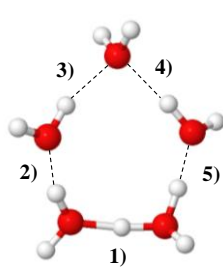
The destabilization effects caused by the continuum aqueous solvent are in good agreement with the previous theoretical results (Chen, McAllister, Lee, and Houk, 1998). Figures 3.1 and 3.2 illustrates the trends of  $\Delta E$ ,  $\Delta E^x$  and  $\Delta E^{\text{sol}}$  with respect to the number of water molecules. The trends of  $\Delta E$ , as well as  $\Delta E^x$ , in the gas phase and continuum aqueous solution are quite similar, with smaller variations in continuum aqueous solution. The solvent effects can be directly observed in Figure 3.1, in which  $\Delta E^{\text{sol}}$  are not substantially different for structures **c** to **h**. This suggested that, when the number of water molecules is the same, the H-bonds inside the protonated water clusters experience comparable uniform electric field (COSMO), with the asymptotic  $\Delta E$  in continuum aqueous solution  $\approx -149$  kJ/mol and  $\Delta E^{\text{sol}} \approx -266$  kJ/mol. Figure 3.2 revealed that the trends of the interaction energies ( $\Delta E^x$ ) remain the same when the counterpoise corrections were applied; the BSSE contributes only about 3% of  $\Delta E^x$ .

**Table 3.1** H-bond distances and energies of the protonated water cluster obtained from B3LYP/TZVP calculations, both in the gas phase and continuum aqueous solution (values in parenthesis). They are in Å and kJ/mol, respectively.

Structure	$R_{O-O}$	$R_{O-H}$	$\Delta E$	$\Delta E^{sol}$	$\Delta E^X$
<b>a)</b> 	2.40 (2.40)	1.20 (1.20)	-158.8 (-58.2)	-316.4	
<b>b)</b> 	1) 2.49 (2.50) 2) 2.49 (2.50)	1.04 (1.05) 1.04 (1.05)	265.7 (-95.2)	-280.3	-290.7 (-121.7)
<b>c)</b> 	1) 2.56 (2.55) 2) 2.56 (2.55) 3) 2.56 (2.54)	1.02 (1.02) 1.01 (1.02) 1.02 (1.02)	-353.7 (129.3)	-260.2	-379.7 (-159.8)
<b>d)</b> 	1) 2.58 (2.64) 2) 2.40 (2.43) 3) 2.58 (2.54)	1.01 (1.00) 1.20 (1.11) 1.01 (1.03)	-340.6 (-116.7)	-260.6	-191.7 (-70.3)

$R_{O-O}$  and  $R_{O-H}$  = H-bond distances;  $\Delta E$  = interaction energy in the protonated water clusters;  $\Delta E^{sol}$  = solvation energy;  $\Delta E^X$  = interaction energy between the central charge species ( $X = H_3O^+$  and  $H_5O_2^+$ ) and water molecules.

**Table 3.1** (Continued).

Structure	$R_{O-O}$	$R_{O-H}$	$\Delta E$	$\Delta E^{\text{sol}}$	$\Delta E^{\text{X}}$
<b>e)</b> 	1) 2.59 (2.64)	1.01(1.00)	-340.5	-261.8	-191.7
	2) 2.39 (2.43)	1.20 (1.11)	(-117.7)		(-74.5)
	3) 2.59 (2.54)	1.01 (1.03)			
<b>f)</b> 	1) 2.66 (2.67)	0.99 (1.00)	-403.2	-253.2	-434.9
	2) 2.45 (2.47)	1.07 (1.07)	(-138.0)		(-171.5)
	3) 2.46 (2.47)	1.07 (1.07)			
	4) 2.66 (2.67)	0.99 (1.00)			
<b>g)</b> 	1) 2.59 (2.57)	1.01 (1.02)	-416.5	-249.7	-415.3
	2) 2.47 (2.50)	1.05 (1.05)	(-147.9)		(-155.2)
	3) 2.59 (2.57)	1.01 (1.02)			
	4) 2.68 (2.69)	0.99 (0.99)			
<b>h)</b> 	1) 2.41 (2.46)	1.12 (1.09)	-402.0	-265.9	-233.1
	2) 2.53 (2.51)	1.03 (1.05)	(-149.5)		(-151.0)
	3) 2.85 (2.75)	0.98 (0.99)			
	4) 2.91 (2.81)	0.97 (0.98)			
	5) 2.61 (2.64)	1.00 (1.00)			

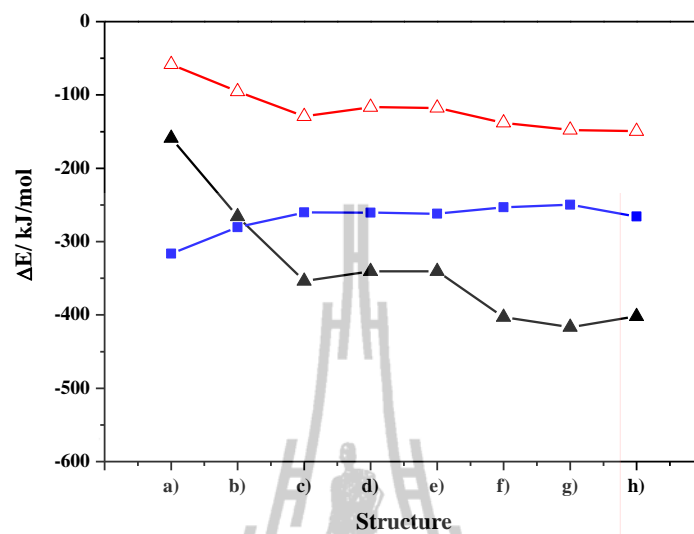


**Figure 3.1** Trends of the interaction ( $\Delta E$ ) and solvation energies ( $\Delta E^{\text{sol}}$ ) with respect to the number of water molecules, obtained from B3LYP/TZVP calculations: -▲- =  $\Delta E$  in the gas phase; -△- =  $\Delta E$  in continuum aqueous solution; -■- =  $\Delta E^{\text{sol}}$ .

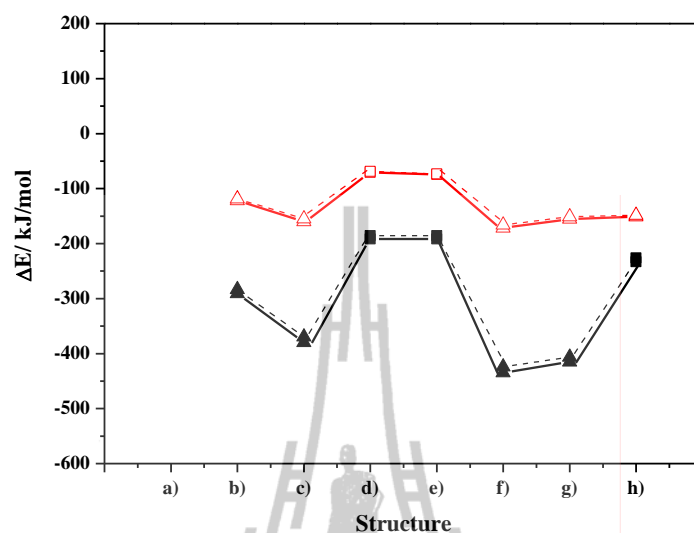


**Figure 3.2** Trends of the interaction energies between the central charged species and water molecules ( $\Delta E^X$ ,  $X = \text{H}_3\text{O}^+$  or  $\text{H}_5\text{O}_2^+$ ) with respect to the number of water molecules, obtained from B3LYP/TZVP calculations: -▲- =  $\text{H}_3\text{O}^+$  in the gas phase; -Δ- =  $\text{H}_3\text{O}^+$  in continuum aqueous solution; -■- =  $\text{H}_5\text{O}_2^+$  in the gas phase; -□- =  $\text{H}_5\text{O}_2^+$  in continuum aqueous solution. \_\_\_\_\_ = calculations without the counterpoise correction. ----- = calculations with the counterpoise correction.

### **Asymmetric stretching coordinates and infrared spectra of transferring protons**

Asymmetric stretching coordinate ( $\Delta d_{DA}$ ), asymmetric stretching frequency ( $\nu^{OH}$ ) and frequency shifts due to continuum aqueous solvent ( $\Delta \nu^{OH}$ ) are displayed in Table 3.2. The trends of  $\Delta d_{DA}$  and  $\nu^{OH}$  with respect to the H-bond distances ( $R_{O-O}$ ) are shown in Figures 3.3a and 3.3b, respectively.

$\Delta d_{DA}$  obtained from static proton transfer potentials could be used to measure the tendency of proton transfer, as well as the strength of H-bond (Morrone, Haslinger, and Tuckerman, 2006; Sagarik, Chaiwongwattana, Vchirawongkwin, and Prueksaaron, 2010).  $\Delta d_{DA}$  in Table 3.2 suggested that the H-bonds in structures **a**, **d**, **e**, **f** and **h** are susceptible to proton transfers in the gas phase, with  $0 \leq \Delta d_{DA} \leq 0.32$ ; whereas the continuum aqueous solvent (COSMO) destabilizes the protonated water clusters, resulting in shifts of the H-bond protons away from the centers, especially for structures **d**, **e** and **h**.

Based on the results of IR and Raman spectra (Buzzoni, Bordiga, Ricchiardi, Spoto, and Zecchina, 1995), the H-bond distance ( $R_{O-O}$ ) in concentrated HCl solution can be divided into three groups namely, the internal, external and solvation groups. The H-bonds linking directly to protons belong to the internal group, with  $R_{O-O}$  in the range of 2.45 – 2.57 Å, whereas  $R_{O-O}$  in the external and solvation groups are in the ranges of 2.60 – 2.70 Å and longer than 2.70 Å, respectively. Figure 3.3a shows linear relationships between  $\Delta d_{DA}$  and  $R_{O-O}$ , with a separation between the internal and external H-bonds at  $R_{O-O} \approx 2.5$  Å, in good agreement with experiment (Buzzoni, Bordiga, Ricchiardi, Spoto, and Zecchina,

1995). The linear relationships for the internal and external H-bonds can be represented by equations (3.1) and (3.2), respectively.

$$\text{Internal H-bonds:} \quad \Delta d_{\text{DA}} = 3.57 \times R_{\text{O-O}} - 8.50 \quad (3.1)$$

$$\text{External H-bonds:} \quad \Delta d_{\text{DA}} = 1.34 \times R_{\text{O-O}} - 2.90 \quad (3.2)$$

Theoretical and experimental results on vibrational spectra of the transferring proton in the Zundel complex were presented in the past decades (Asmis, Pivonka, Santambrogio, Brummer, Kaposta, Neumark, and Woste, 2003; Ifimie, Thomas, Plessis, Marchand, and Ayotte, 2008; Termath and Sauer, 1997), from which the flatness of the potential energy surface was concluded by *ab initio* calculations at different levels to be the most outstanding feature of the transferring proton (Termath and Sauer, 1997). For the Zundel complex in the gas phase ( $\Delta d_{\text{DA}} = 0$ ), B3LYP/TZVP calculations predicted  $\nu^{\text{OH}} = 961 \text{ cm}^{-1}$ , whereas in continuum aqueous solution  $\nu^{\text{OH}} = 677 \text{ cm}^{-1}$ . The former is in reasonable agreement with the theoretical results at the same levels of accuracy (Fridgen, McMahon, MacAleese, Lemaire, and Maitre, 2004; Park, Shin, Singh, and Kim, 2007) and IRMPD experiment (Fridgen, McMahon, MacAleese, Lemaire, and Maitre, 2004; Hammer, Diken, Roscioli, Johnson, Myshakin, Jordan, McCoy, Huang, Bowman, and Carter, 2005). Good agreement between theoretical and experimental data was also found for  $\text{H}_7\text{O}_3^+$ . In the gas phase, B3LYP/TZVP calculations predicted  $\nu^{\text{OH}} = 2304 \text{ cm}^{-1}$ , compared with B3LYP/T(O)DZP calculations of  $2402 \text{ cm}^{-1}$  (Termath and Sauer, 1997) and

experiment between 2200 and 2300  $\text{cm}^{-1}$  (Schwarz, 1977). These  $\nu^{\text{OH}}$  could be associated with the H-bond protons in the  $\text{H}_3\text{O}^+ - \text{H}_2\text{O}$  contact structure. For larger protonated water clusters, the structures with the Zundel complex as the central charged species exhibit higher tendencies of proton transfers, with  $1000 < \nu^{\text{OH}} < 1450 \text{ cm}^{-1}$ , whereas the structures with  $\text{H}_3\text{O}^+$  as the central charged species possess  $1900 < \nu^{\text{OH}} < 2760 \text{ cm}^{-1}$ .

Due to the asymptotic behavior at large  $R_{\text{O-O}}$ , the relationships between  $\nu^{\text{OH}}$  and  $R_{\text{O-O}}$  in Figure 3.3b cannot be approximated by linear functions; at large  $R_{\text{O-O}}$ ,  $\nu^{\text{OH}}$  converges to the asymmetric O-H stretching frequency of the free or non-H-bonded proton in  $\text{H}_3\text{O}^+$ . After several trial fittings, an exponential function similar to the integrated rate expression for the first order reaction was found to be the most appropriate, with the asymptotic values in the gas phase and continuum aqueous solution fixed at  $\nu^{\text{OH}} = 3521$  and  $3566 \text{ cm}^{-1}$ , respectively. The agreements between  $\nu^{\text{OH}}$  obtained from B3LYP/TZVP calculations and the fitted values are included in Figure 3b. The fitted functions in the gas phase and continuum aqueous solution are given in equations (3.3) and (3.4), respectively.

$$\text{Gas phase:} \quad \nu^{\text{OH}} = -1.67 \times 10^{11} e^{-R_{\text{O-O}}/0.1331} + 3521 \quad (3.3)$$

$$\text{Continuum aqueous solution:} \quad \nu^{\text{OH}} = -5.15 \times 10^{10} e^{-R_{\text{O-O}}/0.1438} + 3566 \quad (3.4)$$

Attempt has been made to distinguish between normal and strong H-bonds, however without a concrete result. It was found in general that, when



H-bond is shorter, it becomes stronger, with the strongest attractive interaction at the shortest H-bond distance (Chen, McAllister, Lee, and Houk, 1998; Hibbert and Emsley, 1991). According to the analyses of the H-bond energies with the H-bond distances in crystal structures, the experimental H-bond energies change dramatically at the H-bond distance of 2.45 Å (Hibbert and Emsley, 1991). It was concluded that 2.45 Å is the threshold distance for very strong H-bonds. Theoretical studies, on the other hand, revealed smooth linear relationships between the H-bond energies and the H-bond distances, with no dramatic change when the H-bond distance is between 2.45 and 2.80 Å, a reflection of similar electronic structures of the H-bond complexes within this range (Chen, McAllister, Lee, and Houk, 1998). A similar linear correlation was obtained when the differences between the proton affinities of donor-acceptor pairs ( $\Delta PA$ ) and the H-bond energies were plotted, with no significant deviation in the H-bond energy at  $\Delta PA = 0$ , at which a low-barrier proton transfer potential was anticipated (Chen, McAllister, Lee, and Houk, 1998).

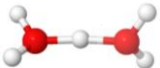
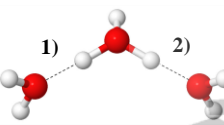
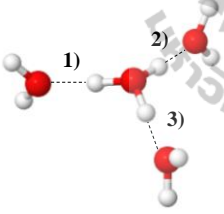
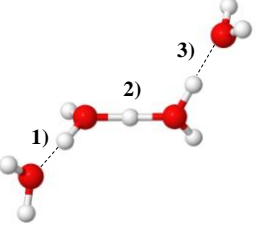
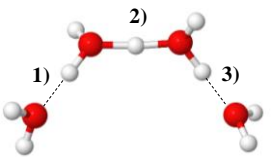
Since strong H-bonds are susceptible to proton transfers, normal and strong H-bonds could be distinguished using IR frequencies of the transferring protons. In the present work,  $\nu^{\text{OH}}$  and  $\Delta d_{\text{DA}}$  were plotted and illustrated in Figure 3.3c, in which an interesting correlation was observed;  $\nu^{\text{OH}}$  could be expressed in terms of  $\Delta d_{\text{DA}}$  using an exponential function resembling the normal distribution function. The fitted functions for the protonated water clusters in the gas phase and continuum aqueous solution are given in equations (3.5) and (3.6), respectively.

*Gas phase:* 
$$\nu^{\text{OH}} = 3521 - \frac{6354}{\sqrt{2\pi}} e^{-4.5 \Delta_{\text{DA}}^2} \quad (3.5)$$

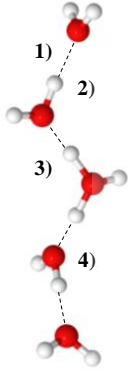
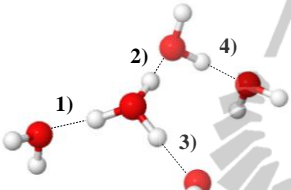
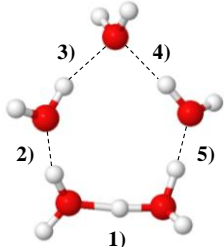
*Continuum aqueous solution:* 
$$\nu^{\text{OH}} = 3566 - \frac{6964}{\sqrt{2\pi}} e^{-3.9 \Delta_{\text{DA}}^2} \quad (3.6)$$

The agreements between  $\nu^{\text{OH}}$  obtained from B3LYP/TZVP calculations and the fitted values are also included in Figure 3.3c. Two inflection points are seen in Figure 3.3c, in the gas phase at  $\Delta d_{\text{DA}} = 0.33$  and in continuum aqueous solution at  $\Delta d_{\text{DA}} = 0.36$  Å. These correspond to  $\nu^{\text{OH}} = 1984$  and  $1881 \text{ cm}^{-1}$ , respectively. It should be mentioned that, for the Zundel complex in the gas phase, the term “critical distance” was used to describe  $R_{\text{O-O}}$  at which symmetric double-well potential with high barrier at the center is transformed into single-well potential without barrier (Benoit and Marx, 2005; Komatsuzaki and Ohmine, 1994). In Figure 3.3a,  $\Delta d_{\text{DA}} = 0.33$  and  $0.36$  Å correspond to  $R_{\text{O-O}} = 2.47$  and  $2.48$  Å, respectively, slightly longer than the critical distance of  $R_{\text{O-O}} = 2.43$  Å (Benoit and Marx, 2005). Therefore, the inflection points in Figure 3.3c could be associated with the “threshold” asymmetric stretching coordinates ( $\Delta d_{\text{DA}}^*$ ) and frequencies ( $\nu^{\text{OH}*}$ ) for proton transfer, and could be used to distinguish between normal and strong H-bonds in the protonated water clusters.

**Table 3.2** Asymmetric stretching coordinates ( $\Delta d_{DA}$ ) and asymmetric O-H stretching frequencies ( $\nu^{OH}$ ) of the protonated water clusters, obtained from B3LYP/TZVP calculations, both in the gas phase and continuum aqueous solution (values in parenthesis). They are in Å and  $\text{cm}^{-1}$ , respectively.

	Structures	$\Delta d_{DA}$	$\nu^{OH}$	$\Delta \nu^{OH}$
a)		0.00 (0.00)	961 (677)	-284
b)		1) 0.41 (0.40) 2) 0.41 (0.40)	2304 (2120) 2304 (2120)	-184 -184
c)		1) 0.52 (0.51) 2) 0.54 (0.51) 3) 0.52 (0.50)	2763 (2531) 2759 (2552) 2764 (2531)	-232 -207 -232
d)		1) 0.56 (0.64) 2) 0.00 (0.21) 3) 0.56 (0.48)	2895 (2985) 998(1240) 2921 (2525)	89 242 -395
e)		1) 0.57 (0.64) 2) 0.00 (0.21) 3) 0.58 (0.49)	2943 (2995) 1002 (1263) 2910 (2537)	52 261 -377

**Table 3.2** (Continued).

Structures	$\Delta d_{DA}$	$\nu^{OH}$	$\Delta\nu^{OH}$
<b>f)</b> 	1) 0.67 (0.68)	3176 (3088)	-88
	2) 0.32 (0.33)	1915 (1778)	-137
	3) 0.32 (0.34)	1915 (1778)	-137
	4) 0.68 (0.68)	3170 (3085)	-85
<b>g)</b> 	1) 0.58 (0.53)	2927 (2748)	-179
	2) 0.37 (0.40)	2230 (2186)	-44
	3) 0.58 (0.53)	2979 (2623)	-356
	4) 0.70 (0.71)	3230 (3153)	-77
<b>h)</b> 	1) 0.18 (0.28)	1298 (1458)	160
	2) 0.47 (0.41)	2587 (2229)	-358
	3) 0.90 (0.78)	3425 (3252)	-173
	4) 0.99 (0.86)	3516 (3376)	-140
	5) 0.63 (0.65)	3072 (2971)	-100

$\Delta\nu^{OH}$  is the frequency shifts due to continuum aqueous solvent. The red shifts are designated by negative values of  $\Delta\nu^{OH}$ .

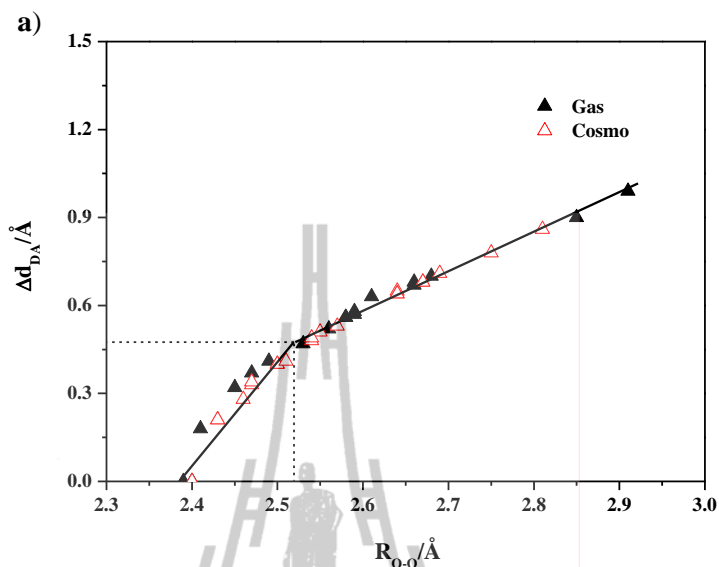


**Figure 3.3** a) Plot of the asymmetric stretching coordinates ( $\Delta d_{DA}$ ) and the O-H..O H-bond distances ( $R_{O-O}$ ), obtained from B3LYP/TZVP calculations. b) Plot of the asymmetric O-H stretching frequencies ( $\nu^{OH}$ ) and the O-H..O H-bond distances ( $R_{O-O}$ ), obtained from B3LYP/TZVP calculations. c) Plot of the asymmetric O-H stretching frequencies ( $\nu^{OH}$ ) and the asymmetric stretching coordinates ( $\Delta d_{DA}$ ), obtained from B3LYP/TZVP calculations.

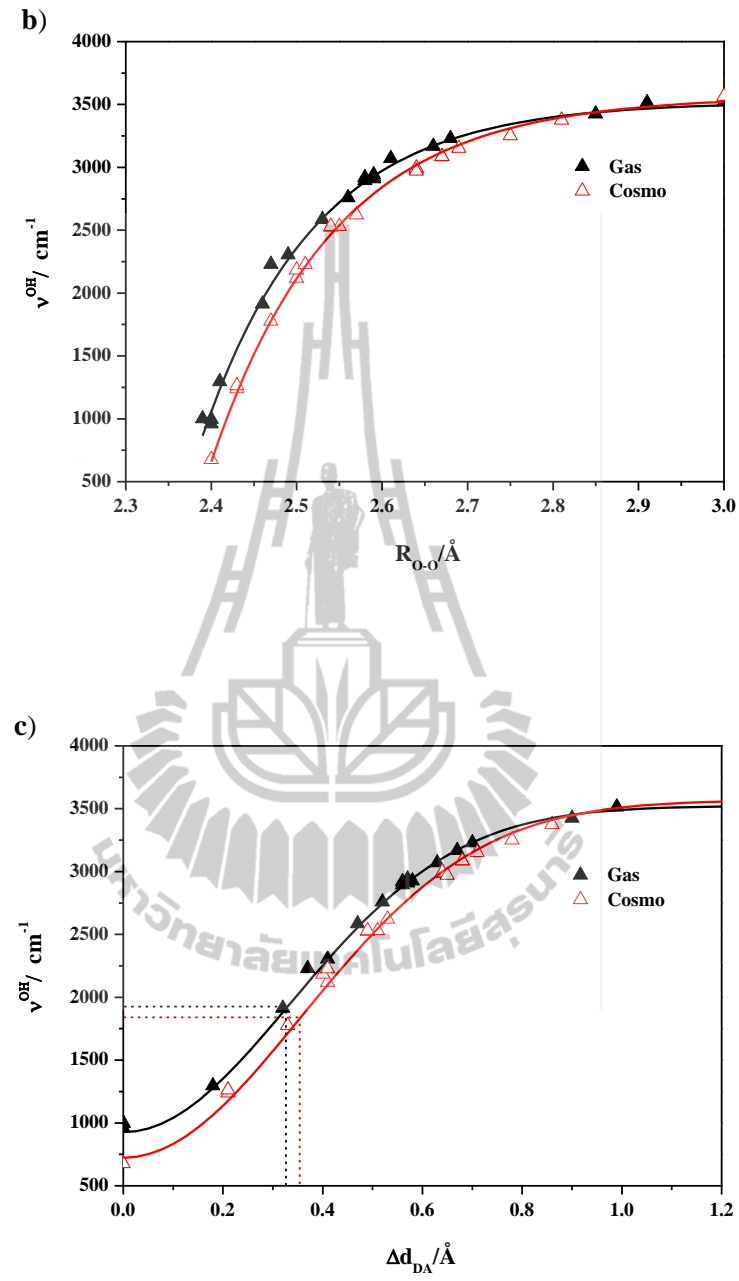


Figure 3.3 (Continued).

### 3.1.2 Dynamic results

All the shared-proton complexes obtained in the previous subsection were investigated in BOMD simulations at 350 K; except structure **h**, for which the cyclic H-bonds were transformed into linear (similar to structure **f**) in the course of BOMD simulations. As pointed out in the previous subsection, the stabilities of the protonated water clusters were substantially decreased in continuum aqueous solution. This and the fact that the model systems did not take into account the H-bond networks of water in the vicinities of the protonated water clusters, especially in the presence of strong thermal energy fluctuations in BOMD simulations, made it difficult to discuss the energetic results. Therefore, only the H-bond structures and IR spectra were used to explain the vibrational behaviors and dynamics of the proton transfer processes.

#### Average H-bond structures and IR spectra

The average H-bond distances ( $\langle R_{O-O} \rangle$  and  $\langle R_{O-H} \rangle$ ) and asymmetric stretching coordinates ( $\langle \Delta d_{DA} \rangle$ ) of the shared-proton complexes obtained from BOMD simulations are listed in Table 3.3. The characteristic asymmetric O-H stretching frequencies ( $\nu^{OH,MD}$ ) of the protons in the shared-proton complexes are included in Table 3.4. Examples of symmetric and asymmetric O-H stretching bands, as well as the O-O vibration band, are shown in Figure 3.4.

Linear relationships between  $\langle \Delta d_{DA} \rangle$  and  $\langle R_{O-O} \rangle$  were also obtained from BOMD simulations. They are illustrated in Figure 3.5a. The fitted functions for the internal and external H-bonds are represented by equations (3.7) and (3.8), respectively.

$$\text{Internal H-bonds:} \quad \langle \Delta d_{\text{DA}} \rangle = 2.74 \times \langle R_{\text{o-o}} \rangle - 6.47 \quad (3.7)$$

$$\text{External H-bonds:} \quad \langle \Delta d_{\text{DA}} \rangle = 1.59 \times \langle R_{\text{o-o}} \rangle - 3.57 \quad (3.8)$$

BOMD simulations at 350 K predicted the separation between the internal and external H-bonds at  $\langle R_{\text{o-o}} \rangle = 2.5 \text{ \AA}$ , the same as that from B3LYP/TZVP calculations.

In order to discuss the dynamics of the structural diffusion mechanism, IR spectra of the transferring protons were analyzed in details, using the Zundel complex as an example. They are broad in general, especially in continuum aqueous solution. The BOMD results in Figures 3.4a to 3.4d show two characteristic asymmetric O-H stretching bands, labeled with **A** and **B**; for the Zundel complex in the gas phase (in Figure 3.4a) at  $\nu_{\text{A}}^{\text{OH, MD}} = 1128$  and  $\nu_{\text{B}}^{\text{OH, MD}} = 1852 \text{ cm}^{-1}$ , and in continuum aqueous solution (in Figure 3.4b) at  $\nu_{\text{A}}^{\text{OH, MD}} = 943$  and  $\nu_{\text{B}}^{\text{OH, MD}} = 1751 \text{ cm}^{-1}$ . The low-frequency bands at **A**, slightly higher frequencies than those from B3LYP/TZVP calculations, are associated with the asymmetric O-H stretching mode, for which proton shuttles back and forth at the center of the H-bond.  $\nu_{\text{A}}^{\text{OH, MD}}$  agree well with the IRMPD experiment (Fridgen, McMahon, MacAleese, Lemaire, and Maitre, 2004) and BOMD simulations at 80 and 270 K (Termath and Sauer, 1997). The higher-frequency bands at **B**, not obtainable from single-well static proton transfer potentials with harmonic approximation, represent the vibrational motion with the center of vibration slightly shifted towards an oxygen atom (Sagarik, Chaiwongwattana, Vchirawongkwin, and Prueksaaron, 2010). Both characteristic IR



bands could be regarded as spectral signatures of proton transfer reactions (Sagarik, Chaiwongwattana, Vchirawongkwin, and Prueksaaron, 2010; Sagarik, Phonyiem, Lao-ngam, and Chaiwongwattana, 2008); the former reflects the extent of the shared-proton complex formation and the latter the product formation. They are comparable with the “oscillatory shuttling motion” and the “Grotthuss shuttling motion” (or “structural diffusion motion”), respectively (Wu, Chen, Wang, Paesani, and Voth, 2007).

A review on the state-of-the-art methods for the calculations of vibrational energies of polyatomic molecules using quantum mechanical, variationally-based approaches was presented (Bowman, Carrington, and Meyer, 2008), in which accurate IR spectra of ionic species in the gas phase were discussed in comparison with experiment (Hammer, Diken, Roscioli, Johnson, Myshakin, Jordan, McCoy, Huang, Bowman, and Carter, 2005). One of the emphases was on the analyses of the middle spectral region ( $800 - 2000 \text{ cm}^{-1}$ ) which can be directly related to the proton transfer in the Zundel complex; experiment (Hammer, Diken, Roscioli, Johnson, Myshakin, Jordan, McCoy, Huang, Bowman, and Carter, 2005) showed a doublet centered at  $1000 \text{ cm}^{-1}$  as the most characteristic feature, with the low-energy component at  $928 \text{ cm}^{-1}$  and the high-energy component at  $1047 \text{ cm}^{-1}$ . Based on the multiconfiguration time-dependent Hartree (MCTDH) method, the most intense band was concluded to be the proton transfer fundamental band (asymmetric O-H stretching mode) and the doublet was attributed to the coupling among the low-frequency water-wagging modes, water-water stretching motion and the proton transfer motion. Additionally, the MCTDH method predicted a water bending state which couples strongly with the proton transfer motion at  $1741 \text{ cm}^{-1}$ , compared with

the experiment at  $1763\text{ cm}^{-1}$  (Hammer, Diken, Roscioli, Johnson, Myshakin, Jordan, McCoy, Huang, Bowman, and Carter, 2005). The present BOMD simulations predicted the proton transfer fundamental frequency in the gas phase close to the MCTDH method and the experiment (Hammer, Diken, Roscioli, Johnson, Myshakin, Jordan, McCoy, Huang, Bowman, and Carter, 2005) ( $1128\text{ cm}^{-1}$  at 350 K, compared with  $1047\text{ cm}^{-1}$  at 275 K). Since one of the main objectives of the present work is to search for an appropriate theoretical method to monitor proton transfer processes in BOMD simulations on larger H-bond systems and it is sufficient to employ the fundamental asymmetric O-H stretching frequencies, the low-frequency band of the doublet was not investigated in details.

### Threshold frequencies and relative probability of proton transfer

Figure 3.5b shows the relationships between  $\nu_A^{\text{OH, MD}}$  (the oscillatory shuttling frequencies) and  $\langle R_{\text{o-o}} \rangle$ . Similar to B3LYP/TZVP calculations, the exponential functions in equations (3.9) and (3.10) can well represent  $\nu_A^{\text{OH, MD}}$  in the gas phase and continuum aqueous solution, respectively.

*Gas phase:*

$$\nu_A^{\text{OH, MD}} = -2.47 \times 10^{13} e^{-\langle R_{\text{o-o}} \rangle / 0.1051} + 3521 \quad (3.9)$$

*Continuum aqueous solution:*

$$\nu_A^{\text{OH, MD}} = -9.14 \times 10^{12} e^{-\langle R_{\text{o-o}} \rangle / 0.1105} + 3566 \quad (3.10)$$

As in the case of B3LYP/TZVP calculations, the relationships between  $\nu_A^{\text{OH, MD}}$  and  $\langle \Delta d_{\text{DA}} \rangle$  in Figure 3.6c were used to approximate the threshold frequencies for

proton transfers in BOMD simulations. They are represented by equations (3.11) and (3.12), in the gas phase and continuum aqueous solution, respectively.

$$\text{Gas phase: } \nu_A^{\text{OH, MD}} = 3521 - \frac{6630}{\sqrt{2\pi}} e^{-4.7 \langle \Delta d_{\text{DA}} \rangle^2} \quad (3.11)$$

$$\text{Continuum aqueous solution: } \nu_A^{\text{OH, MD}} = 3566 - \frac{7563}{\sqrt{2\pi}} e^{-4.9 \langle \Delta d_{\text{DA}} \rangle^2} \quad (3.12)$$

The calculations of the second derivatives of the functions in equation (3.11) and (3.12) yielded two inflection points at  $\langle \Delta d_{\text{DA}} \rangle = 0.32 \text{ \AA}$ , corresponding to the threshold frequencies at  $\nu_A^{\text{OH, MD}} = 1917$  and  $1736 \text{ cm}^{-1}$ , in the gas phase and continuum aqueous solution, respectively. The values are slightly lower than those obtained from B3LYP/TZVP calculations, due to the inclusion of the thermal energy fluctuations and dynamics in BOMD simulations.

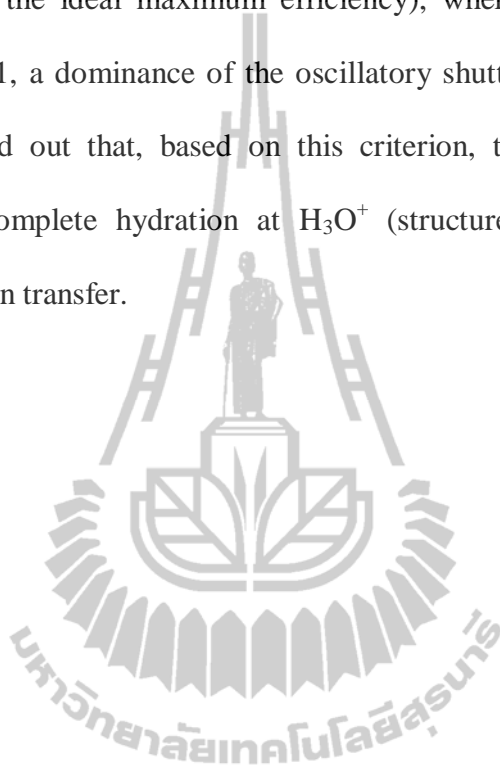
As the proton transfer in H-bond couples with the O-O vibration (Sagarik, Phonyiem, Lao-ngam, and Chaiwongwattana, 2008), the relative probability or the extent of the shared-proton complex formation in BOMD simulations could be approximated from the ratio between the intensity of  $\nu_A^{\text{OH, MD}}$  and the intensity of the O-O vibration ( $\mathbf{I}_{\text{O-O}}$ ) (Sagarik, Chaiwongwattana, Vchirawongkwin, and Prueksaaron, 2010). In Table 3.4,  $\mathbf{I}_A/\mathbf{I}_{\text{O-O}}$  for the Zundel complex in the gas phase and continuum aqueous solution are 0.6 and 0.7, respectively, indicating that, in BOMD simulations in the gas phase, about 60 % of the  $\text{H}_3\text{O}^+ - \text{H}_2\text{O}$  1 : 1 complex are in the form of the Zundel complex, whereas in continuum aqueous solution about

70 %. The values of  $I_A/I_{O-O}$  in Table 3.4 also suggest that the extent of the oscillatory shuttling motion is decreased when the number of water molecule increased; indicating a higher probability of proton transfer in extended H-bond network.

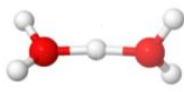
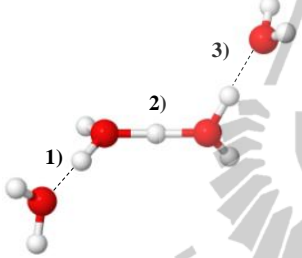
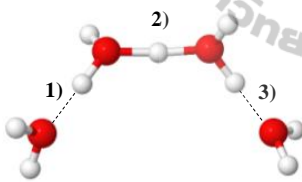
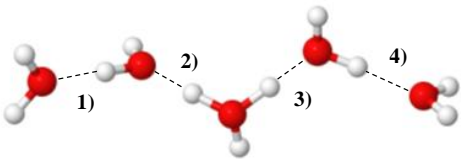
The observation that the proton transfer process in the  $H_3O^+ - H_2O$  1 : 1 complex involves two consecutive steps namely, a quasi-dynamic equilibrium between the precursor (the  $H_3O^+ - H_2O$  1 : 1 complex) and the shared-proton complex (the Zundel complex), followed by the actual proton transfer (Sagarik, Phonyiem, Lao-ngam, and Chaiwongwattana, 2008), made it possible to establish a criterion to measure the extent or the efficiency of proton transfer from IR spectra; the quasi-dynamic equilibrium prevents proton transfer reaction from being concerted and is considered to be the rate-determining step (Sagarik, Chaiwongwattana, Vchirawongkwin, and Prueksaaron, 2010; Sagarik, Phonyiem, Lao-ngam, and Chaiwongwattana, 2008). Hence, an effective proton transfer process should take the reaction path with the shortest lifetime of the quasi-dynamic equilibrium. Therefore, in order to achieve an “ideal” maximum efficiency, according to the transition-state theory, the populations of the shared-proton complex and the product must be the same. In other words, every shared-proton complex formation should lead to the actual proton transfer. This is possible only when the O-O distance undergoes large-amplitude vibration, for which the O-H and O-O vibrations are coherent (Sagarik, Phonyiem, Lao-ngam, and Chaiwongwattana, 2008). It should be emphasized that, since the present model systems involved only the  $O..H^+..O$  H-bonds, the product becomes precursor for the successive proton transfer event.

As the populations of the shared-proton complex and the precursor in BOMD simulations could be approximated from the intensities of the oscillatory

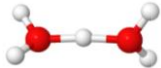
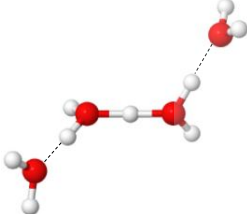
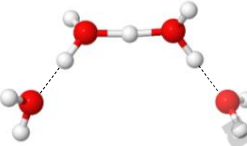
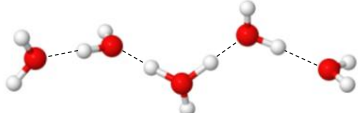
shuttling (**A**) and structural diffusion (**B**) bands, the efficiency of proton transfer could be approximated from the ratio between  $I_B/I_A$  ( $I_B/I_A = 1$  for the ideal maximum efficiency). Table 3.4 reveals that, for the Zundel complex in the gas phase,  $I_B/I_A$  is about 0.5 (half of the ideal maximum efficiency), whereas in continuum aqueous solution  $I_B/I_A < 0.1$ , a dominance of the oscillatory shuttling motion (shared-proton complex). It turned out that, based on this criterion, the most extended H-bond structure with incomplete hydration at  $H_3O^+$  (structure **f**) possesses the highest efficiency for proton transfer.



**Table 3.3** Average H-bond distances ( $\langle R_{O-O} \rangle$  and  $\langle R_{O-H} \rangle$ ) and asymmetric stretching coordinates  $\langle \Delta d_{DA} \rangle$  of the shared-proton complexes, derived from BOMD simulations at 350 K, both in the gas phase and continuum aqueous solution (values in parenthesis). Distances are in Å.

Structure	$\langle R_{O-O} \rangle$	$\langle R_{O-H} \rangle$	$\langle \Delta d_{DA} \rangle$
<b>a)</b> 	2.42 (2.43)	1.21 (1.20)	0.18 (0.20)
<b>d)</b> 	1) 2.64 (2.64) 2) 2.42 (2.48) 3) 2.62 (2.54)	1.01 (1.00) 1.21 (1.15) 1.01 (1.03)	0.65 (0.69) 0.21 (0.35) 0.63 (0.52)
<b>e)</b> 	1) 2.63 (2.64) 2) 2.42 (2.44) 3) 2.62 (2.54)	1.00 (1.00) 1.21 (1.18) 1.02 (1.02)	0.65 (0.69) 0.19 (0.22) 0.53 (0.54)
<b>f)</b> 	1) 2.71 (2.73) 2) 2.47 (2.55) 3) 2.49 (2.55) 4) 2.71 (2.70)	1.00 (1.00) 1.11 (1.10) 1.07 (1.17) 0.99 (1.01)	0.75 (0.75) 0.32 (0.44) 0.36 (0.47) 0.74 (0.71)

**Table 3.4** IR frequencies ( $\text{cm}^{-1}$ ) of the shared-proton complexes, obtained from BOMD simulations at 350 K, both in the gas phase and continuum aqueous solution (values in parenthesis).

Structure	$\nu_{\text{A}}^{\text{OH, MD}}$	$\nu_{\text{B}}^{\text{OH, MD}}$	$I_{\text{A}}/I_{\text{O-O}}$	$I_{\text{B}}/I_{\text{A}}$
a) 	1128 (943)	1852 (1751)	0.57 (0.69)	0.51 (0.09)
d) 	1178 (1448)	1768 (2003)	0.48 (0.14)	0.19 (0.55)
e) 	1263 (1263)	1784 (1650)	—* (0.29)	0.45 (0.23)
f) 	1515 (1734)	2053 (2592)	0.28 (0.17)	0.63 (0.79)

$I_{\text{A}}$  = intensity of the oscillatory shuttling band;  $I_{\text{B}}$  = intensity of the structural diffusion band;  $I_{\text{O-O}}$  = intensity of the O-O stretching band;  $\nu_{\text{A}}^{\text{OH, MD}}$  and  $\nu_{\text{B}}^{\text{OH, MD}}$  = characteristic asymmetric O-H stretching frequencies of the transferring proton.

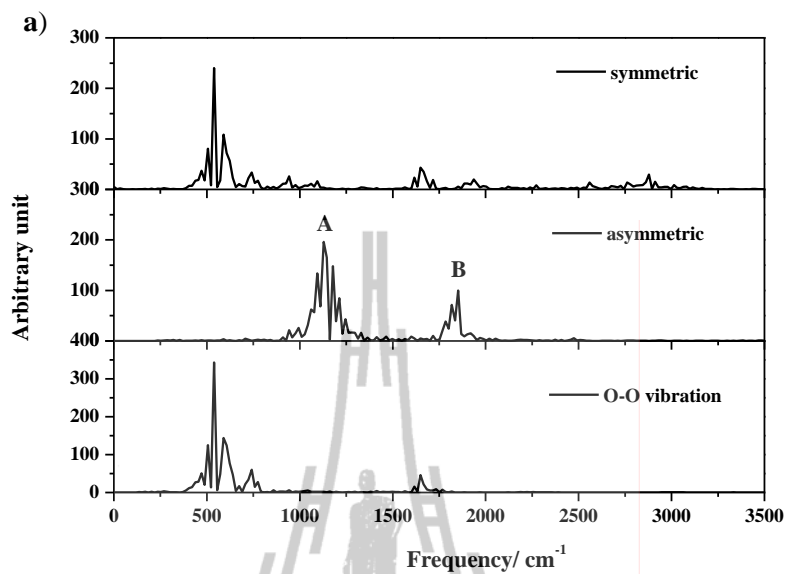


**Figure 3.4** Symmetric and asymmetric O-H stretching bands of the transferring protons in the shared-proton complexes, together with the O-O vibration band, obtained from BOMD simulations at 350 K. a) The Zundel complex (structure **a**) in the gas phase; b) The Zundel complex (structure **a**) in continuum aqueous solution, c) The  $\text{H}_3\text{O}^+ - \text{H}_2\text{O}$  1 : 4 complex (structure **f**) in the gas phase; d) The  $\text{H}_3\text{O}^+ - \text{H}_2\text{O}$  1 : 4 complex (structure **f**) in continuum aqueous solution.



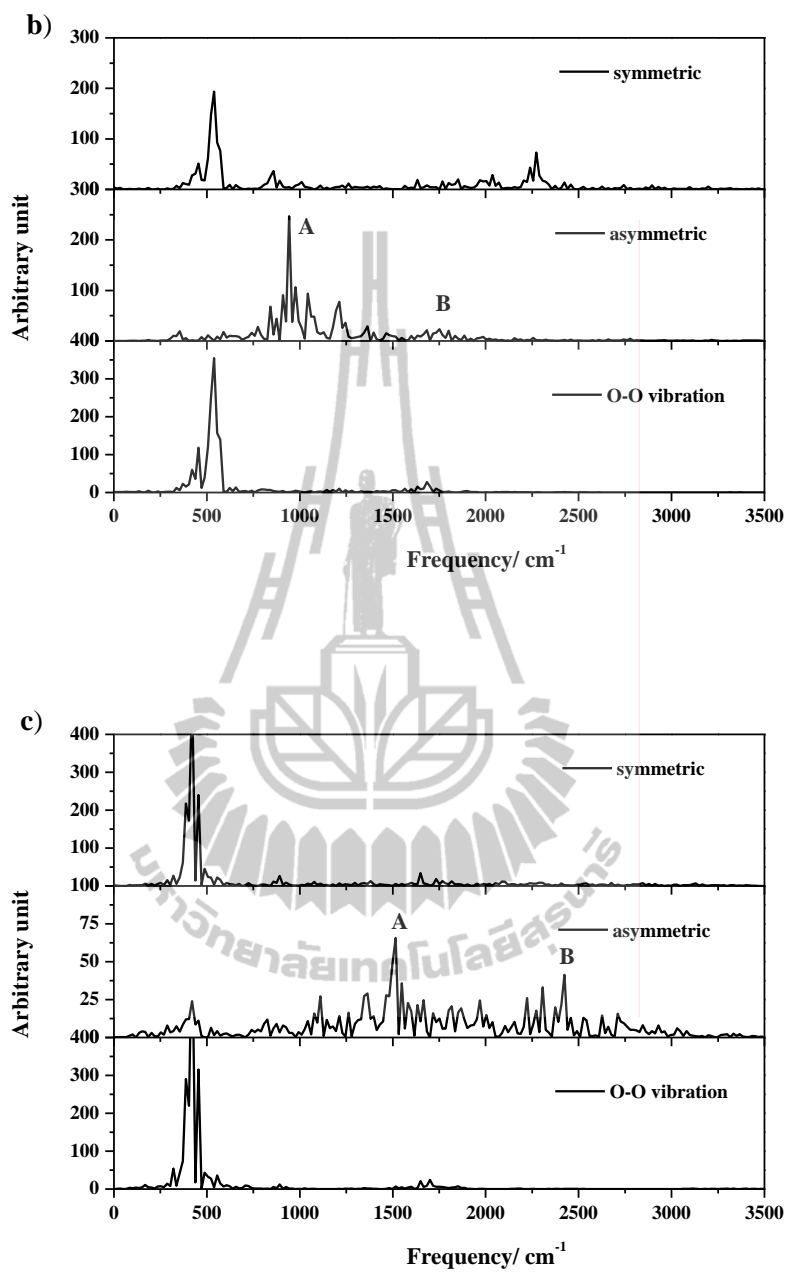


Figure 3.4 (Continued).

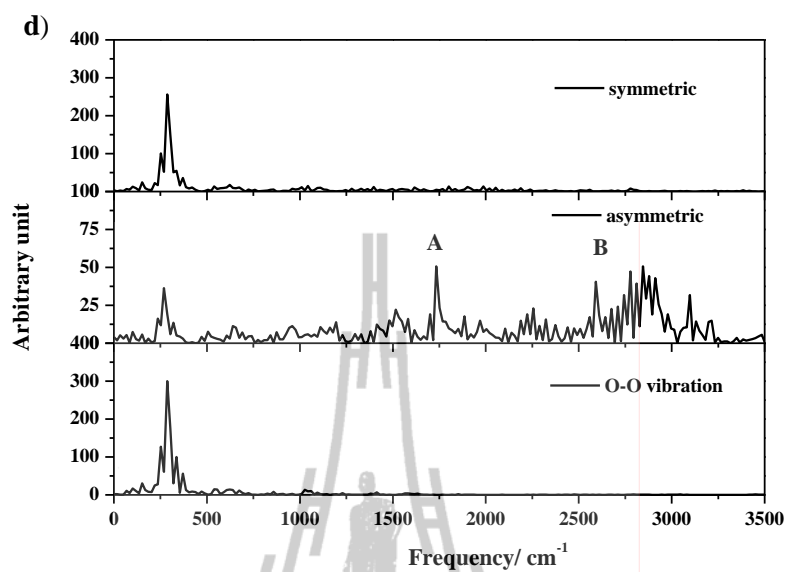
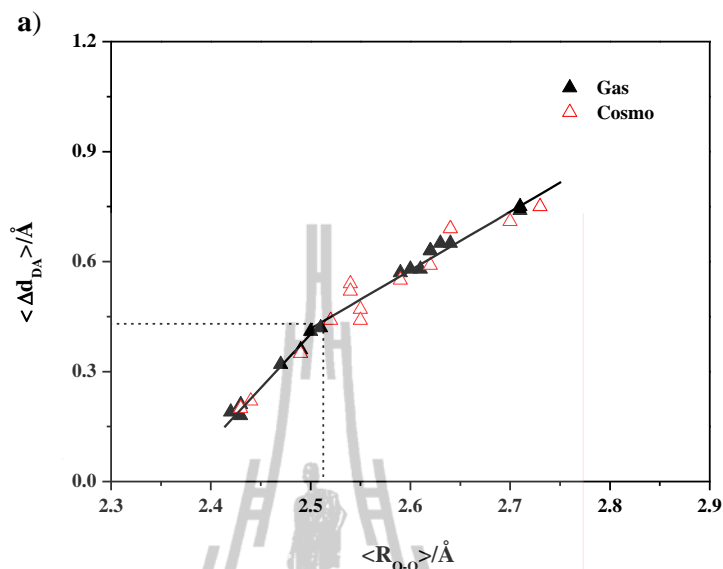


Figure 3.4 (Continued).





**Figure 3.5** a) Plot of the average asymmetric stretching coordinates ( $\langle \Delta d_{DA} \rangle$ ) and the average O-H...O H-bond distances ( $\langle R_{o-o} \rangle$ ), obtained from BOMD simulations at 350 K. b). Plot of the asymmetric O-H stretching frequencies ( $\nu^{\text{OH, MD}}$ ) and the average O-H...O H-bond distances ( $\langle R_{o-o} \rangle$ ), obtained from BOMD simulations at 350 K. c) Plot of the asymmetric O-H stretching frequencies ( $\nu^{\text{OH, MD}}$ ) and the asymmetric stretching coordinates ( $\langle \Delta d_{DA} \rangle$ ), obtained from BOMD simulations at 350 K.

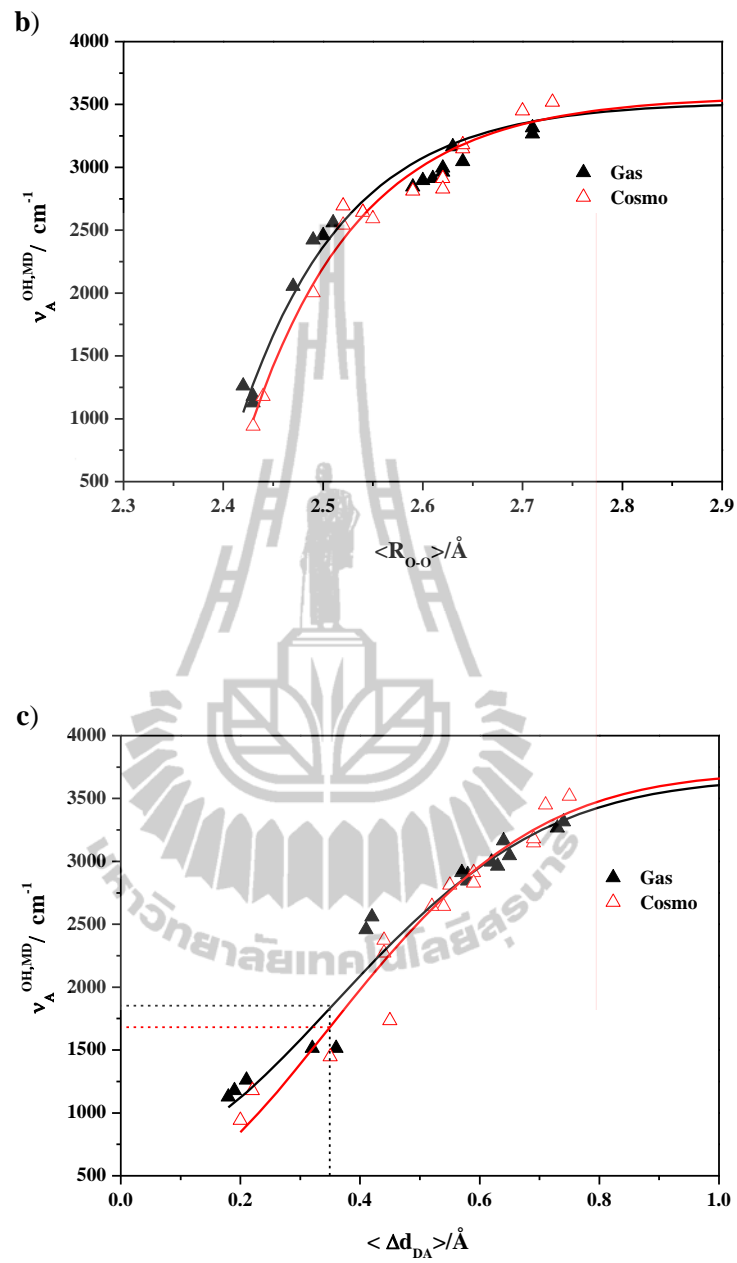


Figure 3.5 (Continued).

### Vibration energy for proton transfer reaction

As reported in the previous section, for the transferring proton ( $\nu^{\text{OH}} < \nu^{\text{OH}^*}$ ), the static proton transfer potential (B3LYP/TZVP calculations) predicted only one asymmetric O-H stretching band, whereas BOMD simulations showed in addition a higher frequency band. The two IR bands are labeled with **A** and **B** in Figures 3.7a and 3.7b. Since the lower frequency band (at  $\nu_{\text{A}}^{\text{OH, MD}}$ ) could be associated with the oscillatory shuttling motion and the higher frequency band (at  $\nu_{\text{B}}^{\text{OH, MD}}$ ) with the structural diffusion motion, the vibrational energy for the interconversion between the two dynamic states ( $\Delta\nu_{\text{BA}}^{\text{OH, MD}}$ ) can be approximated from the difference between  $\nu_{\text{B}}^{\text{OH, MD}}$  and  $\nu_{\text{A}}^{\text{OH, MD}}$ , shown in Table 3.5. It should be noted that the discussion on  $\Delta\nu_{\text{BA}}^{\text{OH, MD}}$  and  $\mathbf{I}_{\text{B}}/\mathbf{I}_{\text{A}}$  is meaningful only when the H-bond considered is susceptible to proton transfer,  $\nu_{\text{A}}^{\text{OH, MD}} < \nu_{\text{A}}^{\text{OH}^*, \text{MD}}$ .

The trend of  $\mathbf{I}_{\text{B}}/\mathbf{I}_{\text{A}}$  in the gas phase and continuum aqueous solution can be explained using  $\Delta\nu_{\text{BA}}^{\text{OH, MD}}$  in Table 3.5; in the gas phase,  $\Delta\nu_{\text{BA}}^{\text{OH, MD}} = 724 \text{ cm}^{-1}$ , and in continuum aqueous solution,  $\Delta\nu_{\text{BA}}^{\text{OH, MD}} = 808 \text{ cm}^{-1}$ . The latter reflects a higher vibrational energy for the interconversion between the oscillatory shuttling and structural diffusion motions, resulting in a higher population of the oscillatory shuttling motion for the Zundel complex in continuum aqueous solution. It should be added that, due to a short BOMD simulation length,  $\mathbf{I}_{\text{B}}/\mathbf{I}_{\text{A}}$  may not be determined precisely. Therefore, attempt was made to alternatively estimate the relative population of the oscillatory shuttling and structural diffusion motions from,  $\Delta\nu_{\text{BA}}^{\text{OH, MD}}$ . For the protonated water clusters, an interesting relationship was observed when

$\Delta v_{BA}^{OH, MD}$  and  $\langle \Delta d_{DA} \rangle$  were plotted. Together with the plot of the standard deviations of the O-H distances ( $\sigma_{R_{O-H}}$ ) and  $\langle \Delta d_{DA} \rangle$ , energetic aspects of the two characteristic vibrations in the protonated water cluster could be studied. The plots of  $\sigma_{R_{O-H}}$  and  $\langle \Delta d_{DA} \rangle$  and  $\Delta v_{BA}^{OH, MD}$  and  $\langle \Delta d_{DA} \rangle$  are shown in Figures 3.6a and 3.6b, respectively. The former could be represented by an exponential decay function, whereas the later by a reflected normal distribution function. They are shown in equations (3.13) and (3.14), respectively.

$$\sigma_{R_{O-H}} = 0.3184e^{-\langle \Delta d_{DA} \rangle / 0.1527} + 0.0300 \quad (3.13)$$

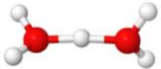
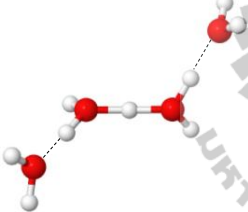
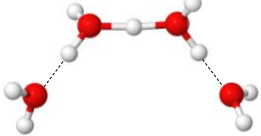
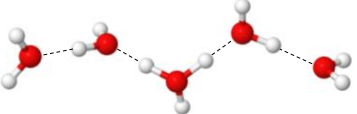
$$\Delta v_{BA}^{OH, MD} = 1339 - \frac{274}{0.1291 \sqrt{2\pi}} e^{-0.5 \left( \frac{\langle \Delta d_{DA} \rangle - 0.2808}{0.1291} \right)^2} \quad (3.14)$$

Due to the thermal energy fluctuations and dynamics,  $\sigma_{R_{O-H}}$  and  $\Delta v_{BA}^{OH, MD}$  in the gas phase and continuum aqueous solution are not well separated. Therefore, the discussion on the relative population of the oscillatory shuttling and structural diffusion motions will be made based on a combined data set. It appeared that, for the protonated water clusters,  $\sigma_{R_{O-H}}$  decreases exponentially with  $\langle \Delta d_{DA} \rangle$ , reflecting characteristics of the oscillatory shuttling and structural diffusion motions; the oscillatory shuttling motion dominates in the H-bond with small  $\langle \Delta d_{DA} \rangle$ . Whereas  $\Delta v_{BA}^{OH, MD}$  decreases exponentially with  $\langle \Delta d_{DA} \rangle$  and reaches a minimum at  $\langle \Delta d_{DA} \rangle = 0.28 \text{ \AA}$  ( $\langle R_{O-O} \rangle = 2.46 \text{ \AA}$ ), corresponding to the lowest vibrational energy

for the interconversion between the oscillatory shuttling and the structural diffusion motions,  $\Delta v_{BA}^{\text{OH, MD}} = 473 \text{ cm}^{-1}$  or 5.7 kJ/mol. Since the probability of finding a physical system in a certain energy state is proportional to the Boltzmann factor, the probability of finding the structural diffusion motion relative to the oscillatory shuttling motion ( $P_B/P_A$ ) is proportional to  $e^{-\Delta v_{BA}^{\text{OH, MD}}/RT}$ . For the protonated water clusters, the plot of  $P_B/P_A$  and  $\langle \Delta d_{DA} \rangle$ , shown in Figure 3.6c, suggested the maximum probability of finding the structural diffusion motion relative to the oscillatory shuttling motion,  $P_B/P_A = 0.17$  at  $\langle \Delta d_{DA} \rangle = 0.27 \text{ \AA}$ . At larger  $\langle \Delta d_{DA} \rangle$ , the H-bond becomes weaker and  $P_B/P_A$  decreases, especially when  $v_A^{\text{OH, MD}} > v_A^{\text{OH}^*, \text{MD}}$ . The relationship between  $P_B/P_A$  and  $\langle \Delta d_{DA} \rangle$  could be represented by normal distribution function. The fitted function for the probability of finding the structural diffusion motion relative to the oscillatory shuttling motion can be written as

$$P_B/P_A = 0.0110 + \frac{0.0225}{0.0564 \sqrt{2\pi}} e^{-0.5 \left( \frac{\langle \Delta d_{DA} \rangle - 0.2693}{0.0564} \right)^2} \quad (3.15)$$

**Table 3.5** The vibrational energy for the interconversion between the oscillatory shuttling and structural diffusion motions ( $\Delta v_{BA}^{OH, MD}$ ), the probability of finding the structural diffusion motion relative to the oscillatory shuttling motion ( $P_B/P_A$ ) and the proton diffusion coefficient ( $D$ ) obtained from BOMD simulations at 350 K, both in the gas phase and continuum aqueous solution (values in parenthesis). They are in  $\text{cm}^{-1}$  and  $\text{cm}^2\text{s}^{-1}$ .

Structure	$\Delta v_{BA}^{OH, MD}$	$P_B/P_A$	$D(10^{-5})$
a) 	724 (808)	0.051 (0.036)	10.26 (9.16)
d) 	589 (557)	0.089 (0.102)	10.89 (10.54)
e) 	522 (471)	0.117 (0.144)	11.09 (12.95)
f) 	539 (859)	0.109 (0.029)	8.89 (8.20)



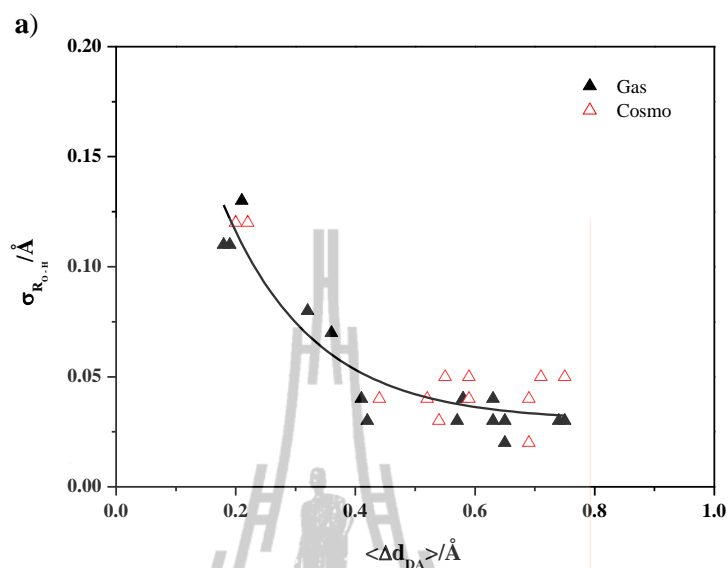


**Figure 3.6** a) Plot of standard deviations of the O-H distances ( $\sigma_{R_{O-H}}$ ) and the asymmetric stretching coordinates ( $\langle \Delta d_{DA} \rangle$ ), obtained from BOMD simulations at 350 K. b) Plot of the vibrational energy for the interconversion between the oscillatory shuttling and structural diffusion motions ( $\Delta v_{BA}^{OH, MD}$ ) and the asymmetric stretching coordinates ( $\langle \Delta d_{DA} \rangle$ ), obtained from BOMD simulations at 350 K. c) Plot of probability of finding the structural diffusion motion relative to the oscillatory shuttling motion ( $P_B/P_A$ ) and the asymmetric stretching coordinates ( $\langle \Delta d_{DA} \rangle$ ), obtained from BOMD simulations at 350 K.

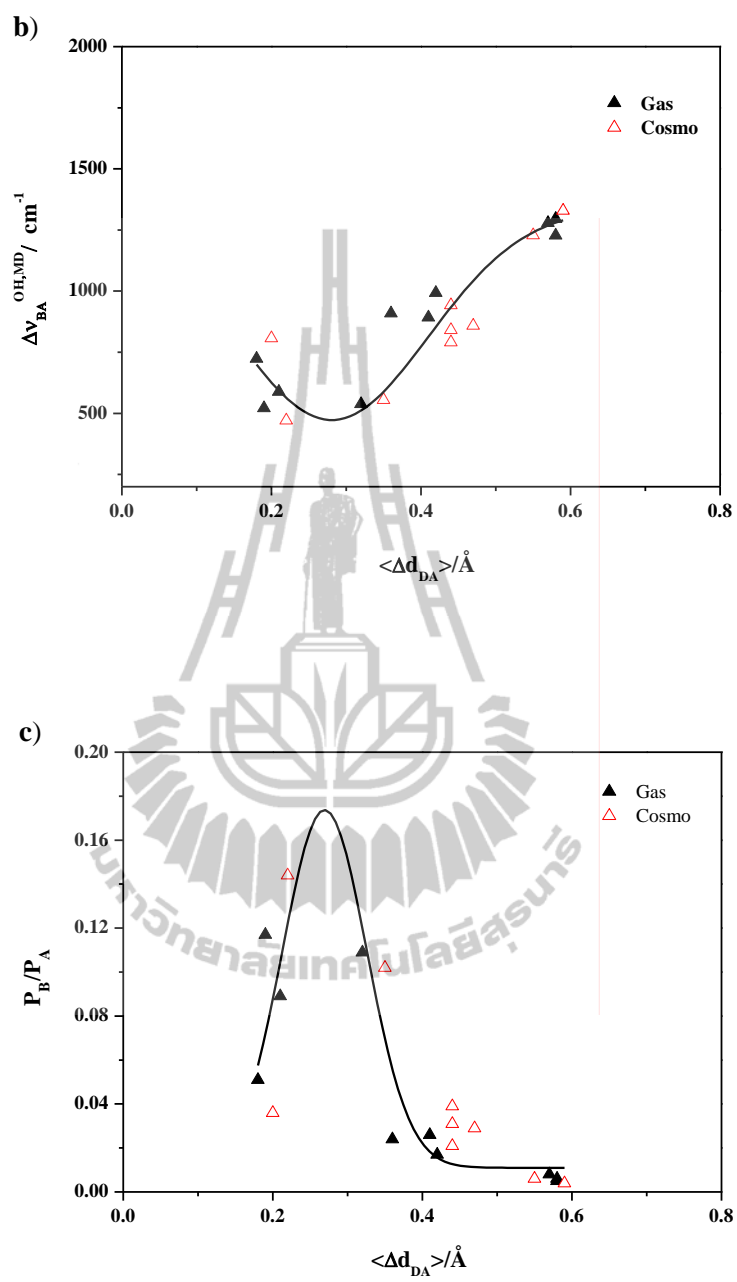


Figure 3.6 (Continued).

### Dynamics of proton transfer and diffusion coefficients

The diffusion coefficients ( $D$ ) of the transferring protons in the shared-proton complexes are listed in Table 3.5. The diffusion coefficients of the Zundel complex in the gas phase and continuum aqueous solution, obtained from BOMD simulations at 350 K, are  $10.3 \times 10^{-5}$  and  $9.2 \times 10^{-5} \text{ cm}^2 \text{ s}^{-1}$ , respectively. Based on the same approach, BOMD simulations predicted the diffusion coefficient at 298 K to be  $5.0 \times 10^{-5} \text{ cm}^2 \text{ s}^{-1}$  (Sagarik, Chaiwongwattana, Vchirawongkwin, and Prueksaaron, 2010), slightly lower than the NMR result (Agmon, 1995); in NMR experiment, the diffusion coefficient of a proton moving across a single water molecule was estimated from the NMR hopping time ( $\tau_p$ ) and the Einstein relation ( $D = l^2/6\tau_p$ ) to be  $7.0 \times 10^{-5} \text{ cm}^2 \text{ s}^{-1}$ ; where  $l$  is the hopping length or the H-bond distance ( $2.5 \text{ \AA}$ ) and  $\tau_p = 1.5 \text{ ps}$ . It should be added that, the reported diffusion coefficient (Agmon, 1995) was derived by subtracting the water self-diffusion coefficient ( $2.3 \times 10^{-5} \text{ cm}^2 \text{ s}^{-1}$ ) from the proton diffusion coefficient ( $9.3 \times 10^{-5} \text{ cm}^2 \text{ s}^{-1}$ ). The deviation of about 28% from the experimental value (Agmon, 1995) could be attributed to the neglect of the H-bond networks connecting the hydration shells of the Zundel complex (Sagarik, Chaiwongwattana, Vchirawongkwin, and Prueksaaron, 2010). For larger protonated water clusters, the shared-proton complex with an extended H-bond network, structure **f**, possess  $D = 8.9 \times 10^{-5}$  and  $8.2 \times 10^{-5} \text{ cm}^2 \text{ s}^{-1}$ , in the gas phase and continuum aqueous solution, respectively. The values are lower than those of the Zundel complex. These support the conclusion that the oscillatory shuttling motion is slightly more important in the  $\text{H}_3\text{O}^+ - \text{H}_2\text{O} \text{ 1 : 1}$  complex, compared to the extended H-bond structures.

### Kinetics of proton transfer in protonated water clusters

In order to assess the reliability of the dynamic results obtained from BOMD simulations, the lifetimes ( $\tau$ ) of the shared-proton structures were computed from VACF of the O-O vibrations (Bopp, 1986). VACF of the O-O vibrations in the Zundel complex and structure **f**, the structure with the highest efficiency of proton transfer in this series, are shown as examples in Figure 3.7. It appeared that an asymptotic exponential relaxation behavior of the envelope of VACF could be approximated, except for the Zundel complex in continuum aqueous solution (Figure 3.7b), for which the envelope of the O-O vibration at short time cannot be fitted with an exponential function. For the Zundel complex in the gas phase, BOMD simulations at 350 K predicted  $\tau$  to be 270 fs, corresponding to the classical first-order rate constant ( $k$ ) for the interconversion between the shared-proton ( $\text{H}_5\text{O}_2^+$ ) and  $\text{H}_3\text{O}^+ - \text{H}_2\text{O}$  contact structures of  $5.1 \text{ ps}^{-1}$ . The shared-proton structure in structure **f** possesses shorter lifetimes,  $\tau = 241$  and  $233$  fs, in the gas phase and continuum aqueous solution, respectively. The values correspond to  $k = 5.8$  and  $6.0 \text{ ps}^{-1}$ , respectively. The lifetimes of the shared-proton structures are in reasonable agreement with the result obtained from the multistate empirical valence bond (MS-EVB) calculations at 280 K,  $\tau = 370$  fs (Lapid, Agmon, Petersen, and Voth, 2005), whereas the rate constants are in accordance with the O-O vibration rate, obtained from quantum MD simulations at 300 K,  $k = 5.0 \text{ ps}^{-1}$  (Tuckerman, Laasonen, Sprik, and Parrinello, 1995).

Finally, in order to ensure that the dynamics and IR results discussed above are reliable, attempt was made to perform NVT BOMD simulations with longer

simulation time. This was successful only for the Zundel complex in the gas phase, and not longer than 5 ps; all the other shared-proton complexes became fragmented after 2.5 ps. It appeared that, for the IR spectra, the oscillatory shuttling and structural diffusion frequencies remain the same (see Figure 3.8), with slight decreases of the intensities,  $I_B/I_A = 0.49$  compared with 0.51. The diffusion coefficient in the gas phase is slightly decreased, from  $10.3 \times 10^{-5}$  to  $9.5 \times 10^{-5}$   $\text{cm}^2 \text{s}^{-1}$ . This leads to a conclusion that, although for small H-bond complexes, the IR spectra obtained from short BOMD simulations show some fine structures, meaningful and reasonable interpretations could be made, especially for all the H-bond complexes investigated here; a similar conclusion was presented by Termath and Sauer (1997) based on a series of BOMD simulations on  $\text{H}_5\text{O}_2^+$  and  $\text{H}_7\text{O}_3^+$ , from which insights into fast dynamic processes in H-bonds (*e.g.* H-bond structures and IR spectra) were obtained from relatively short BOMD trajectories (about 2 ps).

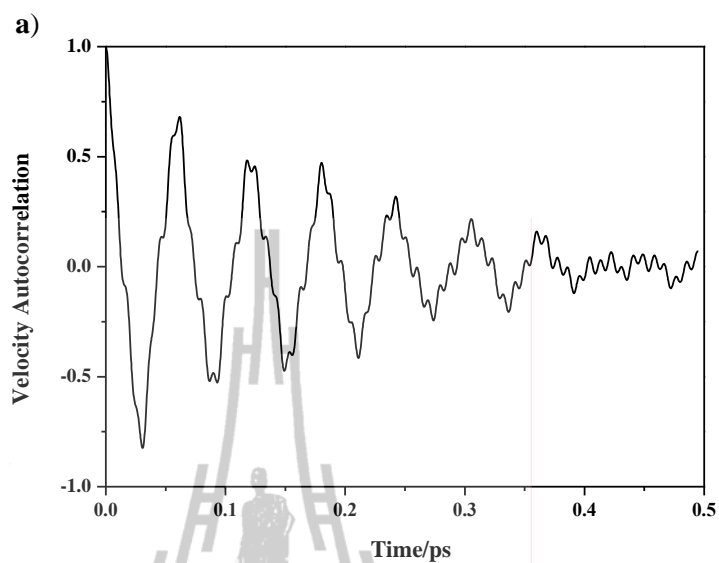


**Figure 3.7** Examples of velocity autocorrelation functions (VACF) of the O-O vibrations in the shared-proton structures, obtained from BOMD simulations at 350 K. a) the Zundel complex in the gas phase; b) the Zundel complex in continuum aqueous solution. c) the  $\text{H}_3\text{O}^+ - \text{H}_2\text{O}$  1 : 4 complex (structure **f**) in the gas phase. d) the  $\text{H}_3\text{O}^+ - \text{H}_2\text{O}$  1 : 4 complex (structure **f**) in continuum aqueous solution.

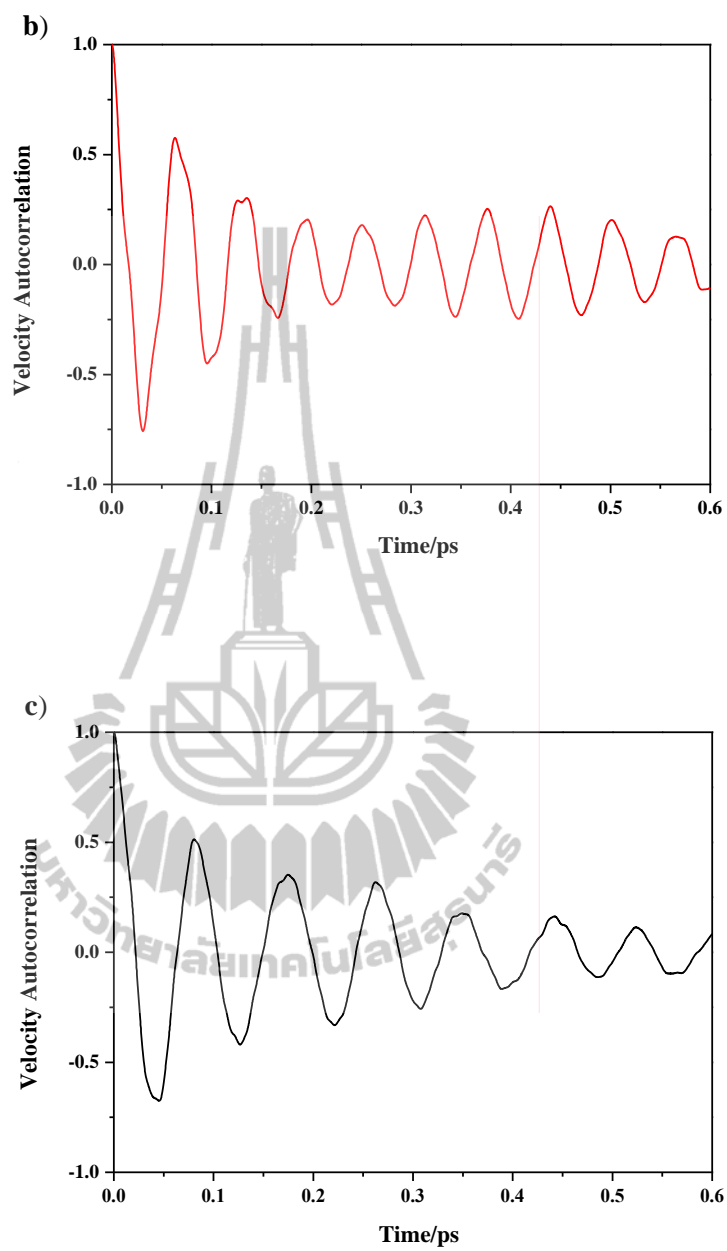


**Figure 3.7** (Continued).

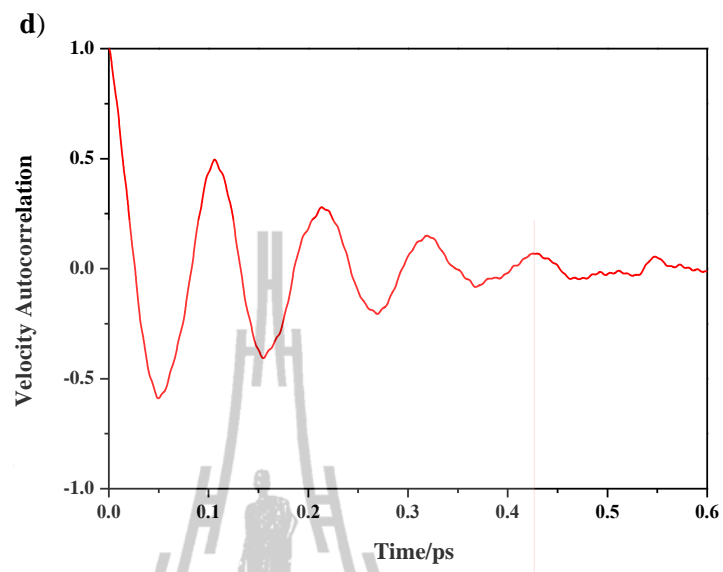
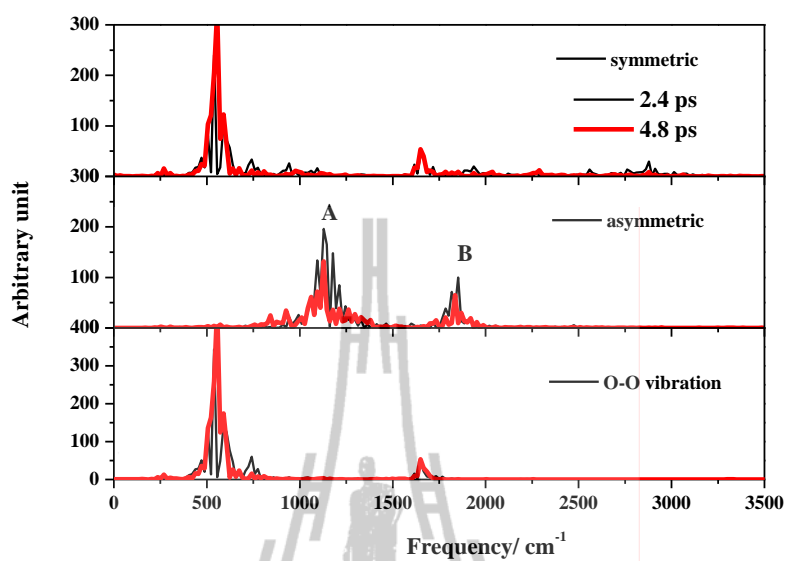


Figure 3.7 (Continued).







**Figure 3.8** Symmetric and asymmetric O-H stretching bands of the transferring protons in Zundel complex (structure **a**) in the gas phase, together with the O-O vibration band, obtained from BOMD simulations at 350 K with the simulation length of 2.4 and 4.8 ps.

## 3.2 The $\text{CF}_3\text{SO}_3^- - \text{H}_3\text{O}^+ - n\text{H}_2\text{O}$ complexes, $n = 1 - 4$

### 3.2.1 Static results

#### Structures and energetic of the shared-proton complexes

Refined equilibrium structures, characteristic H-bond distances and interaction energies ( $\Delta E$ ) of the H-bond complexes in the gas phase and continuum aqueous solution are presented in Table 3.6. In order to simplify the discussion, the H-bonds in Table 3.6 are labeled with numbers in parentheses. The trends of  $\Delta E$  with respect to the number of water molecules in the gas phase and continuum aqueous solution are shown in Figure 3.9.

For the  $\text{CF}_3\text{SO}_3^- - \text{H}_3\text{O}^+ - \text{H}_2\text{O}$  1 : 1 : 1 complexes in the gas phase and continuum aqueous solution, B3LYP/TZVP calculations predicted two important minimum energy geometries, namely structures **a** and **b** in Table 3.6. The most stable one, structure **a**, adopts a compact cyclic H-bond structure in which  $\text{H}_3\text{O}^+$  and  $\text{H}_2\text{O}$  act as proton donors toward two oxygen atoms of  $\text{CF}_3\text{SO}_3^-$ . Structure **a** is about 42 and 35 kJ/mol more stable than structure **b**, in the gas phase and continuum aqueous solutions, respectively. Equilibrium structures of the  $\text{CF}_3\text{SO}_3^- - \text{H}_3\text{O}^+ - \text{H}_2\text{O}$  1 : 1 : 1 complexes in Table 3.6 showed that the H-bond proton (H-bond (1)) tends to protonate at  $\text{CF}_3\text{SO}_3^-$  (structure **a** and **b**) in the gas phase, forming a neutral complex. This agrees well with B3LYP/6-31G\*\* calculations (Paddison, 2003). For structure **a**, the H-bond between  $\text{CF}_3\text{SO}_3^-$  and  $\text{H}_3\text{O}^+$  (H-bond (1)), ( $R_{\text{o-o}} = 2.54 \text{ \AA}$ ), becomes weaker ( $R_{\text{o-o}} = 2.59 \text{ \AA}$ ) in the aqueous solvent. Whereas,  $\text{H}_3\text{O}^+$  and  $\text{H}_2\text{O}$  in structure **a** form strong H-bond

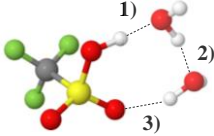
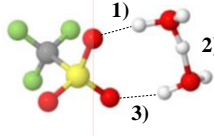
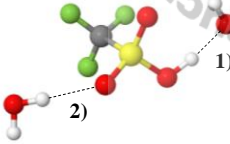
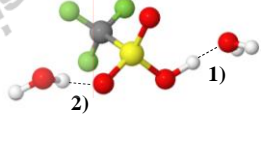
(H-bond (2)), with a considerably shorter distance, with  $R_{\text{o-o}} = 2.44 \text{ \AA}$  and  $R_{\text{o-H}} = 1.10 \text{ \AA}$ .

The absolute and some lowest-lying minimum energy geometries of the  $\text{CF}_3\text{SO}_3^- - \text{H}_3\text{O}^+ - \text{H}_2\text{O}$  1 : 1 : 2 and 1 : 1 : 3 complexes obtained from B3LYP/TZVP calculations were included in Table 3.6. Energetic results suggested that cyclic H-bond structures are slightly more stable than linear H-bond structures, both in the gas phase and continuum aqueous solution; for example for the  $\text{CF}_3\text{SO}_3^- - \text{H}_3\text{O}^+ - \text{H}_2\text{O}$  1 : 1 : 2 complex, structure **c** is more stable than structure **g** about 72 and 45 kJ/mol, in the gas phase and continuum aqueous solution, respectively. It was also observed both in the gas phase and continuum aqueous solution, with completion of coordination at  $\text{H}_3\text{O}^+$ , the H-bond structure **c**, **d**, **h** and **i**, form a solvated  $\text{CF}_3\text{SO}_3^- - \text{H}_3\text{O}^+$  pair. The results are in accordance with the observation that, at least three water molecules are sufficient to yield lowest energy structure, in which proton resides on the water cluster side of the complex, creating a contact ion pair between  $\text{CF}_3\text{SO}_3^-$  group and the solvated  $\text{H}_3\text{O}^+$  (Paddison, 2003). B3LYP/TZVP calculations also revealed that, when the fourth water molecules were added,  $\text{H}_3\text{O}^+$  becomes more hydrated, resulting in the structures capable of forming contact ion pair, a necessary step in structural diffusion. For the H-bond structures with incomplete coordination at  $\text{H}_3\text{O}^+$ , especially in the gas phase (see structure **a**, **b**, **e**, **f**, **g** and **k**), the H-bond protons (see H-bond (1)) tend to protonate at  $\text{CF}_3\text{SO}_3^-$  group, and therefore form neutral complexes. Moreover, the results in Table 3.6 revealed that, in the continuum aqueous solution, the charged species,  $\text{H}_3\text{O}^+$  and

$\text{H}_5\text{O}_2^+$  can be more stabilized in continuum aqueous solution compare to the gas phase.

The trends of  $\Delta E$  with respect to the number of water molecules in the gas phase and continuum aqueous solution are similar, with smaller variations in continuum aqueous solution. The destabilization effects caused by the continuum aqueous solvent are quite large, ranging from 606.3 kJ/mol in the  $\text{CF}_3\text{SO}_3^- - \text{H}_3\text{O}^+ - \text{H}_2\text{O}$  1 : 1 : 1 complex to 668.6 kJ/mol in the  $\text{CF}_3\text{SO}_3^- - \text{H}_3\text{O}^+ - \text{H}_2\text{O}$  1 : 1 : 4 complex. Figure 3.9 also revealed that  $\Delta E^{\text{sol}}$  are not substantially different for the H-bond complexes with the same number of water molecules; when the number of water molecules is the same, the H-bonds inside the clusters experience comparable uniform electric field (COSMO) (Phonyiem, Chaiwongwattana, Lao-ngam, and Sagarik, 2011).

**Table 3.6** H-bond distances and energies of the  $\text{CF}_3\text{SO}_3^- - \text{H}_3\text{O}^+ - n\text{H}_2\text{O}$  complexes,  $n = 1 - 4$ , obtained from B3LYP/TZVP calculations, both in the gas phase and continuum aqueous solution. They are in Å and kJ/mol, respectively.

Gas			Cosmo			
						
$R_{\text{O-O}}$	$R_{\text{O-H}}$	$\Delta E$	$R_{\text{O-O}}$	$R_{\text{O-H}}$	$\Delta E$	$\Delta E^{\text{sol}}$
1) 2.54	1.04	-678.6	1) 2.59	1.01	-97.7	-72.3
2) 2.67	0.99		2) 2.44	1.10		
3) 2.83	0.97		3) 2.77	0.98		
						
$R_{\text{O-O}}$	$R_{\text{O-H}}$	$\Delta E$	$R_{\text{O-O}}$	$R_{\text{O-H}}$	$\Delta E$	$\Delta E^{\text{sol}}$
1) 2.62	1.01	-636.3	1) 2.47	1.08	-62.4	-79.3
2) 3.02	0.97		2) 2.95	0.97		

$R_{\text{O-O}}$  and  $R_{\text{O-H}}$  = H-bond distances;  $\Delta E$  = interaction energy in the  $\text{CF}_3\text{SO}_3^- - \text{H}_3\text{O}^+ - \text{H}_2\text{O}$  clusters;  $\Delta E^{\text{sol}}$  = solvation energy.

Table 3.6 (Continued).

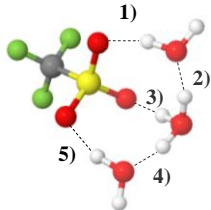
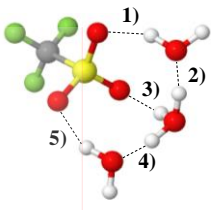
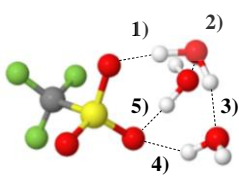
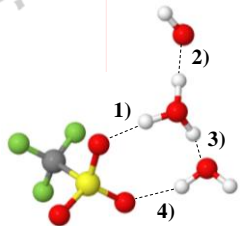
Gas			Cosmo			
						
$R_{O-O}$	$R_{O-H}$	$\Delta E$	$R_{O-O}$	$R_{O-H}$	$\Delta E$	$\Delta E^{sol}$
1) 2.75	0.98	-736.3	1) 2.87	0.98	-123.0	-73.7
2) 2.56	1.03		2) 2.52	1.04		
3) 2.55	1.03		3) 2.72	0.99		
4) 2.55	1.03		4) 2.52	1.05		
5) 2.75	0.98		5) 2.87	0.98		
						
$R_{O-O}$	$R_{O-H}$	$\Delta E$	$R_{O-O}$	$R_{O-H}$	$\Delta E$	$\Delta E^{sol}$
1) 2.51	1.05	-724.3	1) 2.61	1.01	-129.0	-91.7
2) 2.57	1.02		2) 2.54	1.03		
3) 2.58	1.01		3) 2.51	1.04		
4) 2.80	0.98		4) 2.80	0.98		
5) 2.81	0.98					

Table 3.6 (Continued).

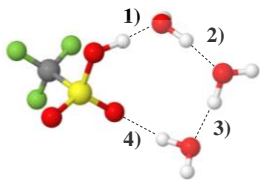
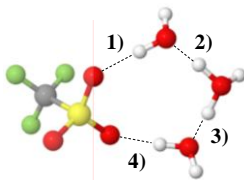
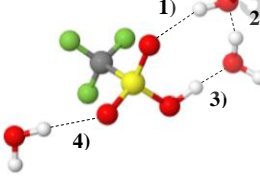
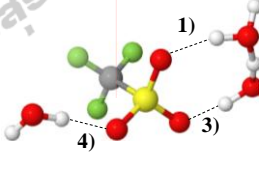
Gas			Cosmo			
e)						
						
$R_{O-O}$	$R_{O-H}$	$\Delta E$	$R_{O-O}$	$R_{O-H}$	$\Delta E$	$\Delta E^{sol}$
1) 2.49	1.06	-724.4	1) 2.72	0.99	-130.2	-92.8
2) 2.64	1.00		2) 2.49	1.06		
3) 2.70	0.99		3) 2.48	1.06		
4) 2.83	0.97		4) 2.72	0.99		
f)						
						
$R_{O-O}$	$R_{O-H}$	$\Delta E$	$R_{O-O}$	$R_{O-H}$	$\Delta E$	$\Delta E^{sol}$
1) 2.84	0.97	-693.4	1) 2.77	0.98	-104.8	-98.5
2) 2.66	0.99		2) 2.44	1.10		
3) 2.52	1.05		3) 2.60	1.01		
4) 3.01	0.97		4) 2.90	0.97		

Table 3.6 (Continued).

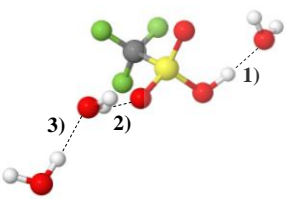
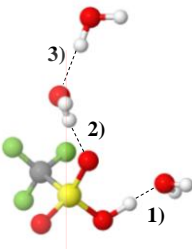
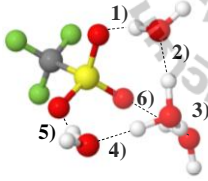
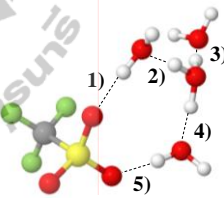
Gas			Cosmo			
g)						
						
$R_{O-O}$	$R_{O-H}$	$\Delta E$	$R_{O-O}$	$R_{O-H}$	$\Delta E$	$\Delta E^{sol}$
1) 2.62	1.01	-664.2	1) 2.47	1.08	-77.4	-100.2
2) 3.00	0.97		2) 2.91	0.97		
3) 2.87	0.97		3) 2.80	0.98		
h)						
						
$R_{O-O}$	$R_{O-H}$	$\Delta E$	$R_{O-O}$	$R_{O-H}$	$\Delta E$	$\Delta E^{sol}$
1) 2.68	0.99	-802.7	1) 2.75	0.98	-159.0	-77.1
2) 2.54	1.03		2) 2.53	1.03		
3) 2.54	1.03		3) 2.57	1.02		
4) 2.54	1.03		4) 2.53	1.04		
5) 2.69	0.99		5) 2.74	0.98		
6) 2.69	0.99					



Table 3.6 (Continued).

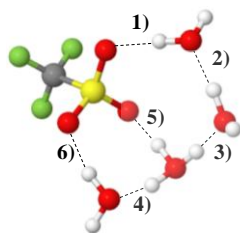
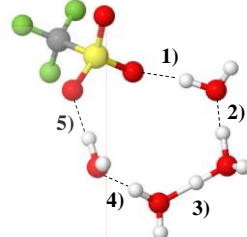
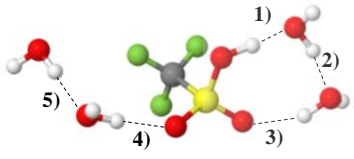
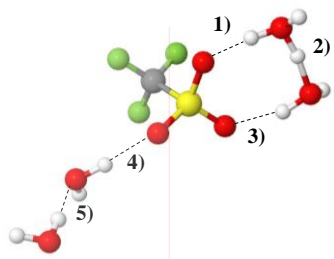
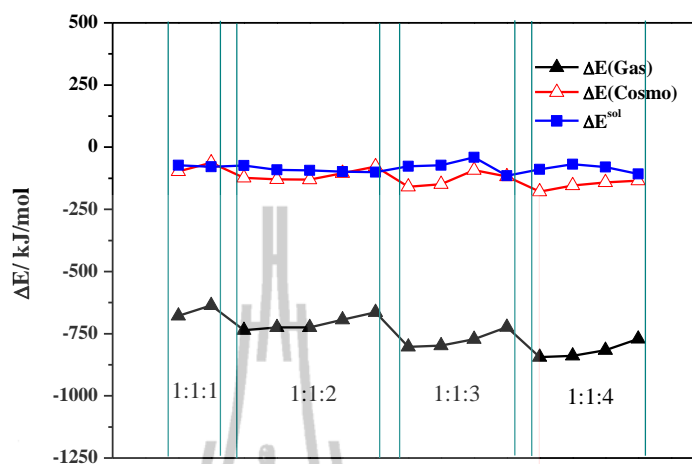
Gas			Cosmo			
i) 						
$R_{O-O}$	$R_{O-H}$	$\Delta E$	$R_{O-O}$	$R_{O-H}$	$\Delta E$	$\Delta E^{sol}$
1) 2.77	0.98	-797.4	1) 2.72	0.98	-149.3	-72.7
2) 2.65	1.00		2) 2.52	1.04		
3) 2.53	1.04		3) 2.44	1.10		
4) 2.56	1.02		4) 2.62	1.00		
5) 2.55	1.03		5) 2.77	0.98		
6) 2.72	0.99					

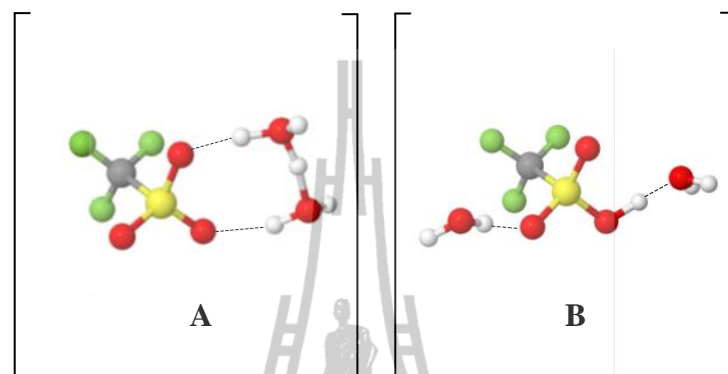
Table 3.6 (Continued).

Gas			Cosmo			
<p>k)</p> 						
$R_{O-O}$	$R_{O-H}$	$\Delta E$	$R_{O-O}$	$R_{O-H}$	$\Delta E$	$\Delta E^{sol}$
1) 2.52	1.05	-723.9	1) 2.61	1.01	-118.5	-115.4
2) 2.66	0.99		2) 2.44	1.10		
3) 2.84	0.97		3) 2.77	0.99		
4) 2.94	0.97		4) 2.86	0.97		
5) 2.86	0.97		5) 2.81	0.98		



**Figure 3.9** Trends of the interaction ( $\Delta E$ ) and solvation energies ( $\Delta E^{\text{sol}}$ ) with respect to the number of water molecules, obtained from B3LYP/TZVP calculations: -▲- =  $\Delta E$  in the gas phase; -△- =  $\Delta E$  in continuum aqueous solution; -■- =  $\Delta E^{\text{sol}}$ .

The results in Table 3.6 anticipated two  $\text{CF}_3\text{SO}_3^- - \text{H}_3\text{O}^+ - \text{H}_2\text{O}$  complexes as the most basic intermediate states in the proton transfer pathways.



Structure **A** is represented by the Zundel complex H-bonding at two oxygen atoms of the  $-\text{SO}_3^-$  group, forming a contact ion pair. In structure **B**,  $-\text{SO}_3^-$  separates  $\text{H}_3\text{O}^+$  and  $\text{H}_2\text{O}$ . The H-bonding features in structures **A** and **B** suggested two important structural diffusion mechanisms at the  $-\text{SO}_3^-$  group. Since the  $-\text{SO}_3^-$  group in structure **B** could be protonated and directly involved in proton transfer, one could regard the structural diffusion through structure **B** as the “pass-through” mechanism. Likewise, since the energetic and dynamics of the proton in the Zundel complex can be affected by the  $-\text{SO}_3^-$  group, one could consider the proton transfer through structures **A** as the “pass-by” mechanism (Phonyiem, Chaiwongwattana, Lao-ngam, and Sagarik, 2011).

### Asymmetric stretching coordinates and IR spectra of transferring protons

Asymmetric stretching coordinate ( $\Delta d_{DA}$ ) and O-H stretching frequency ( $\nu^{OH}$ ) are presented in Table 3.7. Although the H-bond structures in the gas phase and continuum aqueous solution are approximately the same, the trends of proton transfers are quite different. The H-bond distances ( $R_{O-O}$ ) in Table 3.6 and  $\Delta d_{DA}$  and  $\nu^{OH}$  in Table 3.7 suggested that the  $-\text{SO}_3^-$  group is preferentially protonated, forming neutral H-bond complexes (structure **a**, **b**, **f**, **g**, **i** and **k**). Whereas in continuum aqueous solution,  $-\text{SO}_3^- - \text{H}_3\text{O}^+$  contact structures dominate (structure **a**, **f**, **i** and **k**), with the highest tendency of proton transfer through the pass-by mechanism ( $\Delta d_{DA} = 0.24 \text{ \AA}$  and  $\nu^{OH} = 1331 \text{ to } 1389 \text{ cm}^{-1}$ ).

**Table 3.7** Asymmetric stretching coordinate ( $\Delta d_{DA}$ ) and O-H stretching frequency ( $\nu^{OH}$ ) of the  $CF_3SO_3^- - H_3O^+ - nH_2O$  complexes,  $n = 1 - 4$ , obtained from B3LYP/TZVP calculations, both in the gas phase and continuum aqueous solution. They are in Å and  $cm^{-1}$ , respectively.

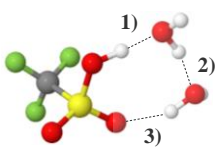
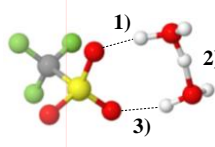
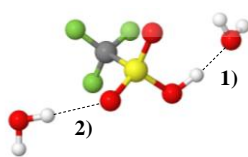
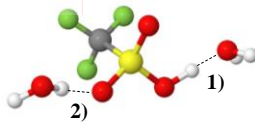
Gas		Cosmo	
<b>a)</b> 			
$\Delta d_{DA}$	$\nu^{OH}$	$\Delta d_{DA}$	$\nu^{OH}$
1) 0.46	2396	1) 0.58	2801
2) 0.71	3194	2) 0.24	1389
3) 0.96	3528	3) 0.85	3360
<b>b)</b> 			
$\Delta d_{DA}$	$\nu^{OH}$	$\Delta d_{DA}$	$\nu^{OH}$
1) 0.62	2898	1) 0.31	1800
2) 1.11	3620	2) 1.01	3570

Table 3.7 (Continued).

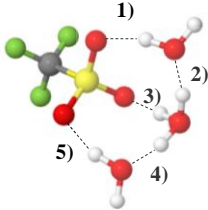
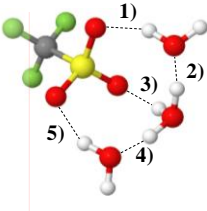
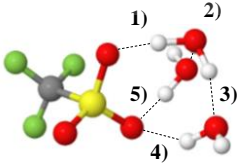
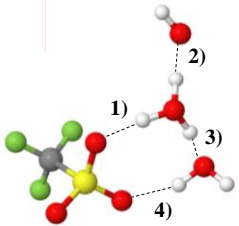
Gas		Cosmo	
c)		c)	
			
$\Delta d_{DA}$	$v^{OH}$	$\Delta d_{DA}$	$v^{OH}$
1) 0.83	3326	1) 0.98	3455
2) 0.52	2584	2) 0.45	-
3) 0.51	2465	3) 0.81	3196
4) 0.52	-	4) 0.43	2191
5) 0.83	3307	5) 0.98	3459
d)		d)	
			
$\Delta d_{DA}$	$v^{OH}$	$\Delta d_{DA}$	$v^{OH}$
1) 0.42	2265	1) 0.60	2906
2) 0.57	2761	2) 0.49	2562
3) 0.60	2911	3) 0.44	2260
4) 0.96	3442	4) 0.99	3415
5) 0.94	3421		

Table 3.7 (Continued).

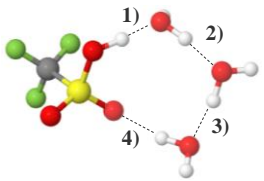
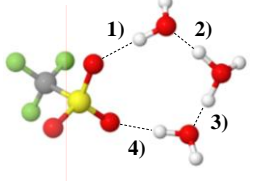
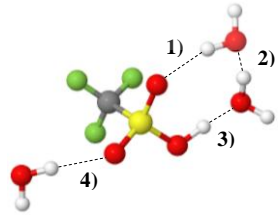
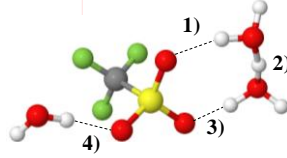
Gas		Cosmo	
e)			
			
$\Delta d_{DA}$	$\nu^{OH}$	$\Delta d_{DA}$	$\nu^{OH}$
1) 0.40	2099	1) 0.75	3270
2) 0.65	3060.8	2) 0.40	1908
3) 0.74	3271	3) 0.36	-
4) 0.91	3498	4) 0.75	3284
f)			
			
$\Delta d_{DA}$	$\nu^{OH}$	$\Delta d_{DA}$	$\nu^{OH}$
1) 0.88	3540	1) 0.87	3371
2) 0.71	3174	2) 0.24	1331
3) 0.43	2295	3) 0.60	2873
4) 1.09	3619	4) 0.96	3529



Table 3.7 (Continued).

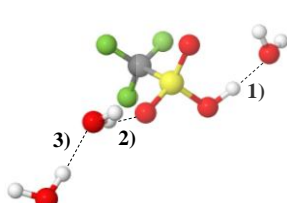
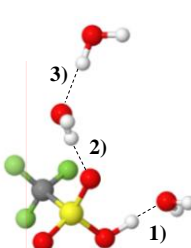
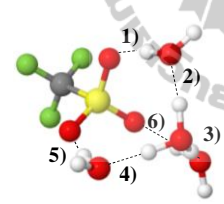
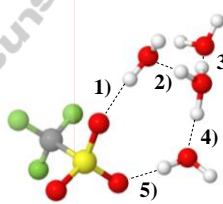
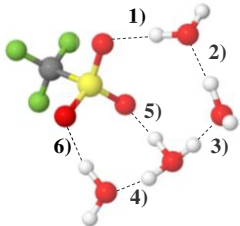
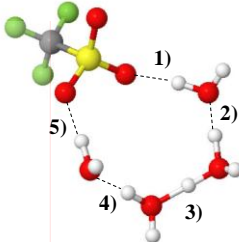
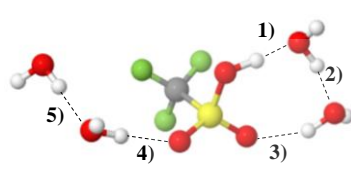
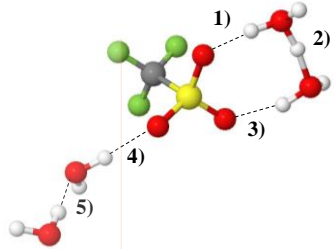
Gas		Cosmo	
<b>g)</b>			
			
$\Delta d_{DA}$	$\nu^{OH}$	$\Delta d_{DA}$	$\nu^{OH}$
1) 0.61	2874	1) 0.31	1795
2) 1.07	3607	2) 0.97	3544
3) 0.93	3504	3) 0.84	3373
<b>h)</b>			
			
$\Delta d_{DA}$	$\nu^{OH}$	$\Delta d_{DA}$	$\nu^{OH}$
1) 0.72	3199	1) 0.79	3330
2) 0.49	2457	2) 0.47	2314
3) 0.49	-	3) 0.53	2728
4) 0.49	2463	4) 0.45	2450
5) 0.72	3110	5) 0.78	3315
6) 0.72	-		

Table 3.7 (Continued).

Gas		Cosmo	
i)		i)	
			
$\Delta d_{DA}$	$v^{OH}$	$\Delta d_{DA}$	$v^{OH}$
1) 0.82	3365	1) 0.77	3300
2) 0.65	3056	2) 0.43	2313
3) 0.46	2403	3) 0.24	1333
4) 0.54	2796	4) 0.62	2924
5) 0.50	2577	5) 0.82	3376
6) 0.77	3290		

**Table 3.7** (Continued).

Gas		Cosmo	
			
$\Delta d_{DA}$	$\nu^{OH}$	$\Delta d_{DA}$	$\nu^{OH}$
1) 0.42	2263	1) 0.61	2906
2) 0.71	3174	2) 0.24	1335
3) 0.98	3538	3) 0.85	3367
4) 1.00	3586	4) 0.83	3499
5) 0.92	3488	5) 0.85	3369

In order to estimate the “threshold” asymmetric stretching coordinates ( $\Delta d_{DA}^*$ ) and frequencies ( $\nu^{OH*}$ ),  $\Delta d_{DA}$  and  $R_{O-O}$ ,  $\nu^{OH}$  and  $R_{O-O}$  and  $\nu^{OH}$  and  $\Delta d_{DA}$  for the pass-through mechanism were plotted and shown in Figures 3.10a to 3.10c, respectively, whereas for the pass-by mechanism in Figures 3.10d to 3.10f, respectively. The trends in Figures 3.10a and 3.10d suggest a separation between the internal and external H-bonds at  $R_{O-O} = 2.59 \text{ \AA}$  for pass-through mechanism and  $2.53 \text{ \AA}$  for pass-by mechanism. For the pass-through mechanism, the linear relationships for the internal and external H-bonds in the gas phase and continuum aqueous solution could be represented by equations (3.15) and (3.16), respectively.

$$\text{Internal H-bonds:} \quad \Delta d_{\text{DA}} = 2.39 \times R_{\text{O-O}} - 5.59 \quad (3.15)$$

$$\text{External H-bonds:} \quad \Delta d_{\text{DA}} = 1.31 \times R_{\text{O-O}} - 2.79 \quad (3.16)$$

For the pass-by mechanism, they are shown in equations (3.17) and (3.18), respectively.

$$\text{Internal H-bonds:} \quad \Delta d_{\text{DA}} = 2.62 \times R_{\text{O-O}} - 6.14 \quad (3.17)$$

$$\text{External H-bonds:} \quad \Delta d_{\text{DA}} = 1.50 \times R_{\text{O-O}} - 3.32 \quad (3.18)$$

Figure 3.10b and 3.10e show the relationships between  $v^{\text{OH}}$  and  $R_{\text{O-O}}$ , represented by the exponential functions in equations (3.19) to (3.22).

Pass-through mechanism

$$\text{Gas phase:} \quad v^{\text{OH}} = -1.80 \times 10^9 e^{-R_{\text{O-O}}/0.1793} + 372 \quad (3.19)$$

$$\text{Continuum aqueous solution:} \quad v^{\text{OH}} = -1.78 \times 10^{10} e^{-R_{\text{O-O}}/0.1540} + 3681 \quad (3.20)$$

Pass-by mechanism

$$\text{Gas phase:} \quad v^{\text{OH}} = -2.30 \times 10^{10} e^{-R_{\text{O-O}}/0.1507} + 3625 \quad (3.21)$$

$$\text{Continuum aqueous solution:} \quad v^{\text{OH}} = -3.15 \times 10^{10} e^{-R_{\text{O-O}}/0.1480} + 3566 \quad (3.22)$$

The relationship between  $\nu^{\text{OH}}$  and  $\Delta d_{\text{DA}}$  for the pass-through mechanism and the pass-by mechanism in the gas phase and continuum aqueous solution are depicted in Figures 3.10c and 3.10f. They are represented by exponential functions resembling the normal distribution function and shown in equations (3.23) to (3.26).

Pass-through mechanism

*Gas phase:* 
$$\nu^{\text{OH, MD}} = 3722 - \frac{6128}{\sqrt{2\pi}} e^{-2.8 < \Delta d_{\text{DA}} >^2} \quad (3.23)$$

*Continuum aqueous solution:* 
$$\nu^{\text{OH, MD}} = 3681 - \frac{6347}{\sqrt{2\pi}} e^{-3.1 < \Delta d_{\text{DA}} >^2} \quad (3.24)$$

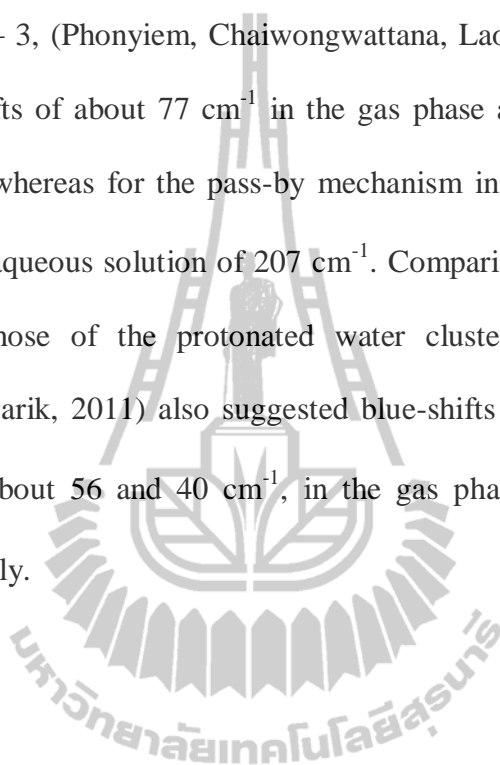
Pass-by mechanism

*Gas phase:* 
$$\nu^{\text{OH, MD}} = 3521 - \frac{6120}{\sqrt{2\pi}} e^{-3.8 < \Delta d_{\text{DA}} >^2} \quad (3.25)$$

*Continuum aqueous solution:* 
$$\nu^{\text{OH, MD}} = 3566 - \frac{6798}{\sqrt{2\pi}} e^{-3.8 < \Delta d_{\text{DA}} >^2} \quad (3.26)$$

Calculations of the second derivatives of the functions in equations (3.23), (3.24), (3.25) and (3.26) yielded inflection points at the threshold frequencies for proton transfer ( $\nu^{\text{OH}^*}$ ), for the pass-through mechanism in the gas phase at  $\nu^{\text{OH}^*} = 2239 \text{ cm}^{-1}$  and  $\Delta d_{\text{DA}}^* = 0.42 \text{ \AA}$ , and in continuum aqueous solution at  $\nu^{\text{OH}^*} = 2145 \text{ cm}^{-1}$  and  $\Delta d_{\text{DA}}^* = 0.40 \text{ \AA}$ . For the pass-by mechanism, Figure 3.10f shows the

inflection points in the gas phase at  $\nu^{\text{OH}^*} = 2040 \text{ cm}^{-1}$  and  $\Delta d_{\text{DA}}^* = 0.36 \text{ \AA}$ , and in continuum aqueous solution at  $\nu^{\text{OH}^*} = 1921 \text{ cm}^{-1}$  and  $\Delta d_{\text{DA}}^* = 0.36 \text{ \AA}$ . Comparison of  $\nu^{\text{OH}^*}$  for the pass-through mechanism and those in the  $\text{CF}_3\text{SO}_3\text{H} - \text{H}_3\text{O}^+ - n\text{H}_2\text{O}$  complexes,  $n = 1 - 3$ , (Phonyiem, Chaiwongwattana, Lao-ngam, and Sagarik, 2011) suggested blue-shifts of about  $77 \text{ cm}^{-1}$  in the gas phase and  $145 \text{ cm}^{-1}$  in continuum aqueous solution, whereas for the pass-by mechanism in the gas phase of  $111 \text{ cm}^{-1}$  and in continuum aqueous solution of  $207 \text{ cm}^{-1}$ . Comparison of  $\nu^{\text{OH}^*}$  for the pass-by mechanism and those of the protonated water clusters (Lao-ngam, Asawakun, Wannarat, and Sagarik, 2011) also suggested blue-shifts due to the presence of the  $-\text{SO}_3^-$  group of about  $56$  and  $40 \text{ cm}^{-1}$ , in the gas phase and continuum aqueous solution, respectively.



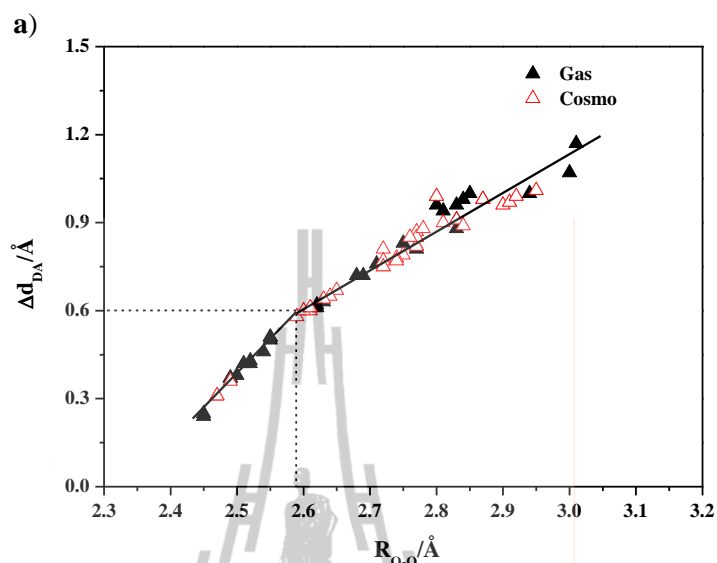


**Figure 3.10** Static results of the  $\text{CF}_3\text{SO}_3^- - \text{H}_3\text{O}^+ - n\text{H}_2\text{O}$  complexes,  $n = 1 - 4$ , obtained from B3LYP/TZVP calculations. a) Plot of the asymmetric stretching coordinates ( $\Delta d_{\text{DA}}$ ) and the O-H...O H-bond distances ( $R_{\text{O-O}}$ ) for the pass-through mechanism. b) Plot of the asymmetric O-H stretching frequencies ( $\nu^{\text{OH}}$ ) and the O - H..O H-bond distances ( $R_{\text{O-O}}$ ) for the pass-through mechanism. c) Plot of the asymmetric O-H stretching frequencies ( $\nu^{\text{OH}}$ ) and the asymmetric stretching coordinates ( $\Delta d_{\text{DA}}$ ) for the pass-through mechanism. d) Plot of the asymmetric stretching coordinates ( $\Delta d_{\text{DA}}$ ) and the O-H..O H-bond distances ( $R_{\text{O-O}}$ ) for the pass-by mechanism. e) Plot of the asymmetric O-H stretching frequencies ( $\nu^{\text{OH}}$ ) and the O - H..O H-bond distances ( $R_{\text{O-O}}$ ) for the pass-by mechanism. f) Plot of the asymmetric O-H stretching frequencies ( $\nu^{\text{OH}}$ ) and the asymmetric stretching coordinates ( $\Delta d_{\text{DA}}$ ) for the pass-by mechanism.

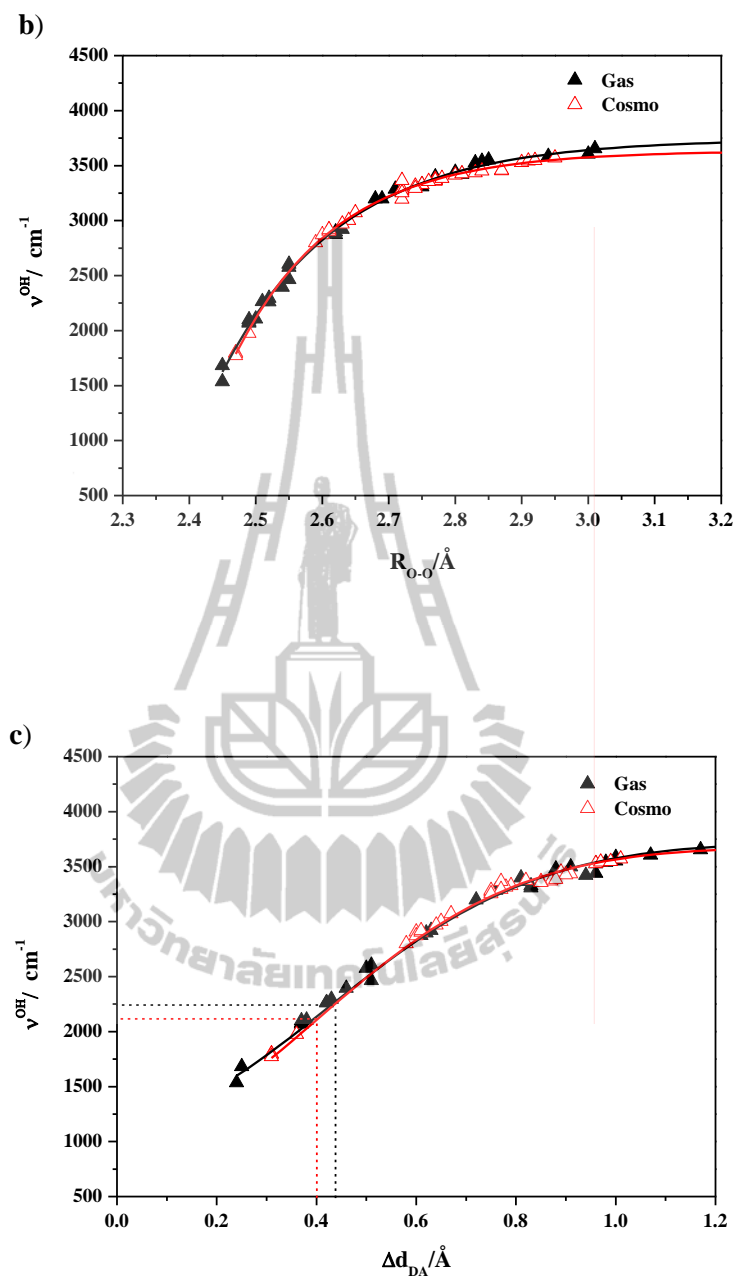


Figure 3.10 (Continued).



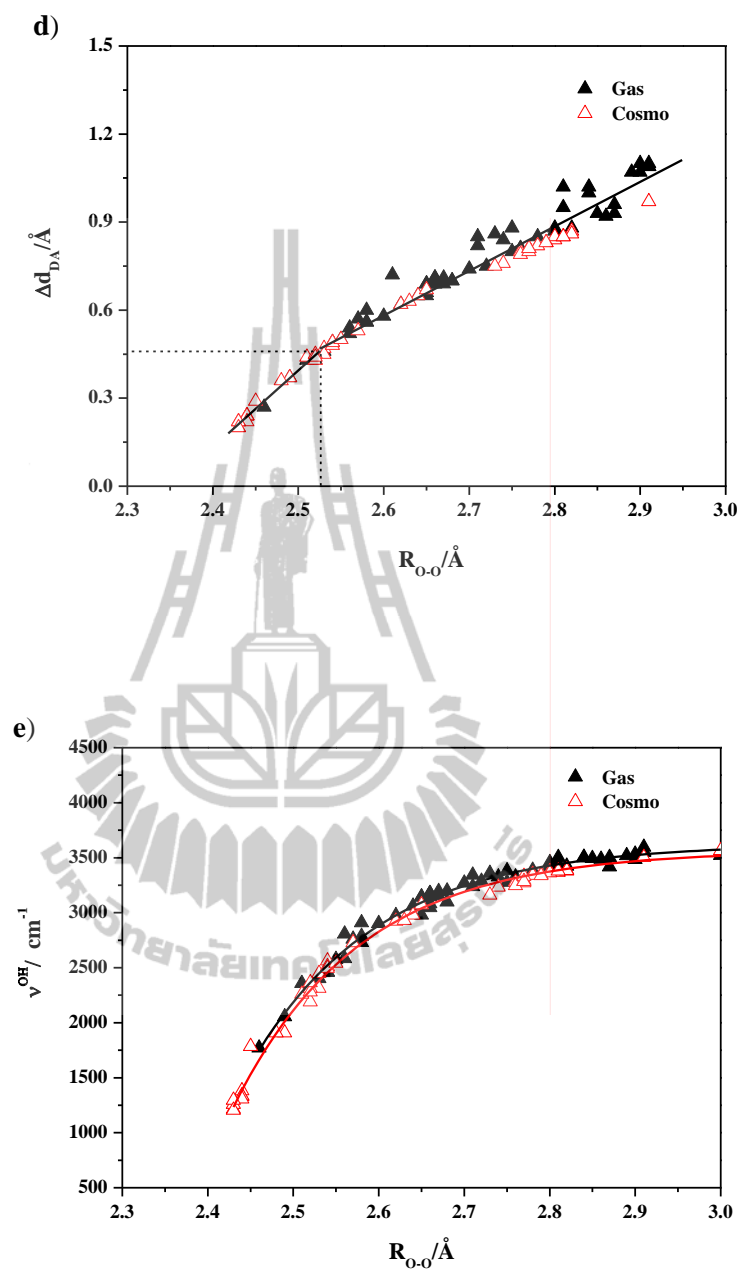
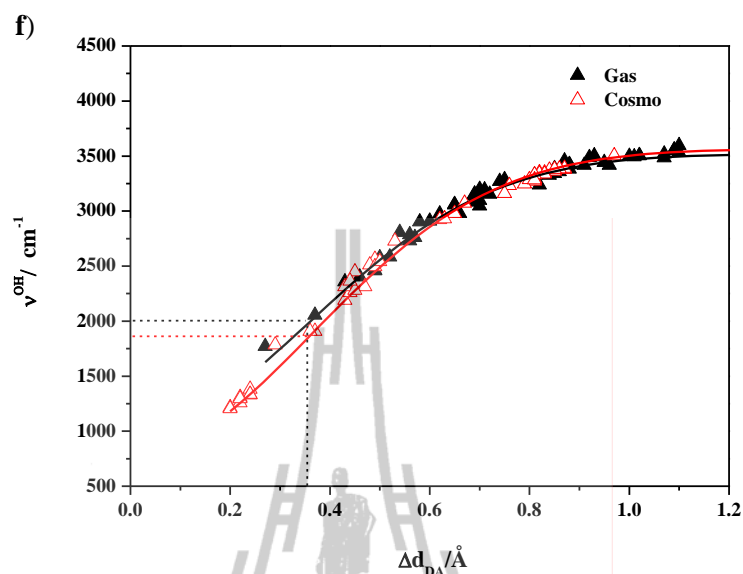


Figure 3.10 (Continued).



**Figure 3.10** (Continued).

Table 3.7 showed that  $\nu^{OH}$  can vary in a quite wide range; in the gas phase from 1100 to 3500  $\text{cm}^{-1}$ , in continuum aqueous solution from 820 to 3600  $\text{cm}^{-1}$ . To resolve these broad IR bands, the H-bonds in Table 3.7 were divided into two groups (Phonyiem, Chaiwongwattana, Lao-ngam, and Sagarik, 2011); the H-bonds connecting directly to the  $-\text{SO}_3\text{H}$  or  $-\text{SO}_3^-$  group belong to **Group 1** (potentially involved in the protonation or deprotonation at the  $-\text{SO}_3\text{H}$  group, as well as the pass-through mechanism) and the H-bonds in the adjacent  $\text{H}_3\text{O}^+ - \text{H}_2\text{O}$  or Zundel complex to **Group 2** (potentially involved in the pass-by mechanism). Investigation of the H-bond structures in Table 3.7 in details allowed **Group 1** and **2** to be further divided into four subgroups. The definitions of the groups and subgroups are summarized as follows:

**Group 1** H-bonds connecting directly to the  $-\text{SO}_3^-$  group.

**Subgroup (I)**; Cyclic H-bonds between the Zundel complex or  $\text{H}_7\text{O}_3^+$  and the two oxygen atoms of  $-\text{SO}_3^-$ , *e.g.* H-bonds (1) and (3) in structures **a**, **f** and **k**, H-bonds (1), (3) and (5) in structure **c**, H-bonds (1), (4) and (5) in structures **d** and **e**, as well as H-bonds (1), (5) and (6) in structures **h** and **i**

**Subgroup (II)**; Linear H-bond between an oxygen atom of the  $-\text{SO}_3^-$  group and,  $\text{H}_3\text{O}^+$ ,  $\text{H}_5\text{O}_2^+$  or  $\text{H}_2\text{O}$ , *e.g.* H-bonds (1) and (2) in structures **b** and **g** and H-bond (4) in structures **f** and **k**.

**Group 2** H-bonds in the adjacent Zundel complex.

**Subgroup (III)**; H-bond in the  $\text{H}_3\text{O}^+ - \text{H}_2\text{O}$  contact structure or the Zundel complex in the structure with Subgroup (II), *e.g.* H-bond (2) in structure **d** in continuum aqueous solution, H-bond (3) in structures **g** and **h** and H-bond (5) in **k**.

**Subgroup (IV)**; H-bond of the Zundel complex in the structure with Subgroup (I), *e.g.* H-bond (2) in structures **a**, **c**, **d** (in the gas phase), **e**, **f**, **h**, **i** and **k**, H-bond (3) in structures **d**, **e**, and **i** and H-bond (4) in structures **c**, **h** and **i**.

The domains of  $\nu^{\text{OH}}$  for the H-bond protons in **Group 1** (Subgroups (I) and (II)) and **Group 2** (Subgroups (III) to (IV)), in the gas phase and continuum aqueous solution, are shown in Figure 3.11. Comparison of Figure 3.11a and 3.11b revealed that the electric field introduced by the continuum aqueous solvent brings about significant shifts of  $\nu^{\text{OH}}$ , especially for the pass-by mechanism, in which most of the H-bonds in Subgroup (IV) are red shifted to  $\nu^{\text{OH}}$  lower than  $\nu^{\text{OH}*}$ . For the pass-through mechanism, only some linear H-bonds in Subgroup (II) are red shifted to  $\nu^{\text{OH}}$

lower than  $\nu^{\text{OH}^*}$ . The cyclic H-bonds between the two oxygen atoms of  $-\text{SO}_3^-$  and the Zundel complex (Subgroup (I)) tend to be destabilized in continuum aqueous solution, leading to blue shifts of  $\nu^{\text{OH}}$  above  $2800 \text{ cm}^{-1}$ .

From the static results, asymmetric stretching coordinate ( $\Delta d_{\text{DA}}$ ) and O-H stretching frequency ( $\nu^{\text{OH}}$ ) suggested higher tendency for proton transfer in the continuum aqueous solution. For the pass-through mechanism in the gas phase,  $\Delta d_{\text{DA}}^*$  was predicted to be  $0.42 \text{ \AA}$ , greater than that the criteria for proton transfer (Morrone, Haslinger, and Tuckerman, 2006), as well as  $\nu^{\text{OH}^*}$  to be  $2239 \text{ cm}^{-1}$ . This observation is in good agreement with the previous study on the  $\text{CF}_3\text{SO}_3\text{H} - \text{H}_3\text{O}^+ - \text{H}_2\text{O}$  clusters (Phonyiem, Chaiwongwattana, Lao-ngam, and Sagarik, 2011); the  $-\text{SO}_3\text{H}$  group is not preferentially dissociated in the gas phase, whereas in continuum aqueous solution,  $-\text{SO}_3\text{H}$  tends to deprotonate, resulting in  $-\text{SO}_3^-$  in close contact with  $\text{H}_3\text{O}^+$ . Therefore, the discussion in the next section will be focused on the H-bond structures, with high tendency of proton transfer through the pass-by mechanism.

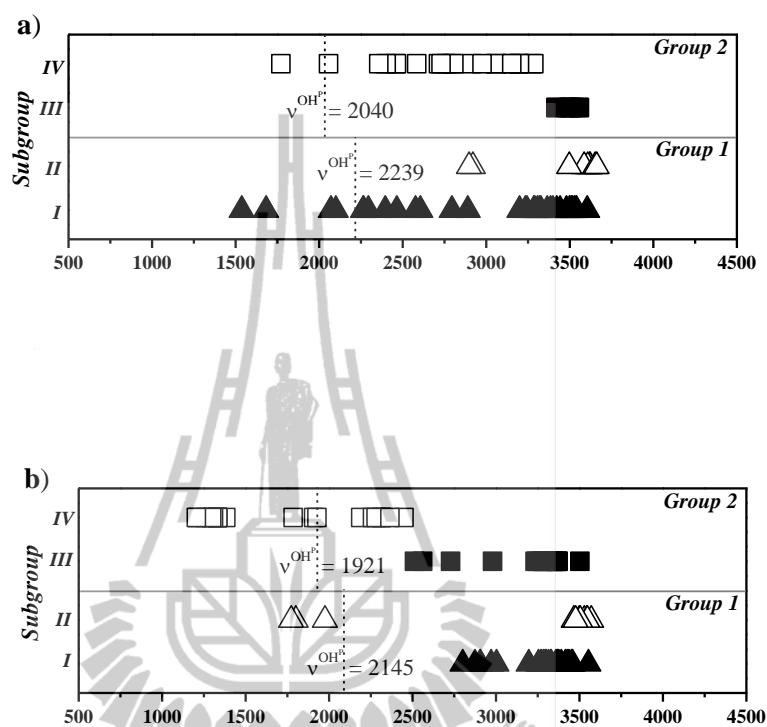


**Figure 3.11** The domains of  $\nu^{\text{OH}}$  for the H-bond protons in **Group 1** and **2**, as well as Subgroup (I) to (IV). a) gas phase. b) continuum aqueous solution.

### 3.2.2 Dynamic results

In the present work, the neglect of extensive H-bond networks of water in the vicinities of the solute ( $\text{CF}_3\text{SO}_3^-$ ), as well as the thermal energy fluctuations in BOMD simulations, made it difficult to analyze the dynamics in the  $\text{CF}_3\text{SO}_3^- - \text{H}_3\text{O}^+ - n\text{H}_2\text{O}$  complexes,  $n = 1 - 4$ . Since the static result showed high tendency for proton transfer in continuum aqueous solution, attention was focused on the H-bond protons in the intermediate states in continuum aqueous solution, in which protons are susceptible to proton transfer through the pass-by mechanism.

#### Average H-bond structures and IR spectra

For the  $\text{CF}_3\text{SO}_3^- - \text{H}_3\text{O}^+ - n\text{H}_2\text{O}$  complexes,  $n = 1 - 4$ , the average H-bond structures,  $\langle R_{\text{O-O}} \rangle$  and  $\langle \Delta d_{\text{DA}} \rangle$ , obtained from BOMD simulations at 350 K, are summarized in Table 3.8, together with,  $v_{\text{A}}^{\text{OH, MD}}$ ,  $v_{\text{B}}^{\text{OH, MD}}$  and the proton diffusion coefficients (D). Plots between  $\langle \Delta d_{\text{DA}} \rangle$  and  $\langle R_{\text{O-O}} \rangle$ ,  $v_{\text{A}}^{\text{OH, MD}}$  and  $\langle R_{\text{O-O}} \rangle$ , and  $v_{\text{A}}^{\text{OH, MD}}$  and  $\langle \Delta d_{\text{DA}} \rangle$  for the pass-by mechanism are shown in Figure 3.12a to 3.12c. The linear relationships between  $\langle \Delta d_{\text{DA}} \rangle$  and  $\langle R_{\text{O-O}} \rangle$  are represented in equation (3.27) and (3.28).

$$\text{Internal H-bonds:} \quad \langle \Delta d_{\text{DA}} \rangle = 2.73 \times \langle R_{\text{O-O}} \rangle - 6.41 \quad (3.27)$$

$$\text{External H-bonds:} \quad \langle \Delta d_{\text{DA}} \rangle = 1.68 \times \langle R_{\text{O-O}} \rangle - 3.73 \quad (3.28)$$

Equation (3.29) shows the relationships between  $\nu_A^{\text{OH, MD}}$  and  $\langle R_{\text{O-O}} \rangle$  and equation (3.30) the relationships between  $\nu_A^{\text{OH, MD}}$  and  $\langle \Delta d_{\text{DA}} \rangle$ .

$$\nu_A^{\text{OH, MD}} = -3.84 \times 10^{12} e^{-\langle R_{\text{O-O}} \rangle / 0.1147} + 3566 \quad (3.29)$$

$$\nu_A^{\text{OH, MD}} = 3566 - \frac{7215}{\sqrt{2\pi}} e^{-4.2 \langle \Delta d_{\text{DA}} \rangle^2} \quad (3.30)$$

Since BOMD simulations were conducted in a short time, the average H-bond structures are not substantially different from the B3LYP/TZVP results. Comparison of  $\nu_A^{\text{OH, MD}}$  in Table 3.8 with  $\nu^{\text{OH}}$  in Table 3.7 showed a general trend. Figure 3.12c showed the inflection point for the pass-by mechanism in the continuum aqueous solvent at  $\langle \Delta d_{\text{DA}} \rangle = 0.34 \text{ \AA}$  and  $\nu_A^{\text{OH*, MD}} = 1820 \text{ cm}^{-1}$ . The latter is higher than the corresponding value for the  $\text{CF}_3\text{SO}_3\text{H} - \text{H}_3\text{O}^+ - n\text{H}_2\text{O}$  complexes,  $n = 1 - 3$ , (Phonyiem, Chaiwongwattana, Lao-ngam, and Sagarik, 2011) and the protonated water clusters (Lao-ngam, Asawakun, Wannarat, and Sagarik, 2011), respectively.

$\Delta \nu_{\text{BA}}^{\text{OH, MD}}$  and  $\mathbf{P_B/P_A}$  for the H-bond protons in the  $\text{CF}_3\text{SO}_3^- - \text{H}_3\text{O}^+ - n\text{H}_2\text{O}$  complexes,  $n = 1 - 4$ , are included in Table 3.8. Examples of the characteristic asymmetric O-H stretching bands for the pass-by mechanisms, obtained from BOMD simulations at 350 K, are shown in Figure 3.12d. Plots of  $\sigma_{\text{R}_{\text{O-H}}}$  and  $\langle \Delta d_{\text{DA}} \rangle$ ,  $\Delta \nu_{\text{BA}}^{\text{OH, MD}}$  and  $\langle \Delta d_{\text{DA}} \rangle$ , and  $\mathbf{P_B/P_A}$  and  $\langle \Delta d_{\text{DA}} \rangle$  are illustrated in Figure 3.12e to 3.12g, respectively.

All the outstanding features discussed in the protonated water clusters were observed in the  $\text{CF}_3\text{SO}_3^- - \text{H}_3\text{O}^+ - n\text{H}_2\text{O}$  complexes,  $n = 1 - 4$ . The same types of functions, as in the case of protonated water cluster in Figure 3.6a to 3.6c, could be employed to represent the relationships in Figure 3.12e to 3.12g.

$$\sigma_{\text{R}_{\text{O-H}}} = -0.4444e^{-\langle \Delta d_{\text{DA}} \rangle / 0.11792} + 0.00827 \quad (3.31)$$

$$\Delta v_{\text{BA}}^{\text{OH, MD}} = 1470 - \frac{380}{0.1347 \sqrt{2\pi}} e^{-0.5 \left( \frac{\langle \Delta d_{\text{DA}} \rangle - 0.3106}{0.1347} \right)^2} \quad (3.32)$$

$$\mathbf{P}_{\text{B}}/\mathbf{P}_{\text{A}} = 0.0036 + \frac{0.0481}{0.0699 \sqrt{2\pi}} e^{-0.5 \left( \frac{\langle \Delta d_{\text{DA}} \rangle - 0.3145}{0.0699} \right)^2} \quad (3.33)$$

Equation (3.31) shows the relationships between  $\sigma_{\text{R}_{\text{O-H}}}$  and  $\langle \Delta d_{\text{DA}} \rangle$ , equation (3.32),  $\Delta v_{\text{BA}}^{\text{OH, MD}}$  and  $\langle \Delta d_{\text{DA}} \rangle$ , and equation (3.33),  $\mathbf{P}_{\text{B}}/\mathbf{P}_{\text{A}}$  and  $\langle \Delta d_{\text{DA}} \rangle$ .

For the pass-by mechanism, due to the presence of the  $\text{CF}_3\text{SO}_3^-$  group, the vibrational energy for the interconversion between the oscillatory shuttling and the structural diffusion motions ( $\Delta v_{\text{BA}}^{\text{OH, MD}}$  in Figure 3.12f) decreases exponentially with  $\langle \Delta d_{\text{DA}} \rangle$ . Comparison of  $\Delta v_{\text{BA}}^{\text{OH, MD}}$  and  $\mathbf{P}_{\text{B}}/\mathbf{P}_{\text{A}}$  in the protonated water clusters and the  $\text{CF}_3\text{SO}_3^- - \text{H}_3\text{O}^+ - n\text{H}_2\text{O}$  complexes,  $n = 1 - 4$ , revealed an increase in the relative probability of finding the structural diffusion motion, from  $\mathbf{P}_{\text{B}}/\mathbf{P}_{\text{A}} = 0.17$  to 0.28, respectively. The H-bonds in the vicinities of maximum  $\mathbf{P}_{\text{B}}/\mathbf{P}_{\text{A}}$  are, for examples, H-bond (2) in structures **a**, **k** and **o**, H-bond (3) in structures **i** and **l**, and H-bond (4) in structures **m** and **n**.

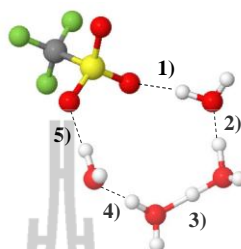


**Table 3.8** Dynamic results of the  $\text{CF}_3\text{SO}_3^- - \text{H}_3\text{O}^+ - n\text{H}_2\text{O}$  complexes,  $n = 1 - 4$ , obtained from BOMD simulation at 350 K in continuum aqueous solution. Distances and IR frequencies are in Å and  $\text{cm}^{-1}$ , respectively

a)						
$\langle R_{\text{O-O}} \rangle$	$\langle \Delta d_{\text{DA}} \rangle$	$\nu_{\text{A}}^{\text{OH, MD}}$	$\nu_{\text{B}}^{\text{OH, MD}}$	$\Delta\nu_{\text{BA}}^{\text{OH, MD}}$	$P_{\text{B}}/P_{\text{A}}$	$D (10^{-5})$
1) 2.77	0.95					
2) 2.44	0.26	1431	1835	404	0.19	3.03
3) 2.59	0.60					
f)						
$\langle R_{\text{O-O}} \rangle$	$\langle \Delta d_{\text{DA}} \rangle$	$\nu_{\text{A}}^{\text{OH, MD}}$	$\nu_{\text{B}}^{\text{OH, MD}}$	$\Delta\nu_{\text{BA}}^{\text{OH, MD}}$	$P_{\text{B}}/P_{\text{A}}$	$D (10^{-5})$
1) 2.77	0.95					
2) 2.44	0.24	1336	1863	527	0.11	2.93
3) 2.60	0.65					
4) 2.90	2.02					

Table 3.8 (Continued).

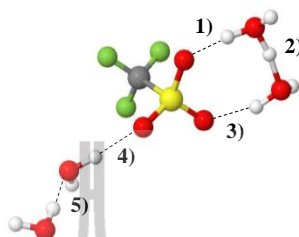
i)



$\langle R_{O-O} \rangle$	$\langle \Delta d_{DA} \rangle$	$V_A^{OH, MD}$	$V_B^{OH, MD}$	$\Delta V_{BA}^{OH, MD}$	$P_B/P_A$	$D (10^{-5})$
1) 2.77	1.96					
2) 2.62	0.65	1728	3198	1470	0.00	5.70
3) 2.44	0.23	1263	1683	421	0.18	6.12
4) 2.52	0.48	1504	2525	1021	0.01	6.10
5) 2.72	1.83					

Table 3.8 (Continued).

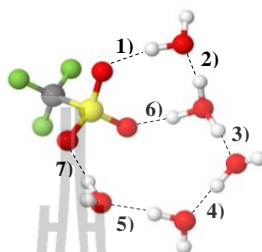
k)



$\langle R_{O-O} \rangle$	$\langle \Delta d_{DA} \rangle$	$V_A^{OH, MD}$	$V_B^{OH, MD}$	$\Delta V_{BA}^{OH, MD}$	$P_B/P_A$	$D (10^{-5})$
1) 2.61	0.64					
2) 2.44	0.24	1420	1829	409	0.19	4.65
3) 2.77	0.93					
4) 2.86	1.10					
5) 2.81	2.23					

**Table 3.8** (Continued).

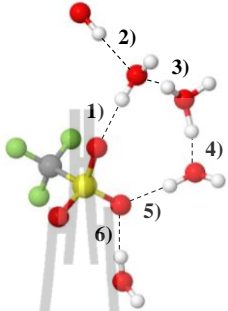
D)



$\langle R_{O-O} \rangle$	$\langle \Delta d_{DA} \rangle$	$v_A^{OH, MD}$	$v_B^{OH, MD}$	$\Delta v_{BA}^{OH, MD}$	$P_B/P_A$	$D (10^{-5})$
1) 2.83	1.96					
2) 2.55	0.54	1689	2665	976	0.02	6.70
3) 2.48	0.37	1582	1930	348	0.24	4.85
4) 2.64	0.69	2110	3165	1055	0.01	9.03
5) 2.74	0.84					
6) 2.65	0.75					
7) 2.84	1.03					

Table 3.8 (Continued).

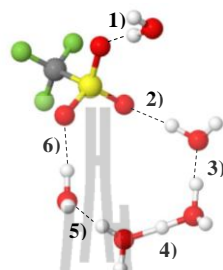
m)



$\langle R_{O-O} \rangle$	$\langle \Delta d_{DA} \rangle$	$v_A^{OH, MD}$	$v_B^{OH, MD}$	$\Delta v_{BA}^{OH, MD}$	$P_B/P_A$	$D (10^{-5})$
1) 2.74	1.66					
2) 2.91	2.20					
3) 2.54	0.48	1504	2407	903	0.01	7.46
4) 2.45	0.32	1521	1852	331	0.26	10.49
5) 2.72	0.87					
6) 2.89	1.43					

Table 3.8 (Continued).

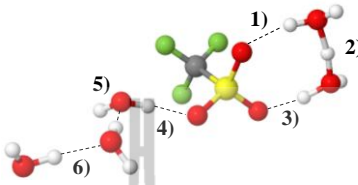
n)



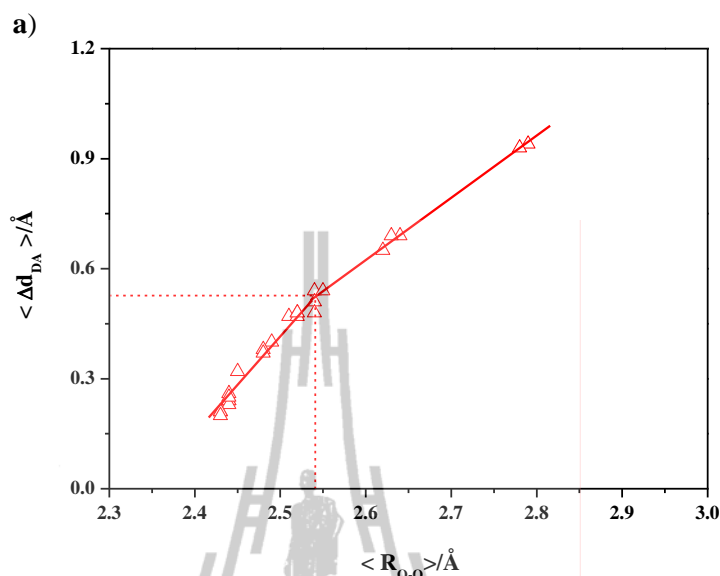
$\langle R_{O-O} \rangle$	$\langle \Delta d_{DA} \rangle$	$v_A^{OH, MD}$	$v_B^{OH, MD}$	$\Delta v_{BA}^{OH, MD}$	$P_B/P_A$	$D (10^{-5})$
1) 2.87	1.26					
2) 2.74	0.84					
3) 2.52	0.48	1616	2576	960	0.02	8.85
4) 2.44	0.25	1369	1728	359	0.23	13.60
5) 2.63	0.69	1751	3199	1448	0.00	6.56
6) 2.79	0.91					

Table 3.8 (Continued).

o)



$\langle R_{O-O} \rangle$	$\langle \Delta d_{DA} \rangle$	$V_A^{OH, MD}$	$V_B^{OH, MD}$	$\Delta V_{BA}^{OH, MD}$	$P_B/P_A$	$D (10^{-5})$
1) 2.76	0.93					
2) 2.43	0.21	1251	1661	410	0.19	-
3) 2.61	0.65					
4) 2.85	1.19					
5) 2.76	0.92					
6) 2.79	0.94					



**Figure 3.12** The results of the  $\text{CF}_3\text{SO}_3^- + \text{H}_3\text{O}^+ - n\text{H}_2\text{O}$  complexes,  $n = 1 - 4$ , in continuum aqueous solution, obtained from BOMD simulations at 350 K. a) Plot of the average asymmetric stretching coordinates ( $\langle \Delta d_{DA} \rangle$ ) and the average O-H..O H-bond distances ( $\langle R_{O-O} \rangle$ ). b) Plot of the asymmetric O-H stretching frequencies ( $\nu^{\text{OH, MD}}$ ) and the average O-H..O H-bond distances ( $\langle R_{O-O} \rangle$ ). c) Plot of the asymmetric O-H stretching frequencies ( $\nu^{\text{OH, MD}}$ ) and the asymmetric stretching coordinates ( $\langle \Delta d_{DA} \rangle$ ). d) Symmetric, asymmetric O-H stretching and O-O vibration bands of the  $\text{CF}_3\text{SO}_3^- + \text{H}_3\text{O}^+ - \text{H}_2\text{O}$  1 : 1 : 4 complex (structure **k**). e) Plot of standard deviations of the O-H distances ( $\sigma_{R_{O-H}}$ ) and the asymmetric stretching coordinates ( $\langle \Delta d_{DA} \rangle$ ). f) Plot of  $\Delta \nu_{BA}^{\text{OH, MD}}$  and the asymmetric stretching coordinates ( $\langle \Delta d_{DA} \rangle$ ). g) Plot of probability of finding the structural diffusion motion relative to the oscillatory shuttling motion ( $\mathbf{P}_B/\mathbf{P}_A$ ) and the asymmetric stretching coordinates ( $\langle \Delta d_{DA} \rangle$ ).



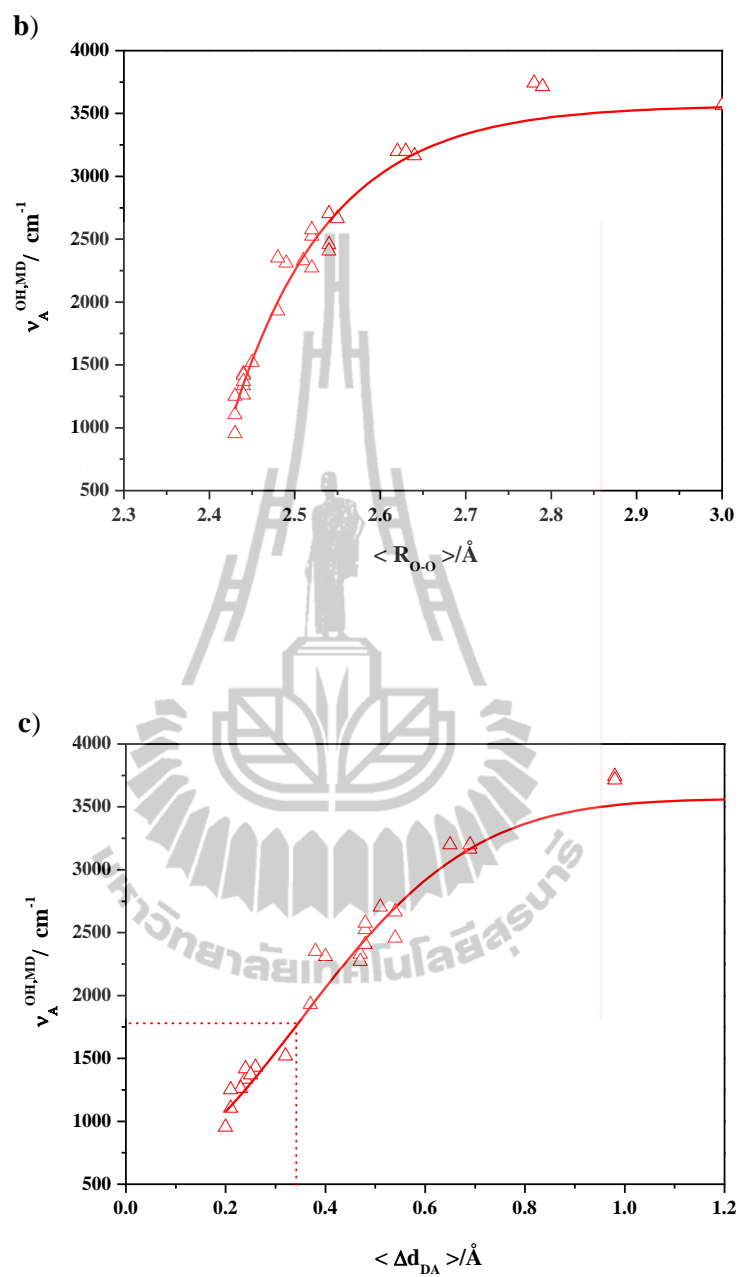


Figure 3.12 (Continued).

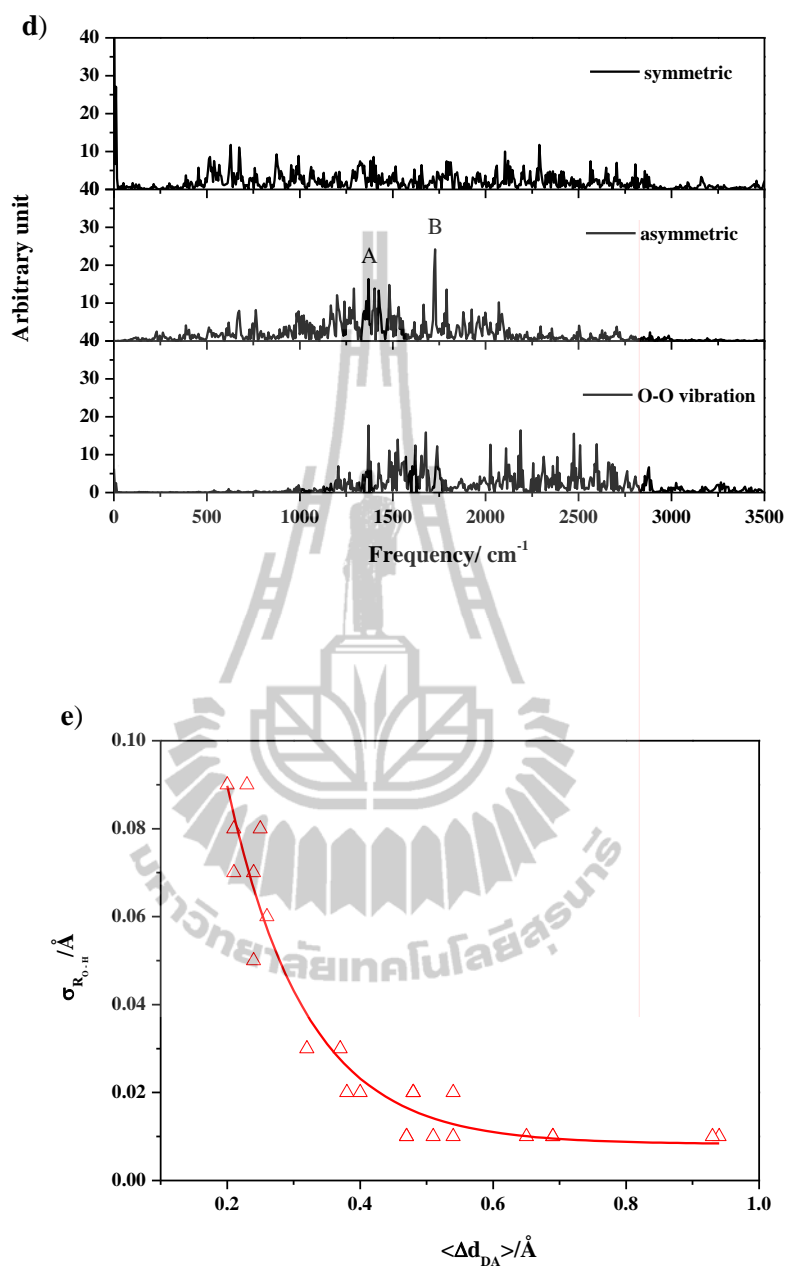


Figure 3.12 (Continued).

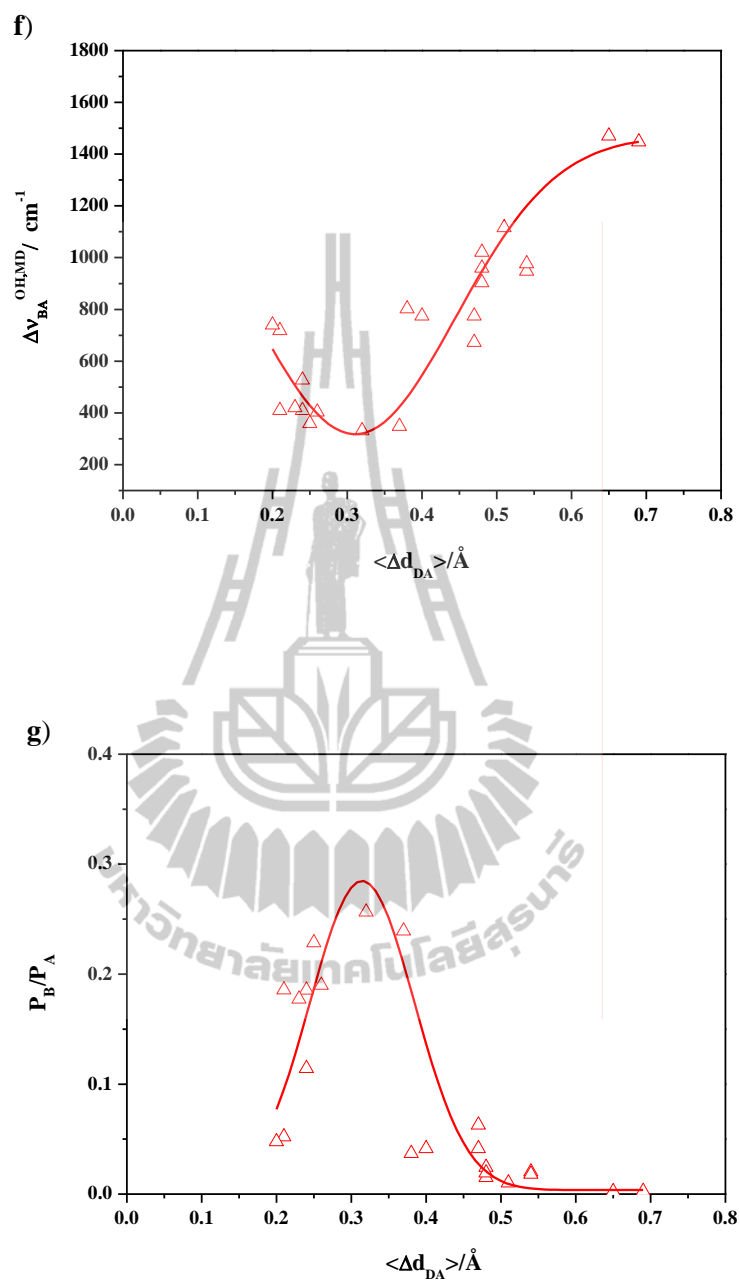


Figure 3.12 (Continued).

### Dynamics of proton transfer and diffusion coefficients

To discuss the dynamics of proton transfer in the  $\text{CF}_3\text{SO}_3^- - \text{H}_3\text{O}^+ - n\text{H}_2\text{O}$  complexes,  $n = 1 - 4$ , the distributions of the proton diffusion coefficients ( $D$ ) for the H-bonds susceptible to proton transfer ( $v_A^{\text{OH}, \text{MD}} < v_A^{\text{OH}^*, \text{MD}}$ ) were computed and shown in Figure 3.13. It appeared that  $D$  can vary in a quite wide range, with a maximum at  $6.7 \times 10^{-5} \text{ cm}^2 \text{ s}^{-1}$  in continuum aqueous solution; represented by the H-bonds in **Group 2** (pass-by mechanism). This could be used in the discussion of the effects of the  $\text{CF}_3\text{SO}_3^-$  group, by comparison with the results in the  $\text{CF}_3\text{SO}_3\text{H} - \text{H}_3\text{O}^+ - n\text{H}_2\text{O}$  complexes,  $n = 1 - 3$ , (Phonyiem, Chaiwongwattana, Lao-ngam, and Sagarik, 2011) and the protonated water clusters (Lao-ngam, Asawakun, Wannarat, and Sagarik, 2011). It should be noted that the most populated proton diffusion coefficient computed in the present work is higher than that in the  $\text{CF}_3\text{SO}_3\text{H} - \text{H}_3\text{O}^+ - n\text{H}_2\text{O}$  complexes,  $n = 1 - 3$ , ( $3.2 \times 10^{-5} \text{ cm}^2 \text{ s}^{-1}$ ), but considerably lower than those in the protonated water clusters.

In order to obtain additional kinetics information from BOMD simulations, the lifetimes ( $\tau$ ) of the H-bonds with high relative probability of finding the structural diffusion motion ( $\mathbf{P}_B/\mathbf{P}_A$ ) were computed from VACF of the O-O vibrations (Bopp, 1986); based on the observation that the relaxation behavior of the envelope of VACF can be approximated by an exponential function and the shared-proton structures possess shorter lifetimes than the contact structures ( $\text{O-H}^+\text{..O}$ ) (Kreuer, 2000) The classical first-order rate constants ( $k$ ) for the interconversion between these two limiting structures were approximated from the lifetimes. In the present study, the lifetimes of H-bond (4) in structure **k** was computed as an

examples;  $\tau = 146$  fs, corresponding to  $k = 9.5$  ps<sup>-1</sup>. The lifetimes are shorter and the first-order rate constants are larger than those obtained from the protonated water cluster (Lao-ngam, Asawakun, Wannarat, and Sagarik, 2011). For the protonated water cluster in continuum aqueous solution, the shared-proton structure with the highest  $\mathbf{P}_B/\mathbf{P}_A$  possesses  $\tau = 233$  fs and  $k = 6.0$  ps<sup>-1</sup>. The values reflect a higher rate for the interconversion between the shared-proton and contact structures in the presence of the  $\text{CF}_3\text{SO}_3^-$  group.

Remarks should be made on the dynamics and kinetics in the presence of the  $\text{CF}_3\text{SO}_3^-$  group. Comparison of the most probable proton diffusion coefficient in the  $\text{CF}_3\text{SO}_3^- - \text{H}_3\text{O}^+ - \text{H}_2\text{O}$  1 : 1 : 4 complexes ( $D = 6.2 \times 10^{-5}$  cm<sup>2</sup> s<sup>-1</sup>, in continuum aqueous solution) and the corresponding value in the protonated water clusters (Lao-ngam, Asawakun, Wannarat, and Sagarik, 2011) leads to an important conclusion; the transferring proton in the protonated water cluster with an extended H-bond network possesses  $D = 8.2 \times 10^{-5}$  cm<sup>2</sup> s<sup>-1</sup>, in the continuum aqueous solution. The values suggested that the  $\text{CF}_3\text{SO}_3^-$  group suppresses the mobility of the transferring proton in the intermediate state. This results in lower proton diffusion coefficients in the  $\text{CF}_3\text{SO}_3^- - \text{H}_3\text{O}^+ - n\text{H}_2\text{O}$  complexes,  $n = 1 - 4$ , compared to the protonated water clusters. However, the presence of the  $-\text{SO}_3^-$  group results in a decrease of  $\Delta v_{\text{BA}}^{\text{OH}, \text{MD}}$  and increases the relative probability of finding the structural diffusion motion ( $\mathbf{P}_B/\mathbf{P}_A$ ) in the shared-proton structure, leading eventually to higher first-order rate constants ( $k$ ) in the  $\text{CF}_3\text{SO}_3^- - \text{H}_3\text{O}^+ - n\text{H}_2\text{O}$  complexes,  $n = 1 - 4$ . One could therefore conclude that the  $\text{CF}_3\text{SO}_3^-$  groups in Nafion<sup>®</sup> act as active

binding sites which provide appropriate structural, energetic and dynamic conditions for effective structural diffusion processes in the intermediate states of proton transfer reactions.

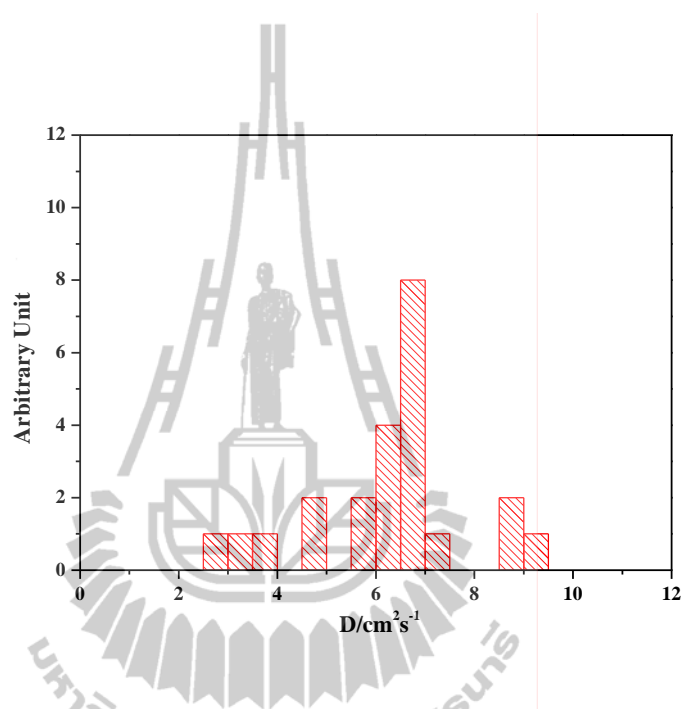


**Figure 3.13** Distributions of the diffusion coefficients (D) of the transferring proton in the  $\text{CF}_3\text{SO}_3^- - \text{H}_3\text{O}^+ - n\text{H}_2\text{O}$  complexes,  $n = 1 - 4$ , for pass-by mechanism, obtained from BOMD simulations at 350 K.

## CHAPTER IV

### CONCLUSION

Attempt has been made in the present work to study proton transfer reactions at a hydrophilic functional group in model Nafion<sup>®</sup>, using theoretical methods which take into account the dynamics of formation and cleavage of covalent and H-bonds. The H-bond complexes formed from  $\text{CF}_3\text{SO}_3^-$ ,  $\text{H}_3\text{O}^+$  and  $n\text{H}_2\text{O}$ ,  $n = 1 - 4$ , were employed as model systems, from which the dynamics of an excess proton and proton defects at and in the vicinity of  $-\text{SO}_3^-$  were systematically studied, with the emphasis on how  $-\text{SO}_3^-$  facilitate or mediate proton transfer reactions at low hydration levels. In order to provide fundamental information for the investigations on the proton transfer reactions at a hydrophobic group of Nafion, characteristics of the transferring protons in protonated water clusters were studied. The theoretical investigations began with searching for the H-bond complexes which could be important in the dynamic proton transfer pathways, as well as characteristic H-bond structures and IR spectra of the transferring protons, both in the gas phase and continuum aqueous solution using the DFT method at the B3LYP/TZVP level of accuracy. A series of BOMD simulations at 350 K was performed based on B3LYP/TZVP calculations. Attention was focused on the precursors and transition states with H-bonds susceptible to proton transfers.

DFT calculations at the B3LYP/TZVP level revealed that the potential H-bond structures consist of the Zundel complex, with the characteristic asymmetric O-H stretching frequencies ( $\nu^{\text{OH}}$ )  $< 1000 \text{ cm}^{-1}$  and the threshold frequencies for proton transfers in the gas phase and continuum aqueous solution at  $\nu^{\text{OH}^*} = 1984$  and  $1881 \text{ cm}^{-1}$ , respectively. According to the results obtained from the static proton transfer potentials, the trends of the interaction energies with respect to the number of water molecules in the gas phase and continuum aqueous solution are quite similar. The destabilization effects caused by the continuum aqueous solvent bring about smaller variation of the interaction energies with respect to the number of water molecules compared to the gas phase. The destabilization effects also lead to shifts of the transferring protons away from the centers, especially for the H-bond complexes with the Zundel complex as the central charged species. The trend of the solvation energies revealed that, when the number of water molecules is the same, the H-bonds inside the protonated water clusters experience comparable uniform electric field.

BOMD simulations at 350 K predicted the characteristic asymmetric O-H stretching frequencies in a quite wide range, from  $940$  to  $1740 \text{ cm}^{-1}$ . Most importantly, BOMD simulations suggested additional characteristic asymmetric O-H stretching bands at higher frequencies. They are in the range of  $1640$  and  $2600 \text{ cm}^{-1}$ . The low-frequency bands are regarded as the “oscillatory shuttling band” and the high-frequency bands the “structural diffusion band”. The latter cannot be determined easily from static proton transfer potentials, due to the anharmonic and dynamic behaviors of the vibrational motions of the transferring protons. The oscillatory shuttling and structural diffusion bands could be considered as the spectroscopic



evidences for the shared-proton complex and product (or precursor) formations, respectively.

The analyses of the H-bond structures and  $\nu^{\text{OH, MD}}$  yielded the threshold frequencies ( $\nu_{\text{A}}^{\text{OH}^*, \text{MD}}$ ) for the proton transfers in the gas phase and continuum aqueous solution at  $\nu_{\text{A}}^{\text{OH}^*, \text{MD}} = 1917$  and  $1736 \text{ cm}^{-1}$ , respectively. Because the quasi-dynamic equilibrium between the Zundel and Eigen complexes was suggested to be the rate-determining step, in order to achieve an “ideal” maximum efficiency, a concerted proton transfer pathway should be taken. The present results anticipated that the effective interconversion between the two proton states, the Zundel-like and hydronium-like structures, could be reflected from comparable intensities of the oscillatory shuttling and structural diffusion bands. The vibrational energy for the interconversion between the two dynamic states ( $\Delta\nu_{\text{BA}}^{\text{OH, MD}}$ ) can be approximated from the difference between  $\nu_{\text{B}}^{\text{OH, MD}}$  and  $\nu_{\text{A}}^{\text{OH, MD}}$ , for the protonated water clusters,  $\Delta\nu_{\text{BA}}^{\text{OH, MD}} = 473 \text{ cm}^{-1}$  or  $5.7 \text{ kJ/mol}$ . The probability of finding a physical system in a certain energy state is proportional to the Boltzmann factor, the probability of finding the structural diffusion motion relative to the oscillatory shuttling motion ( $\mathbf{P}_{\text{B}}/\mathbf{P}_{\text{A}}$ ) is proportional to  $e^{-\Delta\nu_{\text{BA}}^{\text{OH, MD}}/RT}$ , the plot of  $\mathbf{P}_{\text{B}}/\mathbf{P}_{\text{A}}$  and  $\langle \Delta d_{\text{DA}} \rangle$  suggested the maximum probability of finding the structural diffusion motion relative to the oscillatory shuttling motion,  $\mathbf{P}_{\text{B}}/\mathbf{P}_{\text{A}} = 0.17$  at  $\langle \Delta d_{\text{DA}} \rangle = 0.27 \text{ \AA}$ . At larger  $\langle \Delta d_{\text{DA}} \rangle$ , the H-bond becomes weaker and  $\mathbf{P}_{\text{B}}/\mathbf{P}_{\text{A}}$  decreases, especially when  $\nu_{\text{A}}^{\text{OH, MD}} > \nu_{\text{A}}^{\text{OH}^*, \text{MD}}$ . These pieces of information could provide an appropriate IR spectroscopic method to investigate proton transfer reactions in larger model systems, and iterated the

necessity to incorporate the thermal energy fluctuations and dynamics in the model calculations.

For proton transfer reactions and dynamics at a hydrophilic group of Nafion<sup>®</sup>, the B3LYP/TZVP results suggested two types of structural diffusion mechanisms namely, the pass-through mechanism, involving the protonation and deprotonation at the  $-\text{SO}_3^-$  group, and the pass-by mechanism, the proton transfer in the adjacent Zundel complex. From the static results, asymmetric stretching coordinate ( $\Delta d_{\text{DA}}$ ) and O-H stretching frequency ( $\nu^{\text{OH}}$ ) suggested higher tendency for proton transfer in the continuum aqueous solution with  $\Delta d_{\text{DA}}^* = 0.36 \text{ \AA}$   $\nu^{\text{OH}*} = 1921 \text{ cm}^{-1}$ .

BOMD simulations at 350 K predicted slightly lower threshold frequencies for proton transfer,  $\nu_{\text{A}}^{\text{OH}, \text{MD}} = 1820 \text{ cm}^{-1}$ , compared to those in B3LYP/TZVP results. The analyses of  $\nu_{\text{A}}^{\text{OH}, \text{MD}}$  and  $\nu_{\text{B}}^{\text{OH}, \text{MD}}$  suggested the lowest  $\Delta \nu_{\text{BA}}^{\text{OH}, \text{MD}}$  for pass-by mechanisms of  $318 \text{ cm}^{-1}$ . This is about 80 and  $155 \text{ cm}^{-1}$  lower than those observed in  $\text{CF}_3\text{SO}_3\text{H} - \text{H}_3\text{O}^+ - n\text{H}_2\text{O}$ ,  $n = 1 - 3$ , and the protonated water clusters; an indication of a decrease of the vibrational energy for the interconversion between the oscillatory shuttling and structural diffusion motions in the presence of the  $-\text{SO}_3^-$  group.

The proton diffusion coefficients obtained in the  $\text{CF}_3\text{SO}_3^- - \text{H}_3\text{O}^+ - n\text{H}_2\text{O}$  complexes,  $n = 1 - 4$ , was slightly predicted higher than those in the  $\text{CF}_3\text{SO}_3\text{H} - \text{H}_3\text{O}^+ - n\text{H}_2\text{O}$  complexes,  $n = 1 - 3$ , but lower than those in the protonated water clusters, indicated that the  $-\text{SO}_3^-$  group suppresses the mobility of the transferring proton in the intermediate states, by introducing strong electrostatic effect at the shared-proton structures. These are however accompanied by a decrease

of the vibrational energy for the interconversion between the oscillatory shuttling and structural diffusion motions and a higher relative probability of finding the structural diffusion motion in the  $\text{CF}_3\text{SO}_3^- - \text{H}_3\text{O}^+ - n\text{H}_2\text{O}$  complexes,  $n = 1 - 4$ , compared to those in the protonated water clusters. One could, therefore, conclude that the  $-\text{SO}_3^-$  groups in Nafion<sup>®</sup> act as active binding sites which provide appropriate structural, energetic and dynamic conditions for effective structural diffusion processes in the intermediate states of proton transfer reactions. The present results confirmed that, due to the coupling among various vibrational modes in H-bonds, the discussions on proton transfer reactions cannot be made based solely on static proton transfer potentials. Inclusion of thermal energy fluctuations and dynamics in the model calculations, as in the case of BOMD simulations, together with systematic IR spectral analyses, has been proved to be the most appropriate theoretical approaches.



## REFERENCES

## REFERENCES

- Agmon, N. (1995). The Grotthuss mechanism. **Chemical Physics Letters**. 244: 456-462.
- Ahlrichs, R., Bär, M., Häser, M., Horn, H. and Kölmel, C. (1989). Electronic structure calculations on workstation computers: The program system turbomole. **Chemical Physics Letters**. 162: 165-169.
- Allen, M. P. and Tildesley, D. J. (1987). **Computer Simulation of Liquids**. New York: Oxford University Press.
- Asbury, J. B., Steinel, T. and Fayer, M. D. (2004). Vibrational echo correlation spectroscopy probes of hydrogen bond dynamics in water and methanol. **Journal of Luminescence**. 107: 271-286.
- Asmis, K. R., Pivonka, N. L., Santambrogio, G., Brummer, M., Kaposta, C., Neumark, D. M. and Woste, L. (2003). Gas-phase infrared spectrum of the protonated water dimer. **Science**. 299: 1375-1377.
- Balbuena, P. B. and Seminario, J. M. (1999). **Theoretical and Computational Chemistry 7**. Amsterdam: Elsevier.
- Barnett, R. N. and Landman, U. (1993). Born-Oppenheimer molecular-dynamics simulations of finite systems: Structure and dynamics of (H<sub>2</sub>O)<sub>2</sub>. **Physical Review B**. 48: 2081.

- Becke, A. D. (1993). Density-functional thermochemistry. III. The role of exact exchange. **The Journal of Chemical Physics**. 98: 5648-5652.
- Benoit, M. and Marx, D. (2005). The shapes of protons in hydrogen bonds depend on the bond length. **ChemPhysChem**. 6: 1738-1741.
- Bernal, J. D. and Fowler, R. H. (1933). A Theory of water and ionic solution, with particular reference to hydrogen and hydroxyl ions. **The Journal of Chemical Physics**. 1: 515-548.
- Bopp, P. (1986). A study of the vibrational motions of water in an aqueous  $\text{CaCl}_2$  solution. **Chemical Physics**. 106: 205-212.
- Botti, A., Bruni, F., Imberti, S., Ricci, M. A. and Soper, A. K. (2005). Solvation shell of  $\text{H}^+$  ions in water. **Journal of Molecular Liquids**. 117: 77-79.
- Boys, S. F. and Bernardi, F. (1970). The calculation of small molecular interactions by the differences of separate total energies. Some procedures with reduced errors **Molecular Physics**. 19: 533-556.
- Bowman, J. M., Carrington, T. and Meyer, H.-D. (2008). Variational quantum approaches for computing vibrational energies of polyatomic molecules. **Molecular Physics**. 106: 2145-2182.
- Buzzoni, R., Bordiga, S., Ricchiardi, G., Spoto, G. and Zecchina, A. (1995). Interaction of  $\text{H}_2\text{O}$ ,  $\text{CH}_3\text{OH}$ ,  $(\text{CH}_3)_2\text{O}$ ,  $\text{CH}_3\text{CN}$ , and pyridine with the superacid perfluorosulfonic membrane Nafion: An IR and Raman study. **The Journal of Physical Chemistry**. 99: 11937-11951.

- Cappa, C. D., Smith, J. D., Messer, B. M., Cohen, R. C. and Saykally, R. J. (2005). The electronic structure of the hydrated proton: A comparative x-ray absorption study of aqueous HCl and NaCl solutions. **The Journal of Physical Chemistry B**. 110: 1166-1171.
- Chen, J., McAllister, M. A., Lee, J. K. and Houk, K. N. (1998). Short, strong hydrogen bonds in the gas phase and in solution: Theoretical exploration of pKa matching and environmental effects on the strengths of hydrogen bonds and their potential roles in enzymatic catalysis. **The Journal of Organic Chemistry**. 63: 4611-4619.
- Cheng, H.-P. and Krause, J. L. (1997). The dynamics of proton transfer in  $\text{H}_3\text{O}_2^+$ . **The Journal of Chemical Physics**. 107: 8461-8468.
- Choe, Y.-K., Tsuchida, E., Ikeshoji, T., Ohira, A. and Kidena, K. (2010). An *ab initio* modeling study on a modeled hydrated polymer electrolyte membrane, sulfonated polyethersulfone (SPES). **The Journal of Physical Chemistry B**. 114: 2411-2421.
- Conway, B. E., Bockris, J. O. M. and Linton, H. (1956). Proton conductance and the existence of the  $\text{H}_3\text{O}^+$  ion. **The Journal of Chemical Physics**. 24: 834-850.
- Cramer, C. J. (2002). **Essentials of Computational Chemistry: Theory and models**: John Wiley & Sons, Ltd.
- Deeying, N. (2005). **Influence of metal ion and solute conformation change on hydration of small amino acid**. Ph.D. Dissertation, Suranaree University of Technology, Thailand.

- Devanathan, R., Venkatnathan, A. and Dupuis, M. (2007). Atomistic simulation of Nafion membrane. 2. Dynamics of water molecules and hydronium Ions. **The Journal of Physical Chemistry B**. 111: 13006-13013.
- Eikerling, M., Paddison, S. J., Pratt, L. R. and Zawodzinski, T. A. (2003). Defect structure for proton transport in a triflic acid monohydrate solid. **Chemical Physics Letters**. 368: 108-114.
- Fridgen, T. D., McMahon, T. B., MacAleese, L., Lemaire, J. and Maitre, P. (2004). Infrared spectrum of the protonated water dimer in the gas phase. **The Journal of Physical Chemistry A**. 108: 9008-9010.
- Gejji, S. P., Hermansson, K. and Lindgren, J. (1994). Structure and vibrational frequencies of the molecular trichloromethanesulfonic acid and its anion from *ab initio* calculations. **The Journal of Physical Chemistry**. 98: 8687-8692.
- Gierke, T. D., Munn, G. E. and Wilson, F. C. (1981). The morphology in nafion perfluorinated membrane products, as determined by wide- and small-angle x-ray studies. *Journal of Polymer Science: Polymer Physics Edition*. 19: 1687-1704.
- Giguere, P. A. (1979). The great fallacy of the  $H^+$  ion: And the true nature of  $H_3O^+$ . **Journal of Chemical Education**. 56: 571-null.
- Glezakou, V.-A., Dupuis, M. and Mundy, C. J. (2007). Acid/base equilibria in clusters and their role in proton exchange membranes: Computational insight. **Physical Chemistry Chemical Physics**. 9: 5752-5760.
- Haile, J. M. (1997). **Molecular Dynamics Simulations**. New York: John Wiley & Sons Ltd.



- Hammer, N. I., Diken, E. G., Roscioli, J. R., Johnson, M. A., Myshakin, E. M., Jordan, K. D., McCoy, A. B., Huang, X., Bowman, J. M. and Carter, S. (2005). The vibrational predissociation spectra of the  $\text{H}_5\text{O}_2^+$ .  $\text{RG}_n(\text{RG} = \text{Ar,Ne})$  clusters: Correlation of the solvent perturbations in the free OH and shared proton transitions of the Zundel ion. **The Journal of Chemical Physics**. 122: 244301.
- Han, J., Zhou, X. and Liu, H. (2006). Ab initio simulation on the mechanism of proton transport in water. **Journal of Power Sources**. 161: 1420-1427.
- Hermida-Ramón, J. M. and Karlström, G. (2004). Study of the hydronium ion in water. A combined quantum chemical and statistical mechanical treatment. **Journal of Molecular Structure: THEOCHEM**. 712: 167-173.
- Hibbert, F. and Emsley, J. (1991). Hydrogen bonding and chemical reactivity. **Advances in Physical Organic Chemistry**. 26: 255-379.
- Huisken, F., Mohammad-Pooran, S. and Werhahn, O. (1998). Vibrational spectroscopy of single methanol molecules attached to liquid water clusters. **Chemical Physics**. 239: 11-22.
- Hunter, E. P. L. and Lias, S. G. (1998). Evaluated Gas Phase Basicities and Proton Affinities of Molecules: An Update. **Journal of Physical and Chemical Reference Data**. 27: 413-656.
- Idupulapati, N., Devanathan, R. and Dupuis, M. (2010). *Ab initio* study of hydration and proton dissociation in ionomer membranes. **The Journal of Physical Chemistry A**. 114: 6904-6912.

- Iftimie, R., Thomas, V., Plessis, S., Marchand, P. and Ayotte, P. (2008). Spectral signatures and molecular origin of acid dissociation intermediates. **Journal of the American Chemical Society**. 130: 5901-5907.
- Jiang, J. C., Chaudhuri, C., Lee, Y. T. and Chang, H. C. (2002). Hydrogen bond rearrangements and interconversions of  $\text{H}^+(\text{CH}_3\text{OH})_4\text{H}_2\text{O}$  cluster isomers. **The Journal of Physical Chemistry A**. 106: 10937-10944.
- Jing, X., Troullier, N., Dean, D., Binggeli, N., Chelikowsky, J. R., Wu, K. and Saad, Y. (1994). Ab initio molecular-dynamics simulations of Si clusters using the higher-order finite-difference-pseudopotential method. **Physical Review B**. 50: 12234.
- Komatsuzaki, T. and Ohmine, I. (1994). Energetics of proton transfer in liquid water. I. Ab initio study for origin of many-body interaction and potential energy surfaces. **Chemical Physics**. 180: 239-269.
- Kornyshev, A. A., Kuznetsov, A. M., Spohr, E. and Ulstrup, J. (2003). Kinetics of proton transport in water. **The Journal of Physical Chemistry B**. 107: 3351-3366.
- Kreuer, K.-D. (1996). Proton conductivity: Materials and applications. **Chemistry of Materials**. 8: 610-641.
- Kreuer, K.-D. (2000). On the complexity of proton conduction phenomena. **Solid State Ionics** 136: 149-160.
- Kreuer, K.-D., Paddison, S. J., Spohr, E. and Schuster, M. (2004). Transport in proton conductors for fuel-cell applications: simulations, elementary reactions, and phenomenology. **Chemical Reviews**. 104: 4637-4678.

- Lao-ngam, C., Asawakun, P., Wannarat, S. and Sagarik, K. (2011). Proton transfer reactions and dynamics in protonated water clusters. **Physical Chemistry Chemical Physics**. 13: 4562-4575.
- Lapid, H., Agmon, N., Petersen, M. K. and Voth, G. A. (2005). A bond-order analysis of the mechanism for hydrated proton mobility in liquid water. **The Journal of Chemical Physics**. 122: 014506.
- Laporta, M., Pegoraro, M. and Zanderighi, L. (1999). Perfluorosulfonated membrane (Nafion): FT-IR study of the state of water with increasing humidity. **Physical Chemistry Chemical Physics**. 1: 4619-4628.
- Larminie, J. and Dicks, A. (2001). *Fuel Cell Systems Explained*. Chichester: John Wiley & Son, Ltd.
- Leach, A. R. (1996). **Molecular Modelling: Principles and Applications**. : Addison Wesley Longman Limited.
- Lee, C., Yang, W. and Parr, R. G. (1988). Development of the Colle-Salvetti correlation-energy formula into a functional of the electron density. **Physical Review B**. 37: 785.
- Lobaugh, J. and Voth, G. A. (1995). The quantum dynamics of an excess proton in water. **The Journal of Chemical Physics**. 104: 2056-2069.
- Marx, D., Tuckerman, M. E., Hutter, J. and Parrinello, M. (1999). The nature of the hydrated excess proton in water. **Nature**. 397: 601-604.
- Mauritz, K. A. and Moore, R. B. (2004). State of understanding of Nafion. **Chemical Reviews**. 104: 4535-4586.

- Morrone, J. A., Haslinger, K. E. and Tuckerman, M. E. (2006). *Ab initio* molecular dynamics simulation of the structure and proton transport dynamics of methanol-water solutions. **The Journal of Physical Chemistry B**. 110: 3712-3720.
- Okumura, M., Yeh, L. I., Myers, J. D. and Lee, Y. T. (1990). Infrared spectra of the solvated hydronium ion: Vibrational predissociation spectroscopy of mass-selected  $\text{H}_3\text{O}^+(\text{H}_2\text{O})_n(\text{H}_2)_m$ . **The Journal of Physical Chemistry**. 94: 3416-3427.
- Paddison, S. J. (2001). The modeling of molecular structure and ion transport in sulfonic acid based ionomer membranes. **Journal of New Materials for Electrochemical Systems**. 4: 197-207.
- Paddison, S. J. (2003). Proton conduction mechanisms at low degrees of hydration in sulfonic acid-based polymer electrolyte membranes. **Annual Review of Materials Research**. 33: 289-319.
- Paddison, S. J. and Elliott, J. A. (2005). Molecular modeling of the short-side-chain perfluorosulfonic acid membrane. **The Journal of Physical Chemistry A**. 109: 7583-7593.
- Paddison, S. J. and Elliott, J. A. (2006). On the consequences of side chain flexibility and backbone conformation on hydration and proton dissociation in perfluorosulfonic acid membranes. **Physical Chemistry Chemical Physics**. 8: 2193-2203.
- Paddison, S. J., Pratt, L. R. and Zawodzinski Jr., T. A. (1999). Conformations of perfluoroether sulfonic acid side chains for the modeling of Nafion. **Journal of New Materials for Electrochemical Systems**. 2: 183-188.

- Paddison, S. J., Pratt, L. R. and Zawodzinski Jr., T. A. (2001). Variation of the Dissociation Constant of Triflic Acid with Hydration. **The Journal of Physical Chemistry A**. 105: 6266-6268.
- Paddison, S. J. and Zawodzinski Jr, T. A. (1998). Molecular modeling of the pendant chain in Nafion. **Solid State Ionics**. 115: 333-340.
- Park, M., Shin, I., Singh, N. J. and Kim, K. S. (2007). Eigen and Zundel forms of small protonated water clusters: Structures and infrared spectra. **The Journal of Physical Chemistry A**. 111: 10692-10702.
- Parthasarathi, R., Subramanian, V. and Sathyamurthy, N. (2007). Hydrogen bonding in protonated water clusters: An atoms-in-molecules perspective. **The Journal of Physical Chemistry A**. 111: 13287-13290.
- Phonyiem, M., Chaiwongwattana, S., Lao-ngam, C. and Sagarik, K. (2011). Proton transfer reactions and dynamics of sulfonic acid group of Nafion<sup>®</sup>. **Physical Chemistry Chemical Physics**. 13: 10923-10939.
- Rapaport, D. C. (1995). **The Art of Molecular Dynamics Simulation**. London: Cambridge University Press.
- Rejnek, J., Hanus, M., Kabelac, M., Ryjacek, F. and Hobza, P. (2005). Correlated ab initio study of nucleic acid bases and their tautomers in the gas phase, in a microhydrated environment and in aqueous solution. Part 4. Uracil and thymine. **Physical Chemistry Chemical Physics**. 7: 2006-2017.
- Rospenk, M., Fritsch, J. and Zundel, G. (1984). Solvent effect on the proton-transfer equilibria and thermodynamic data of the hydrogen bond in a Mannich base. **The Journal of Physical Chemistry**. 88: 321-323.

- Sadeghi, R. R. and Cheng, H.-P. (1999). The dynamics of proton transfer in a water chain. **The Journal of Chemical Physics**. 111: 2086-2094.
- Sagarik, K. (1999). Theoretical studies on hydrogen bonding in hydroxylamine clusters and liquid. **Journal of Molecular Structure: THEOCHEM**. 465: 141-155.
- Sagarik, K. and Ahlrichs, R. (1987). A test particle model potential for formamide and molecular dynamics simulations of the liquid. **The Journal of Chemical Physics**. 86: 5117-5126.
- Sagarik, K. and Asawakun, P. (1997). Intermolecular potential for phenol based on the test particle model. **Chemical Physics**. 219: 173-191.
- Sagarik, K., Chaiwongwattana, S. and Sisot, P. (2004). A theoretical study on clusters of benzoic acid-water in benzene solutions. **Chemical Physics**. 306: 1-12.
- Sagarik, K., Chaiwongwattana, S., Vchirawongkwin, V. and Prueksaaron, S. (2010). Proton transfer reactions and dynamics in  $\text{CH}_3\text{OH}-\text{H}_3\text{O}^+-\text{H}_2\text{O}$  complexes. **Physical Chemistry Chemical Physics**. 12: 918-929.
- Sagarik, K. and Chaiyapongs, S. (2005). Structures and stability of salt-bridge in aqueous solution. **Biophysical Chemistry**. 117: 119-140.
- Sagarik, K., Phonyiem, M., Lao-ngam, C. and Chaiwongwattana, S. (2008). Mechanisms of proton transfer in Nafion: Elementary reactions at the sulfonic acid groups. **Physical Chemistry Chemical Physics**. 10: 2098-2112.
- Sagarik, K., Pongpituk, V., Chaiyapongs, S. and Sisot, P. (1991). Test-particle model potentials for hydrogen-bonded complexes: Complexes formed from HCN, HF,  $\text{H}_2\text{O}$ ,  $\text{NH}_3$ ,  $\text{HCONH}_2$ ,  $\text{HCONHCH}_3$ , guanine and cytosine. **Chemical Physics**. 156: 439-456.

- Sagarik, K. and Rode, B. M. (2000). Intermolecular potential for benzoic acid-water based on the test-particle model and statistical mechanical simulations of benzoic acid in aqueous solutions. **Chemical Physics**. 260: 159-182.
- Sagarik, K. and Spohr, E. (1995). Statistical mechanical simulations on properties of liquid pyridine. **Chemical Physics**. 199: 73-82.
- Santambrogio, G., Brummer, M., Woste, L., Dobler, J., Sierka, M., Sauer, J., Meijer, G. and Asmis, K. R. (2008). Gas phase vibrational spectroscopy of mass-selected vanadium oxide anions. **Physical Chemistry Chemical Physics**. 10: 3992-4005.
- Schafer, A., Huber, C. and Ahlrichs, R. (1994). Fully optimized contracted Gaussian basis sets of triple zeta valence quality for atoms Li to Kr. **The Journal of Chemical Physics**. 100: 5829-5835.
- Schmitt, U. W. and Voth, G. A. (1999). The computer simulation of proton transport in water. **The Journal of Chemical Physics**. 111: 9361-9381.
- Schwarz, H. A. (1977). Gas phase infrared spectra of oxonium hydrate ions from 2 to 5  $\mu$ . **The Journal of Chemical Physics**. 67: 5525-5534.
- Scott, A. P. and Radom, L. (1996). Harmonic vibrational frequencies: An evaluation of Hartree-Fock, Moller-Plesset, quadratic configuration interaction, density functional theory, and semiempirical scale factors. **The Journal of Physical Chemistry**. 100: 16502-16513.
- Smitha, B., Sridhar, S. and Khan, A. A. (2005). Solid polymer electrolyte membranes for fuel cell applications-a review. **Journal of Membrane Science**. 259: 10-26.

- Spohr, E., Commer, P. and Kornyshev, A. A. (2002). Enhancing proton mobility in polymer electrolyte membranes: Lessons from molecular dynamics simulations. **The Journal of Physical Chemistry B**. 106: 10560-10569.
- Stearn, A. E. and Eyring, H. (1937). The deduction of reaction mechanisms from the theory of absolute rates. **The Journal of Chemical Physics**. 5: 113-124.
- Termath, V. and Sauer, J. (1997). *Ab initio* molecular dynamics simulation of  $\text{H}_5\text{O}_2^+$  and  $\text{H}_7\text{O}_3^+$  gas phase clusters based on density functional theory **Molecular Physics**. 91: 963-975.
- Treutler, O. and Ahlrichs, R. (1995). Efficient molecular numerical integration schemes. **The Journal of Chemical Physics**. 102: 346-354.
- Tsuda, M., Arboleda Jr, N. B. and Kasai, H. (2006). Initial driving force for proton transfer in Nafion. **Chemical Physics**. 324: 393-397.
- Tuckerman, M. E., Laasonen, K., Sprik, M. and Parrinello, M. (1995). *Ab initio* molecular dynamics simulation of the solvation and transport of hydronium and hydroxyl ions in water. **The Journal of Chemical Physics**. 103: 150-161.
- Tuckerman, M. E., Marx, D., Klein, M. L. and Parrinello, M. (1997). On the quantum nature of the shared proton in hydrogen bonds. **Science**. 275: 817-820.
- Vuilleumier, R. and Borgis, D. (1999). Transport and spectroscopy of the hydrated proton: A molecular dynamics study. **The Journal of Chemical Physics**. 111: 4251-4266.
- Wu, C. C., Chaudhuri, C., Jiang, J. C., Lee, Y. T. and Chang, H. C. (2003). Structural isomerism and competitive proton solvation between methanol and water in  $\text{H}^+(\text{CH}_3\text{OH})_m(\text{H}_2\text{O})_n$ ,  $m + n = 4$ . **The Journal of Physical Chemistry A**. 108: 2859-2866.



- Wu, C. C., Jiang, J. C., Boo, D. W., Lin, S. H., Lee, Y. T. and Chang, H.-C. (2000). Behaviors of an excess proton in solute-containing water clusters: A case study of  $\text{H}^+(\text{CH}_3\text{OH})(\text{H}_2\text{O})_{1-6}$ . **The Journal of Chemical Physics**. 112: 176-188.
- Wu, Y., Chen, H., Wang, F., Paesani, F. and Voth, G. A. (2007). An improved multistate empirical valence bond model for aqueous proton solvation and transport. **The Journal of Physical Chemistry B**. 112: 467-482.
- Xenides, D., Randolph, B. R. and Rode, B. M. (2005). Structure and ultrafast dynamics of liquid water: A quantum mechanics/molecular mechanics molecular dynamics simulations study. **The Journal of Chemical Physics**. 122: 174506.
- Zundel, G. and Fritsch, J. (1984). Environmental interaction of hydrogen bonds showing a large proton polarizability. Molecular processes and the thermodynamics of acid dissociation. **The Journal of Physical Chemistry**. 88: 6295-6302.



**APPENDICES**



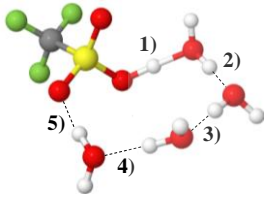
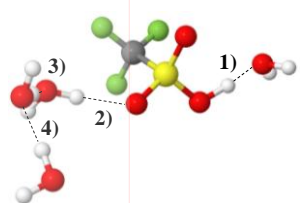
**APPENDIX A**

**SUPPLEMENTARY RESULTS**

**FOR THE  $\text{CF}_3\text{SO}_3^- - \text{H}_3\text{O}^+ - n\text{H}_2\text{O}$  complexes,**

**$n = 1 - 4$**

**Table A.1** Static results of the  $\text{CF}_3\text{SO}_3^- - \text{H}_3\text{O}^+ - n\text{H}_2\text{O}$  complexes,  $n = 1 - 4$ , obtained from B3LYP/TZVP calculations, both in the gas phase and continuum aqueous solution. Distances and energies are in Å and kJ/mol, respectively

Gas			Cosmo			
						
$R_{\text{O}-\text{O}}$	$R_{\text{O}-\text{H}}$	$\Delta E$	$R_{\text{O}-\text{O}}$	$R_{\text{O}-\text{H}}$	$\Delta E$	$\Delta E^{\text{sol}}$
1) 2.45	1.10	-259.9	1) 2.47	1.08	-100.9	-40.7
2) 2.60	1.01		2) 2.92	0.97		
3) 2.67	0.99		3) 2.77	0.98		
4) 2.72	0.99		4) 2.78	0.98		
5) 2.83	0.98					

$R_{\text{O}-\text{O}}$  and  $R_{\text{O}-\text{H}}$  = H-bond distances;  $\Delta E$  = interaction energy in the  $\text{CF}_3\text{SO}_3^- - \text{H}_3\text{O}^+ - \text{H}_2\text{O}$  clusters;  $\Delta E^{\text{sol}}$  = solvation energy.

Table A.1 (Continued).

Gas			Cosmo			
$R_{O-O}$	$R_{O-H}$	$\Delta E$	$R_{O-O}$	$R_{O-H}$	$\Delta E$	$\Delta E^{sol}$
1) 2.71	0.99	-876.5	1) 2.83	0.98	-209.0	-88.9
2) 2.56	1.02		2) 2.55	1.03		
3) 2.55	1.02		3) 2.48	1.07		
4) 2.51	1.04		4) 2.64	1.00		
5) 2.62	1.00		5) 2.74	0.99		
6) 2.68	0.99		6) 2.65	1.00		
7) 2.77	0.98		7) 2.84	0.98		

Table A.1 (Continued).

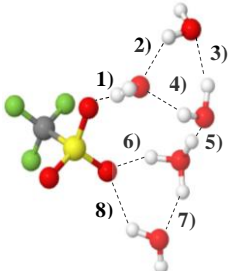
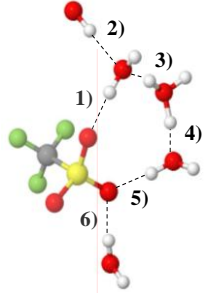
Gas			Cosmo			
m) 						
$R_{O-O}$	$R_{O-H}$	$\Delta E$	$R_{O-O}$	$R_{O-H}$	$\Delta E$	$\Delta E^{sol}$
1) 2.68	0.99	-863.4	1) 2.74	0.99	-205.12	-79.79
2) 2.84	0.97		2) 2.91	0.97		
3) 2.71	0.98		3) 2.54	1.03		
4) 2.75	0.98		4) 2.45	1.08		
5) 2.46	1.09		5) 2.72	0.99		
6) 2.55	1.02		6) 2.89	0.97		
7) 2.61	1.00					
8) 2.82	0.97					

Table A.1 (Continued).

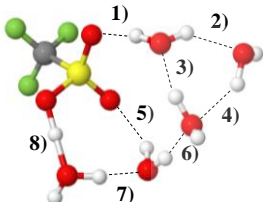
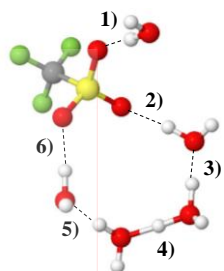
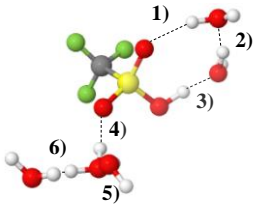
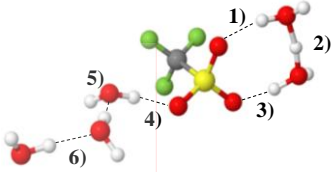
Gas			Cosmo			
						
$R_{O-O}$	$R_{O-H}$	$\Delta E$	$R_{O-O}$	$R_{O-H}$	$\Delta E$	$\Delta E^{sol}$
1) 2.95	0.97	-296.16	1) 2.87	0.97	-202.06	-117.4
2) 2.81	0.97		2) 2.74	0.98		
3) 2.66	1.00		3) 2.52	1.04		
4) 2.91	0.97		4) 2.44	1.11		
5) 2.91	0.97		5) 2.63	1.00		
6) 2.76	0.98		6) 2.79	0.98		
7) 2.58	1.02					
8) 2.45	1.10					

Table A.1 (Continued).

Gas			Cosmo			
o)						
						
$R_{O-O}$	$R_{O-H}$	$\Delta E$	$R_{O-O}$	$R_{O-H}$	$\Delta E$	$\Delta E^{sol}$
1) 3.01	0.97	-232.14	1) 2.76	(0.98)	-175.60	-107.39
2) 2.66	0.99		2) 2.43	(1.12)		
3) 2.51	1.05		3) 2.61	(1.01)		
4) 2.83	0.97		4) 2.85	(0.97)		
5) 2.79	0.98		5) 2.76	(0.98)		
6) 2.74	0.98		6) 2.79	(0.98)		
7) 2.83	0.97					



**Table A.2** Asymmetric stretching coordinate ( $\Delta d_{DA}$ ) and O-H stretching frequency ( $\nu^{OH}$ ) of the  $CF_3SO_3^- - H_3O^+ - nH_2O$  complexes,  $n = 1 - 4$ , obtained from B3LYP/TZVP calculations, both in the gas phase and continuum aqueous solution. They are in Å and  $cm^{-1}$ , respectively.

	Gas		Cosmo	
j)				
	$\Delta d_{DA}$	$\nu^{OH}$	$\Delta d_{DA}$	$\nu^{OH}$
	0.24	1537	0.31	1773
	0.58	2903	0.99	3548
	0.69	3156	0.81	3297
	0.75	3286	0.82	3350
	0.88	3481		

Table A.2 (Continued).

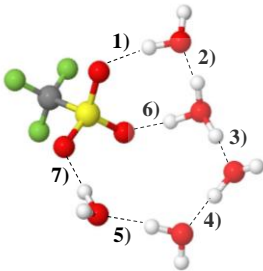
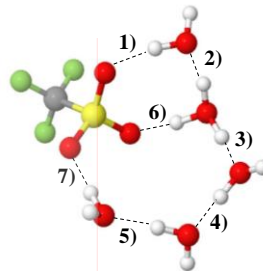
Gas		Cosmo	
d) 			
$\Delta d_{DA}$	$\nu^{OH}$	$\Delta d_{DA}$	$\nu^{OH}$
0.76	3287	0.91	3437
0.54	2807	0.50	2542
0.51	2606	0.35	1927
0.43	2358	0.65	2980
0.62	2976	0.76	3234
0.70	3199	0.67	3072
0.81	3398	0.89	3452

Table A.2 (Continued).

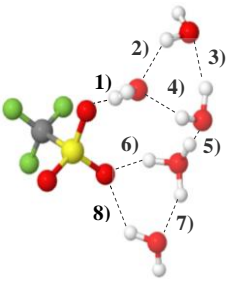
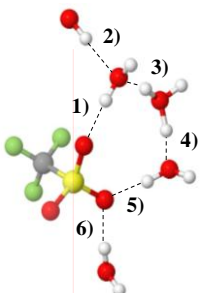
Gas		Cosmo	
m) 			
$\Delta d_{DA}$	$\nu^{OH}$	$\Delta d_{DA}$	$\nu^{OH}$
0.72	3243	0.77	3294
1.02	3507	0.97	3504
0.85	3342	0.49	2495
0.88	3383	0.29	1786
0.27	1771	0.75	3255
0.57	2795	0.95	3514
0.72	3154		
1.09	3516		

Table A.2 (Continued).

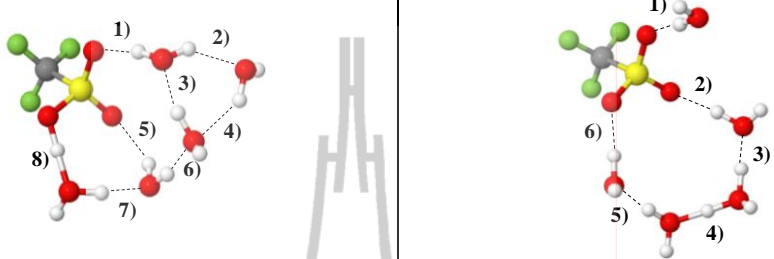
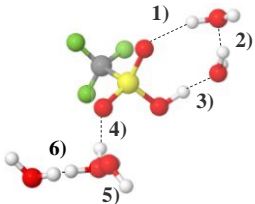
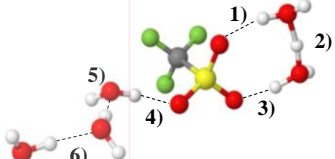
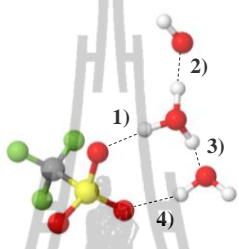
Gas		Cosmo	
n)			
$\Delta d_{DA}$	$\nu^{OH}$	$\Delta d_{DA}$	$\nu^{OH}$
1.04	3507	0.93	3504
1.02	3503	0.78	3328
0.69	3081	0.44	2364
1.10	3596	0.22	1308
1.11	3603	0.63	2929
0.81	3325	0.83	3391
0.56	2785		
0.25	1682		

Table A.2 (Continued).

Gas		Cosmo	
o)			
			
$\Delta d_{DA}$	$\nu^{OH}$	$\Delta d_{DA}$	$\nu^{OH}$
1.17	3653	0.85	3356
0.70	3174	0.20	1214
0.42	2261	0.61	2919
1.01	3496	0.90	3477
0.91	3417	0.80	3279
0.84	3326	0.83	3347
1.01	3494		

**Table A.3** Dynamic results of the  $\text{CF}_3\text{SO}_3^- - \text{H}_3\text{O}^+ - n\text{H}_2\text{O}$  complexes,  $n = 1 - 4$ , obtained from B3LYP/TZVP calculations, both in the gas phase and continuum aqueous solution (the values in parenthesis). Distances and energies are in Å and kJ/mol, respectively

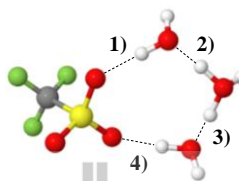
d)



$\langle R_{\text{O-O}} \rangle$	$\langle \Delta d_{\text{DA}} \rangle$	$V_{\text{A}}^{\text{OH, MD}}$	$V_{\text{B}}^{\text{OH, MD}}$	$\Delta v_{\text{BA}}^{\text{OH, MD}}$	$P_{\text{B}}/P_{\text{A}}$	$D (10^{-5})$
1) 2.61	0.66					
2) 2.54	0.54	1509.6	2457.8	948.3	0.02	3.93
3) 2.51	0.47	1554.3	2328.7	774.4	0.04	6.02
4) 2.80	1.56					

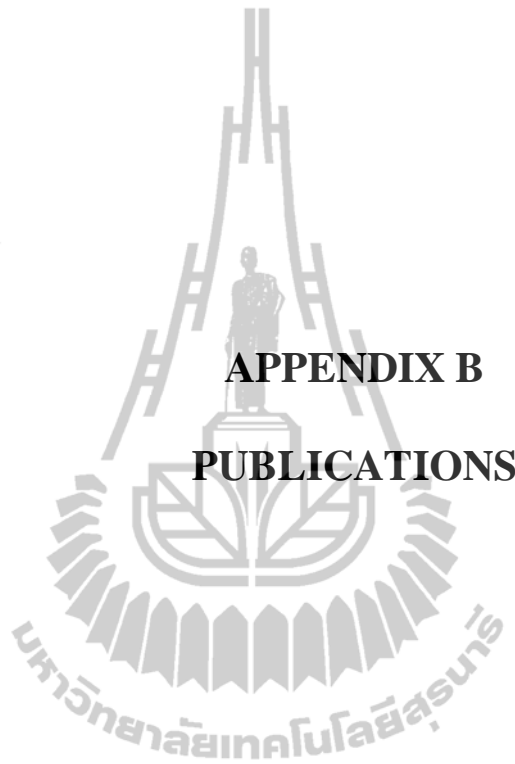
Table A.3 (Continued).

e)



$\langle R_{O-O} \rangle$	$\langle \Delta d_{DA} \rangle$	$V_A^{OH, MD}$	$V_B^{OH, MD}$	$\Delta V_{BA}^{OH, MD}$	$P_B/P_A$	$D (10^{-5})$
1) 2.72	0.83					
2) 2.49	0.40	1537.5	2311.9	774.3	0.04	6.70
3) 2.48	0.38	1548.7	2351.2	802.4	0.03	6.42
4) 2.72	0.83					





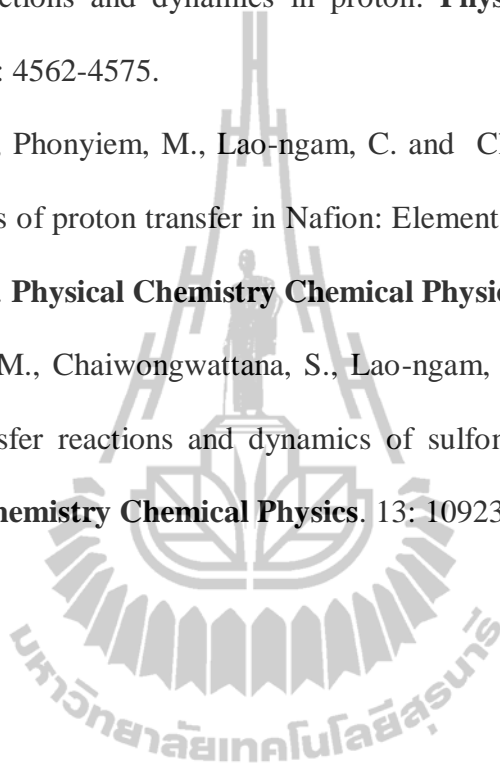
**APPENDIX B**

**PUBLICATIONS**



**Publications:**

1. Lao-ngam, C., Asawakun, P., Wannarat, S. and Sakarik, K. (2011). Proton transfer reactions and dynamics in proton. **Physical Chemistry Chemical Physics**. 13: 4562-4575.
2. Sagarik, K., Phonyiem, M., Lao-ngam, C. and Chaiwongwattana, S. (2008). Mechanisms of proton transfer in Nafion: Elementary reactions at the sulfonic acid groups. **Physical Chemistry Chemical Physics**. 10: 2098-2112.
3. Phonyiem, M., Chaiwongwattana, S., Lao-ngam, C. and Sagarik, K. (2011). Proton transfer reactions and dynamics of sulfonic acid group of Nafion<sup>®</sup>. **Physical Chemistry Chemical Physics**. 13: 10923-10939.



## Proton transfer reactions and dynamics in protonated water clusters

Charoensak Lao-ngam,<sup>a</sup> Prapasri Asawakun,<sup>b</sup> Sornthep Wannarat<sup>c</sup> and Kritsana Sagarik<sup>\*a</sup>

Received 7th October 2010, Accepted 26th November 2010

DOI: 10.1039/c0cp02068k

Proton transfer reactions and dynamics were theoretically studied using the hydrogen-bond (H-bond) complexes formed from  $\text{H}_3\text{O}^+$  and  $n\text{H}_2\text{O}$ ,  $n = 1-4$ , as model systems. The investigations began with searching for characteristics of transferring protons in the gas phase and continuum aqueous solution using DFT method at the B3LYP/TZVP level, followed by Born–Oppenheimer molecular dynamics (BOMD) simulations at 350 K. B3LYP/TZVP calculations revealed the threshold asymmetric O–H stretching frequencies ( $\nu^{\text{OH}*}$ ) for the proton transfers in the Zundel complex ( $\text{H}_5\text{O}_2^+$ ) in the gas phase and continuum aqueous solution at 1984 and 1881  $\text{cm}^{-1}$ , respectively. BOMD simulations suggested lower threshold frequencies ( $\nu^{\text{OH,MD}*} = 1917$  and  $1736 \text{ cm}^{-1}$ , respectively), with two characteristic  $\nu^{\text{OH,MD}}$  being the IR spectral signatures of the transferring protons. The low-frequency band could be associated with the “oscillatory shuttling motion” and the high-frequency band with the “structural diffusion motion”. These can be regarded as the spectroscopic evidences of the formations of the shared-proton structure ( $\text{O} \cdots \text{H}^+ \cdots \text{O}$ ) and the  $\text{H}_3\text{O}^+ - \text{H}_2\text{O}$  contact structure ( $\text{O} - \text{H}^+ \cdots \text{O}$ ), respectively. Since the quasi-dynamic equilibrium between the Zundel and Eigen complexes was suggested to be the rate-determining step, in order to achieve an “ideal” maximum efficiency of proton transfer, a concerted reaction pathway should be taken. The most effective interconversion between the two proton states, the shared-proton structure and the  $\text{H}_3\text{O}^+ - \text{H}_2\text{O}$  contact structure, can be reflected from comparable intensities of the oscillatory shuttling and structural diffusion bands. The present results iterated the previous conclusions that static proton transfer potentials cannot provide complete description of the structural diffusion process and it is essential to incorporate thermal energy fluctuations and dynamics in the model calculations.

### Introduction

Proton transfer reactions have been of interest especially in connection with the understanding of elementary reactions in electrochemical and biological systems.<sup>1–3</sup> Although some theoretical and experimental information has been accumulated in the past decades,<sup>4–7</sup> precise mechanisms of proton transfer reactions in liquids and solids are not completely known. Because some basic chemistry of proton transfer processes has been discussed in detail in many review articles,<sup>4,5,7</sup> only the theoretical and experimental information pertinent to the present work will be briefly summarized.

According to experimental and theoretical studies,<sup>8,9</sup> there are three basic structures involved in proton transfer reactions in aqueous solution namely, the hydronium ion ( $\text{H}_3\text{O}^+$ ), the Eigen complex ( $\text{H}_9\text{O}_4^+$ ) and the dihydrated cation known as the Zundel ( $\text{H}_5\text{O}_2^+$ ) complex. The latter is represented by an excess proton equally shared between two neutral water molecules. Various concepts have been proposed to explain the unusually high mobility of protons in aqueous solution.<sup>5,8–11</sup> Apart from the diffusion of hydrated proton through the so called “vehicle mechanism”, by which protons bound with a fraction of water molecules travel through the electrolyte *via* mutual diffusion, Eigen and De Maeyer<sup>11</sup> demonstrated that the “structural diffusion”, the diffusion of the H-bond structure in which an excess proton is shuttling back and forth, represents an important elementary reaction in the proton transfer processes.

There has been a controversy as to whether the species containing an excess proton could be described as  $\text{H}_3\text{O}_4^+$  or  $\text{H}_5\text{O}_2^+$ .<sup>5</sup> The controversy was partly resolved by Tuckerman *et al.*<sup>12,13</sup> According to the results of quantum molecular

<sup>a</sup>School of Chemistry, Institute of Science, Suranaree University of Technology, Nakhon Ratchasima 30000, Thailand.

E-mail: kritsana@sut.ac.th; Fax: + (6644) 224635;

Tel: + (6644) 224635

<sup>b</sup>School of Mathematics, Institute of Science, Suranaree University of Technology, Nakhon Ratchasima 30000, Thailand

<sup>c</sup>National Electronics and Computer Technology Center (NECTEC), National Science and Technology Development Agency (NSTDA), Pathumthani 12120, Thailand

dynamics (MD) simulations, a single proton in H-bond network, regarded as "proton defect", could belong to either  $\text{H}_5\text{O}_2^+$  or  $\text{H}_9\text{O}_4^+$ , with the center of the area having the excess proton coinciding with the center of symmetry of the H-bond structure. It was demonstrated that, changes in these H-bond structures and those in the vicinities through the H-bond breaking and forming processes displace the center of symmetry in space and also the center of the excess charge.<sup>12,13</sup> In this way,  $\text{H}_5\text{O}_2^+$  can be converted to  $\text{H}_9\text{O}_4^+$  and, therefore, regarded as structural diffusion. The proposed mechanism for the diffusion of an excess proton in water was supported by Agmon,<sup>10</sup> based on the interpretation of NMR data.

One of the most powerful experimental techniques in H-bond research is vibrational spectroscopy. The most evident effects of H-bond formations in aqueous solution are the red shift of the high-frequency hydroxyl (O–H) stretching mode, accompanied by its intensity increase and band broadening.<sup>14–16</sup> The broad and intense IR absorption bands ranging from 1000 to 3000  $\text{cm}^{-1}$  were interpreted as spectral signatures of protonated water networks.<sup>17</sup> The correlation between the O–H stretching frequency and the probability of proton transfer in H-bond has been discussed in detail;<sup>16–18</sup> the probability of proton transfer could be related to a strong red shift of the asymmetric O–H stretching frequency ( $\nu^{\text{OH}}$ ), compared to the corresponding "free" or "non-H-bonded" one.<sup>16</sup> The red shift cannot be detected easily in experiments due to the coupling and overlapping of various vibrational modes, as well as the detection limit of IR equipment,<sup>19–21</sup> whereas, the harmonic approximation employed in conventional *ab initio* calculations is inadequate to predict accurately the asymmetric O–H stretching frequency of the active proton in  $\text{H}_5\text{O}_2^+$ .<sup>20,22</sup>

Theories<sup>23</sup> and experiments<sup>19,24</sup> indicated that the IR spectra of protonated water clusters in the gas phase and aqueous solution could be divided into three distinct regions. Born–Oppenheimer molecular dynamics (BOMD) simulations at 225 and 360 K<sup>23</sup> suggested that the vibrational frequencies above 3000  $\text{cm}^{-1}$  are associated with the symmetric and asymmetric O–H stretching modes of individual water molecules, whereas those between 1000 and 2000  $\text{cm}^{-1}$  are the characteristic vibrational frequencies of the transferring protons.<sup>25</sup> The IR multiple photon dissociation (IRMPD) spectra of  $\text{H}_5\text{O}_2^+$  were measured in the gas phase,<sup>22,24</sup> from which two different possible assignments of the observed IR bands were discussed. The IRMPD spectra showed a characteristic asymmetric O–H stretching frequency at 990  $\text{cm}^{-1}$ , in good agreement with B3LYP/6-31+G\*\* calculations with harmonic approximation.<sup>24</sup>

In our previous work, proton transfer reactions at a hydrophilic group of Nafion<sup>®</sup>, a widely used polymer electrolyte membrane in fuel cells (PEMFC), were studied using the H-bond complexes formed from methanol ( $\text{CH}_3\text{OH}$ ),  $\text{H}_3\text{O}^+$  and  $\text{H}_2\text{O}$ ,<sup>26</sup> and from triflic acid ( $\text{CF}_3\text{SO}_3\text{H}$ ),  $\text{H}_3\text{O}^+$  and  $\text{H}_2\text{O}$ ,<sup>27</sup> as model systems. For the most basic unit in aqueous solution, the  $\text{H}_3\text{O}^+$ – $\text{H}_2\text{O}$  complexes, BOMD simulations at 350 K revealed that a quasi-dynamic equilibrium is established between the Eigen and Zundel complexes and considered to be the most important elementary reaction in the proton transfer process.<sup>27</sup>

It was demonstrated that proton transfer reactions are not concerted due to the thermal energy fluctuations and dynamics. The BOMD results and IR spectra of the transferring protons also revealed that, the proton transfer processes in the protonated  $\text{CH}_3\text{OH}$ – $\text{H}_2\text{O}$  clusters involve the  $\text{CH}_3\text{OH}$ – $\text{H}_3\text{O}^+$ – $\text{H}_2\text{O}$  1 : 1 : 1 complex as the most effective mediator;<sup>26</sup> whereas for the protonated  $\text{CF}_3\text{SO}_3\text{H}$ – $\text{H}_2\text{O}$  clusters, the  $-\text{SO}_3\text{H}$  group could be directly and indirectly involved in proton transfer reactions, through the formation of proton defects, as well as  $-\text{SO}_3^-$  and  $-\text{SO}_3\text{H}_2^+$ .<sup>26</sup> It was concluded that, due to the coupling among various modes of vibrations, the discussions on proton transfer reactions cannot be made based only on static proton transfer potentials.<sup>26,27</sup>

In order to provide fundamental information for further investigations on the proton transfer reactions at a hydrophilic group of Nafion<sup>®</sup>, characteristics of the transferring protons in protonated water clusters were studied in the present work. The investigations began with searching for the equilibrium structures of the protonated water clusters which could be important in proton transfer pathways using pair potentials. The computed equilibrium structures were refined using a density functional theory (DFT) method, and employed as starting configurations in BOMD simulations at 350 K, an operation temperature in PEMFC. As proton transfer reactions are governed by various modes of vibrations, IR spectra of the H-bond protons susceptible to proton transfers were computed from DFT calculations and BOMD simulations. The characteristic IR frequencies and dynamics of the transferring protons, obtained from BOMD simulations, were analyzed, discussed and compared with available theoretical and experimental data.

## Computational methods

Our experience<sup>26,27</sup> revealed that elementary reactions and dynamics of proton transfer in H-bond could be studied reasonably well by taking the following three basic steps namely; (1) searching for the H-bond structures which could be intermediate states in the dynamic proton transfer pathways using pair potentials; (2) refining the computed structures using an accurate quantum chemical method; (3) BOMD simulations using the refined structures as the starting configurations. These basic steps were adopted in the present work to investigate proton transfer reactions in the protonated water clusters.

Since proton transfer reactions involve formation and cleavage of covalent bonds, inclusion of too many water molecules in the model systems could lead to difficulties in the analyses of the elementary reactions and dynamics.<sup>20,26,27</sup> It was, therefore, the strategy of the previous<sup>26,27</sup> and present works to restrict the number of water molecules to not more than four; according to a neutron diffraction experiment with hydrogen isotope substitutions and Monte Carlo (MC) simulations,<sup>8</sup> the first hydration shell of  $\text{H}_3\text{O}^+$  consists of four water molecules and only three of them strongly H-bond to the hydrogen atoms of  $\text{H}_3\text{O}^+$ . As the electric field introduced by polar solvent could determine the potential energy surface, on which the transferring proton in H-bond moves,<sup>26,28–31</sup> a continuum solvent model had to be included in the model

calculations. To approximate the solvent effects, a conductor-like screening model (COSMO) was proved to be applicable on similar H-bond systems.<sup>26,32</sup> Therefore, to partially account for the effects of the extended H-bond networks of water, COSMO with the dielectric constant ( $\epsilon$ ) of 78 was employed in the present quantum chemical calculations and BOMD simulations.

#### Static calculations

**Equilibrium structures and asymmetric stretching coordinates.** In the present investigation, attention was focused on the H-bond structures which could be involved in proton transfer processes. The T-model potentials for  $\text{H}_3\text{O}^+$  and  $\text{H}_2\text{O}$  were taken from ref. 26 and employed in the calculations of the equilibrium structures of the  $\text{H}_3\text{O}^+ - n\text{H}_2\text{O}$  complexes,  $n = 1-4$ . Because the T-model had been discussed in details in the previous studies,<sup>33-41</sup> only some important aspects relevant to the geometry optimizations will be briefly summarized using the Eigen complex as an example. The experimental geometries<sup>42</sup> of  $\text{H}_3\text{O}^+$  and  $\text{H}_2\text{O}$  were kept constant in the T-model geometry optimizations. For the Eigen complex, a rigid  $\text{H}_3\text{O}^+$  was placed at the origin of the Cartesian coordinate system. The coordinates of  $\text{H}_2\text{O}$  molecules were randomly generated in the vicinities of  $\text{H}_3\text{O}^+$ . Based on the T-model potentials, equilibrium structures of the Eigen complex were searched using a minimization technique. Fifty configurations were generated randomly and employed as starting configurations in the T-model geometry optimizations.

Because the T-model is based on rigid molecules, in which the cooperative effects are neglected, further structural refinements had to be made using an appropriate quantum chemical method. Literature survey showed that, DFT methods have been frequently chosen due to the ability to treat molecules of relatively large sizes with reasonable accuracies compared to other non-empirical methods.<sup>43-47</sup> Especially in the present case, calculations of IR spectra and BOMD simulations with thousands of time steps had to be made, it was necessary to compromise between the accuracy of theoretical methods and available computer resources. In order to achieve all the objectives, DFT calculations were made using the B3LYP hybrid functional,<sup>48,49</sup> with the triple-zeta valence basis sets augmented by polarization functions (TZVP). The TZVP basis sets were developed and tested by Ahlrichs and coworkers.<sup>50</sup> The applicability of the TZVP basis sets in DFT calculations on structures and IR spectra was discussed.<sup>51</sup> It was concluded that the TZVP basis sets are sufficient for the systems with and without occupied d-states, and could be applied well in the calculations of equilibrium structures and interaction energies, as well as IR spectra, of such systems.<sup>51</sup> The applicability of B3LYP calculations on protonated water clusters was also analyzed and discussed in details.<sup>20</sup>

In the present work, all quantum chemical calculations were made using TURBOMOLE 6.0.<sup>52,53</sup> The absolute and local minimum energy geometries of the protonated water clusters obtained from the T-model potentials were employed as starting configurations in the B3LYP/TZVP geometry optimizations. In order to ensure that the optimized structures were at the stationary points and to obtain reasonable IR frequencies, a

tight SCF energy convergence criterion (less than  $10^{-8}$  au), with the maximum norm of Cartesian gradients less than  $10^{-4}$  au, was employed in the B3LYP/TZVP geometry optimizations.

The interaction energies ( $\Delta E$ ) of the optimized structures were computed as  $\Delta E = E(\text{H}_3\text{O}^+ - n\text{H}_2\text{O}) - [E(\text{H}_3\text{O}^+) + nE(\text{H}_2\text{O})]$ ;  $E(\text{H}_3\text{O}^+ - n\text{H}_2\text{O})$  is the total energy of the optimized structures of the  $\text{H}_3\text{O}^+ - n\text{H}_2\text{O}$  complexes;  $E(\text{H}_3\text{O}^+)$  and  $E(\text{H}_2\text{O})$  are the total energies of the isolated  $\text{H}_3\text{O}^+$  and  $\text{H}_2\text{O}$  at their optimized structures, respectively. The energetic effects due to the continuum aqueous solvent (COSMO with  $\epsilon = 78$ ) were estimated from the solvation energy ( $\Delta E^{\text{sol}}$ ), approximated as  $\Delta E^{\text{sol}} = E(\text{H}_3\text{O}^+ - n\text{H}_2\text{O})^{\text{COSMO}} - E(\text{H}_3\text{O}^+ - n\text{H}_2\text{O})$ ;  $E(\text{H}_3\text{O}^+ - n\text{H}_2\text{O})^{\text{COSMO}}$  and  $E(\text{H}_3\text{O}^+ - n\text{H}_2\text{O})$  are the total energies of the optimized structures, obtained from B3LYP/TZVP calculations with and without COSMO, respectively. The interaction energies between the central charged species and the surrounding water molecules ( $\Delta E^{\text{X}}$ ,  $\text{X} = \text{H}_3\text{O}^+$  or  $\text{H}_2\text{O}$ ) were computed with and without the continuum aqueous solvent as  $\Delta E^{\text{X}} = E(\text{X} - n\text{H}_2\text{O}) - [E(\text{X}) + nE(\text{H}_2\text{O})]$ ;  $E(\text{X} - n\text{H}_2\text{O})$  is the total energy of the optimized structures;  $E(\text{X})$  and  $E(n\text{H}_2\text{O})$  are the total energies obtained by removing water molecules and the central charged species from the optimized structures, respectively. In order to test the reliability of the energetic results obtained from B3LYP/TZVP calculations, the basis set superposition errors (BSSE) were estimated for  $\Delta E^{\text{X}}$  using the counterpoise correction.<sup>54</sup>

An attempt was made to anticipate the tendency of proton transfer in H-bond using the asymmetric stretching coordinate ( $\Delta d_{\text{DA}}$ ),<sup>26,55</sup> for which a concept of the "most active" H-bond<sup>56</sup> was employed in the discussion of the Grotthuss mechanism. Within the framework of the most active H-bond,  $\Delta d_{\text{DA}}$  of a H-bond donor (D)-acceptor (A) pair is defined by  $\Delta d_{\text{DA}} = |d_{\text{A-H}} - d_{\text{B}\cdots\text{H}}|$ ; where  $d_{\text{A-H}}$  and  $d_{\text{B}\cdots\text{H}}$  are the A-H and B $\cdots$ H distances in the A-H $\cdots$ B H-bond, respectively. The H-bond with small  $\Delta d_{\text{DA}}$  is considered to be susceptible to proton transfer;<sup>26</sup> "active" with respect to proton transfer when  $\Delta d_{\text{DA}} < 0.1 \text{ \AA}$ , and "inactive" when  $\Delta d_{\text{DA}} > 0.4 \text{ \AA}$ .<sup>57</sup>

**Infrared spectra and normal mode analyses.** Because the theoretical results on the IR spectra of the  $\text{CH}_3\text{OH} - \text{H}_3\text{O}^+ - \text{H}_2\text{O}$  complexes<sup>26</sup> revealed interesting correlations between the asymmetric O-H stretching frequencies ( $\nu^{\text{OH}}$ ) and the H-bond distances ( $R_{\text{O}\cdots\text{O}}$ ),  $\nu^{\text{OH}}$  of the H-bond protons in the protonated water clusters were investigated in detail. Using the optimized H-bond structures obtained in the previous subsection, harmonic IR frequencies were computed from the numerical second derivatives of the B3LYP/TZVP total energies. The calculations of the second derivatives and the analyses of the normal modes in terms of internal coordinates were performed using NUMFORCE and AOFORCE programs, respectively. They were incorporated in TURBOMOLE 6.0 software package.<sup>52,53</sup>  $\nu^{\text{OH}}$  derived from the static proton transfer potentials (B3LYP/TZVP calculations) were used to estimate the tendencies of proton transfers in the protonated water clusters.

It should be mentioned that the vibrational frequencies derived from quantum chemical calculations are in general larger than those from experiments. Therefore, a scaling factor which partially account for the anharmonicities and systematic

errors is required. Although in the present study, only the changes in the O–H stretching frequencies due to different H-bond environments were of interest, a scaling factor was used throughout; a scaling factor of 0.9614<sup>58</sup> was proved to be appropriate for B3LYP/TZVP calculations with comparable basis sets.<sup>58,59</sup>

#### Dynamic calculations

**Born–Oppenheimer MD simulations.** Dynamics of rapid covalent and H-bond formations and cleavages could be studied reasonably well using quantum MD simulations,<sup>60</sup> among which BOMD simulations have been widely used in recent years.<sup>61–66</sup> Within the framework of BOMD simulations, classical equations of motions of nuclei on the Born–Oppenheimer (BO) surfaces are integrated, whereas forces on nuclei are calculated in each MD step from quantum energy gradients, with the molecular orbitals (MO) updated by solving Schrödinger equations in the BO approximation; the nuclei thus undergo classical Newtonian dynamics on quantum potential hypersurface. BOMD simulations are therefore more accurate, as well as considerably CPU time consuming, compared to classical MD simulations, in which forces on nuclei are determined from predefined empirical or quantum pair potentials. It should be mentioned that, although the high mobility of excess proton was initially attributed to quantum mechanical (QM) tunneling,<sup>67</sup> the results of BOMD simulations<sup>25</sup> and conductivity measurements<sup>68</sup> indicated that mechanisms of proton transfers could be explained reasonably well without assuming the proton tunneling as an important pathway.

As proton transfers in aqueous solution involve dynamic processes with different timescales,<sup>10,42,69</sup> the complexity of proton transfer reactions could be reduced using various approaches. The observation that the actual proton transfer occurs in femtosecond (fs) timescale,<sup>42</sup> which is faster than solvent structure reorganization,<sup>10</sup> made it possible to perform BOMD simulations by focusing on short-lived phenomena taking place before the H-bond structure reorganization. The present BOMD simulations were performed with canonical (NVT) ensemble at 350 K, by applying a Nosé–Hoover chain thermostat to each degree of freedom in the system. In order to ensure that all important dynamics in the gas phase and continuum aqueous solution (COSMO) were taken into account, the shared-proton complexes predicted in the previous subsection were used as the starting configurations. Since in aqueous solution, the rapid interconversion between the Zundel and Eigen complexes takes place within 100 fs ( $10^{-13}$  s),<sup>69</sup> the timestep used in solving dynamic equations was set to 0.24 fs. In each BOMD simulations, 2000 steps were devoted to equilibration, after which 10 000 steps to property calculations, corresponding to about 2.4 ps. All BOMD simulations were performed using FROG program included in TURBOMOLE 6.0;<sup>52,53</sup> the MD program employs the Leapfrog Verlet algorithm to turn the electronic potential energy gradients into new atomic positions and velocities.

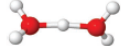
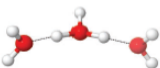


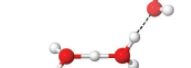


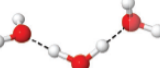
Remarks should be made on the ensemble and simulation length chosen in the present study. The applicability and performance of NVE and NVT BOMD simulations on small

H-bond chains were investigated and discussed in detail.<sup>70</sup> For NVE BOMD simulations, it was demonstrated that the potential energy of the system decreases quite rapidly in the course of BOMD simulations. Once the proton stays at the center of the H-bond, the potential energy is at the lowest point and the proton is trapped in the minimum; no proton transfer can be observed in the later timesteps. Since NVE BOMD simulations are conducted at constant energy, a decrease in the potential energy is accompanied by an increase in the kinetic energy, as well as temperature, leading to the H-bond structure reorganization and fragmentation. For NVT BOMD simulations, the energy released during the proton transfer processes can be absorbed by the thermostat bath, allowing the H-bond structure and local temperature to be maintained for a longer time (2–5 ps), depending upon the size and the complexity of the H-bond structure. Thus, NVT BOMD simulations are more appropriate for the present investigations.

Additional comments should be made on BOMD simulations, in comparison with another theoretical method. In order to obtain a quantitative description of reaction path networks, special algorithms,<sup>71</sup> such as “discrete path sampling (DPS)” method, have been developed.<sup>72</sup> The DPS method is based on path sampling using information about stationary points on the potential energy surface. Thermodynamics and dynamic properties (rate constants) could be computed from model density of state (*e.g.* employing classical pair potentials or databases of local minima and transition states). The method is therefore suitable for the reactions, in which the pathways consist of sequences of local minima and transition states. The DPS method can also be applied on the dynamic properties with large samples of minima, *e.g.* the rates of isomerization of water clusters.<sup>72</sup> One of the problems of the DPS method is the number of local minima on the potential energy surface which can grow exponentially with the system size. Since we focused attention on the motions of individual protons in small H-bond clusters, not many local energy minima and pathways had to be considered; the quasi-dynamic equilibria between the two limiting structures, the Zundel and  $\text{H}_3\text{O}^+-\text{H}_2\text{O}$  complexes, in various H-bond environments are the most important issues, as they can determine the dynamic behaviors of proton transfers in aqueous solution. BOMD simulations are therefore the most appropriate choice in this case.

**Infrared spectra and diffusion coefficients.** Since proton transfer reactions in H-bonds are strongly coupled with various degrees of freedom, especially the O–O vibration,<sup>4,23,26</sup> attention was focused on the symmetric and asymmetric O–H stretching modes, as well as the O–O vibrations. In the present work, the IR spectra of the transferring protons were computed from BOMD simulations by Fourier transformations of the velocity autocorrelation function (VACF).<sup>73</sup> This approach is appropriate as it allows the coupled vibrations to be distinguished, characterized and analyzed separately. Fourier transformations of VACF were made within a short time limit of 100 fs. This choice is justified by the observation that the average lifetime of the most important shared-proton complex, the Zundel complex, is about 100 fs.<sup>12,69</sup> The diffusion coefficients (D) of the transferring protons were computed

**Table 1** Static results of the protonated water clusters obtained from B3LYP/TZVP calculations. Distances, energies and IR frequencies are in Å, kJ/mol and  $\text{cm}^{-1}$ , respectively<sup>a</sup>

Structure		$R_{\text{O-O}}$	$R_{\text{O-H}}$	$\Delta d_{\text{DA}}$	$\Delta E$	$\Delta E^{\text{sol}}$	$\Delta E^{\text{X}}$	$\nu^{\text{OH}}$	
a		Gas	2.40	1.20	0.00	-158.8	-316.4	961.3	
		Cosmo	2.40	1.20	0.00	-58.2		676.8	
b		Gas	2.49	1.04	0.41	-265.7	-280.3	-290.7 (-283.2)	2304.5
		Cosmo	2.50	1.05	0.40	-95.2		-121.7 (-118.3)	2120.1
c		Gas	2.56	1.02	0.52	-353.7	-260.2	-379.7 (-369.7)	2759.7
		Cosmo	2.55	1.02	0.51	-129.3		-159.8 (-154.7)	2531.4
d		Gas	2.40	1.20	0.00	-340.6	-260.6	-191.7 (-185.4)	997.9
		Cosmo	2.43	1.11	0.21	-116.7		-70.3 (-68.5)	1240.4
e		Gas	2.39	1.20	0.00	-340.5	-261.8	-191.7 (-185.3)	1001.9
		Cosmo	2.43	1.11	0.21	-117.7		-74.5 (-73.2)	1263.6
f		Gas	2.45	1.07	0.32	-403.2	-253.2	-434.9 (-424.2)	1914.7
		Cosmo	2.47	1.07	0.33	-138.0		-171.5 (-166.1)	1778.0
g		Gas	2.47	1.05	0.37	-416.5	-249.7	-415.3 (-406.4)	2229.6
		Cosmo	2.50	1.05	0.40	-147.9		-155.2 (-150.9)	2185.8
h		Gas	2.41	1.12	0.18	-402.0	-265.9	-233.1 (-226.1)	1296.8
		Cosmo	2.46	1.09	0.28	-149.5		-151.0 (-148.4)	1457.7

<sup>a</sup>  $R_{\text{O-O}}$  and  $R_{\text{O-H}}$  = H-bond distances;  $\Delta d_{\text{DA}}$  = asymmetric stretching coordinate;  $\Delta E$  = interaction energy in the protonated water clusters;  $\Delta E^{\text{sol}}$  = solution energy;  $\Delta E^{\text{X}}$  interaction energy between the central charged species ( $X = \text{H}_3\text{O}^+$  or  $\text{H}_5\text{O}_2^+$ ) and water molecules (the values in parentheses computed with the counterpoise corrections);  $\nu^{\text{OH}}$  = asymmetric O-H stretching frequency.

from BOMD simulations using the Einstein relation,<sup>74,75</sup> by which  $D$  were determined from the slopes of the mean-square displacements (MSD). Because the transferring proton is confined in a short H-bond distance, care must be exercised in selecting the time interval in which MSD is computed.<sup>76</sup> Our previous<sup>26</sup> and present experience showed that, linear relationship between MSD and simulation time could be obtained when the time intervals are not larger than 0.5 ps.

## Results and discussion

In this section, all important results are presented, with the emphasis on the H-bonds in the shared-proton complexes. The discussions are made primarily on the static results obtained from B3LYP/TZVP calculations, both in the gas phase and continuum aqueous solution. Then, the BOMD results are analyzed and discussed in comparison with the B3LYP/TZVP results, with special attentions on the relationships among the H-bond structures, characteristic IR frequencies and dynamics in connection with the mechanisms of proton transfer reactions.

### Static results

**Shared-proton complexes and infrared spectra of transferring protons.** Equilibrium structures, interaction energies ( $\Delta E$  and  $\Delta E^X$ ,  $X = \text{H}_3\text{O}^+$  or  $\text{H}_5\text{O}_2^+$ ) and solvation energies ( $\Delta E^{\text{sol}}$ ) of the  $\text{H}_3\text{O}^+ - n\text{H}_2\text{O}$  complexes,  $n = 1-4$ , obtained from B3LYP/TZVP calculations are summarized in Table 1. The characteristic H-bond distances ( $R_{\text{O-O}}$  and  $R_{\text{O-H}}$ ), asymmetric stretching coordinates ( $\Delta d_{\text{DA}}$ ) and asymmetric O-H stretching frequencies ( $\nu^{\text{OH}}$ ) of the transferring protons are included in Table 1. The trends of  $\Delta E$ ,  $\Delta E^{\text{sol}}$  and  $\Delta E^X$  with respect to the number of water molecules are compared in Fig. 1.

The equilibrium structures,  $\Delta E$  and  $\Delta E^X$  obtained from B3LYP/TZVP calculations agree in general with the results in the literature.<sup>20,24,77-79</sup> The Zundel complex with  $C_2$  symmetry (structure **a** in Table 1) represents the absolute minimum energy geometry of the  $\text{H}_3\text{O}^+ - \text{H}_2\text{O}$  1:1 complex, both in the gas phase and continuum aqueous solution. The equilibrium structure of the  $\text{H}_3\text{O}^+ - \text{H}_2\text{O}$  1:2 complex (structure **b** in Table 1) consists of two symmetric O-H...O H-bonds at  $\text{H}_3\text{O}^+$ , with  $R_{\text{O-H}}$  about 0.2 Å shorter than the Zundel complex. For the  $\text{H}_3\text{O}^+ - \text{H}_2\text{O}$  1:3 complex, three equilibrium structures were predicted by B3LYP/TZVP calculations (structures **c**, **d** and **e** in Table 1). With a complete water coordination at  $\text{H}_3\text{O}^+$ ,  $\Delta E$  of the Eigen complex (structure **c**) is about 13 kJ/mol more stable than the structures with the Zundel complex as the central charged species (structures **d** and **e**). Structures **f**, **g** and **h** are three important equilibrium structures of the  $\text{H}_3\text{O}^+ - \text{H}_2\text{O}$  1:4 complex. Having the Eigen complex as the central charged species, structure **g** in the gas phase is about 14 kJ/mol more stable than structures **f** and **h**, whereas in the continuum aqueous solvent (COSMO) structure **h** is about 2 kJ/mol more stable than structure **g**. The stabilization effects at the central charged species can be confirmed by the values of  $\Delta E^X$ ,  $X = \text{H}_3\text{O}^+$  or  $\text{H}_5\text{O}_2^+$ . It appeared that, for the same number of water coordination,  $\text{H}_3\text{O}^+$  can be more effectively stabilized by water molecules compared to the Zundel complex; as an example,  $\Delta E^{\text{H}_3\text{O}^+}$  of

structure **b** in the gas phase is  $-290.7$  kJ/mol, whereas  $\Delta E^{\text{H}_5\text{O}_2^+}$  of structures **d** and **e** are  $-191.7$  kJ/mol.

The environmental effects on the stabilities of charged H-bonds were investigated using *ab initio* SCRf (self-consistent reaction field) calculations at the Hartree-Fock level, from which the dependence of  $\Delta E$  on a wide range of dielectric constant ( $\epsilon$ ) was established.<sup>28</sup> It was reported that small increases in  $\epsilon$  from the gas-phase value ( $\epsilon = 1$ ) rapidly reduce the stabilities of the charged H-bonds. In the present work, although the equilibrium structures in the gas phase and continuum aqueous solution are almost the same,  $\Delta E$  and  $\Delta E^X$  are considerably higher (less negative) in continuum aqueous solution (see Fig. 1). The destabilization effects caused by the continuum aqueous solvent are in good agreement with ref. 28. Fig. 1 also illustrates the trends of  $\Delta E$ ,  $\Delta E^X$  and  $\Delta E^{\text{sol}}$  with respect to the number of water molecules. The trends of  $\Delta E$ , as well as  $\Delta E^X$ , in the gas phase and continuum aqueous solution are quite similar, with smaller variations in continuum aqueous solution. The solvent effects can be directly observed in Fig. 1a, in which  $\Delta E^{\text{sol}}$  are not substantially different for structures **c** to **h**. This suggested that, when the number of water molecules is the same, the H-bonds inside the protonated water clusters experience comparable uniform electric field (COSMO), with the asymptotic  $\Delta E$  in continuum aqueous solution  $\approx -149$  kJ/mol and  $\Delta E^{\text{sol}} \approx -266$  kJ/mol. Fig. 1b revealed that the trends of the interaction energies ( $\Delta E^X$ ) remain the same when the counterpoise corrections were applied; the BSSE contributes only about 3% of  $\Delta E^X$ .

As concluded in the previous work,<sup>26,57</sup>  $\Delta d_{\text{DA}}$  obtained from static proton transfer potentials could be used to measure the tendency of proton transfer, as well as the strength of H-bond. Based on the criteria in ref. 57 and  $\Delta d_{\text{DA}}$  in Table 1, The H-bonds in structures **a**, **d**, **e**, **f** and **h** are susceptible to proton transfers in the gas phase, with  $0 \leq \Delta d_{\text{DA}} \leq 0.32$ ; whereas the continuum aqueous solvent (COSMO) destabilizes the protonated water clusters, resulting in shifts of the H-bond protons away from the centers, especially for structures **d**, **e** and **h**.

As reported in ref. 18, the H-bond distance ( $R_{\text{O-O}}$ ) in concentrated HCl solution can be divided into three groups namely, the internal, external and solvation groups. The H-bonds linking directly to protons belong to the internal group, with  $R_{\text{O-O}}$  in the range of 2.45–2.57 Å, whereas  $R_{\text{O-O}}$  in the external and solvation groups are in the ranges of 2.60–2.70 Å and longer than 2.70 Å, respectively. Fig. 2a shows linear relationships between  $\Delta d_{\text{DA}}$  and  $R_{\text{O-O}}$ , with a separation between the internal and external H-bonds at  $R_{\text{O-O}} \approx 2.5$  Å, in good agreement with ref. 18. The linear relationships for the internal and external H-bonds can be represented by eqn (1) and (2), respectively.

$$\text{Internal H-bonds: } \Delta d_{\text{DA}} = 3.57 \times R_{\text{O-O}} - 8.50 \quad (1)$$

$$\text{External H-bonds: } \Delta d_{\text{DA}} = 1.34 \times R_{\text{O-O}} - 2.90 \quad (2)$$

Theoretical and experimental results on vibrational spectra of the transferring proton in the Zundel complex were presented in the past decades,<sup>17,20,22</sup> from which the flatness of the potential energy surface was concluded by *ab initio* calculations at different levels to be the most outstanding feature of the H-bond proton.<sup>20</sup> For the Zundel complex in the gas phase ( $\Delta d_{\text{DA}} = 0$ ),

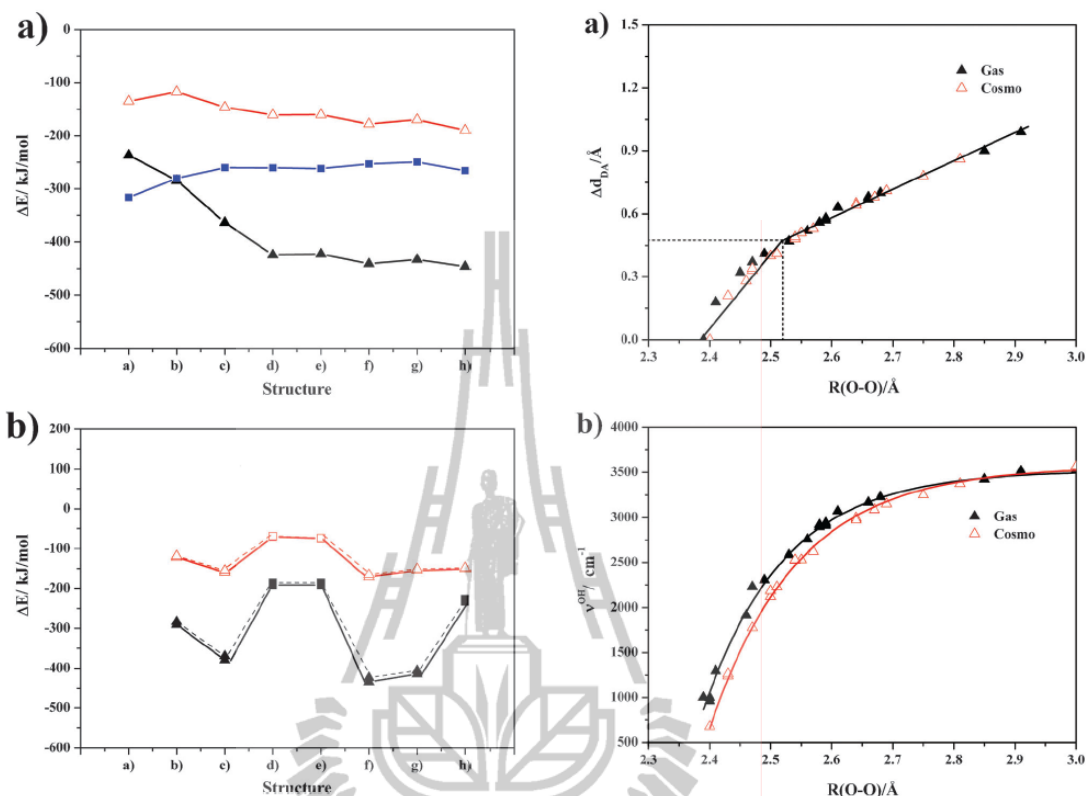


**Fig. 1** (a) Trends of the interaction ( $\Delta E$ ) and solvation energies ( $\Delta E^{sol}$ ) with respect to the number of water molecules, obtained from B3LYP/TZVP calculations:  $\blacktriangle$  =  $\Delta E$  in the gas phase;  $\blacktriangle$  =  $\Delta E$  in continuum aqueous solution;  $\blacksquare$  =  $\Delta E^{sol}$ . (b) Trends of the interaction energies between the central charged species and water molecules ( $\Delta E^X$ , X =  $H_3O^+$  or  $H_5O_2^+$ ) with respect to the number of water molecules, obtained from B3LYP/TZVP calculations:  $\blacktriangle$  =  $H_3O^+$  in the gas phase;  $\blacktriangle$  =  $H_3O^+$  in the continuum aqueous solution;  $\blacksquare$  =  $H_5O_2^+$  in the gas phase;  $\blacksquare$  =  $H_5O_2^+$  in continuum aqueous solution. — = calculations without the counterpoise correction. - - - - = calculations with the counterpoise correction.

B3LYP/TZVP calculations predicted  $\nu^{OH} = 961 \text{ cm}^{-1}$ , whereas in continuum aqueous solution  $\nu^{OH} = 677 \text{ cm}^{-1}$ . The former is in reasonable agreement with the theoretical results at the same levels of accuracy<sup>24,77</sup> and IRMPD experiment.<sup>24,80</sup>

Good agreement between theoretical and experimental data was also found for  $H_7O_3^+$ . In the gas phase, B3LYP/TZVP calculations predicted  $\nu^{OH} = 2304 \text{ cm}^{-1}$ , compared with B3LYP/T(O)DZP calculations of  $2402 \text{ cm}^{-1}$ ,<sup>20</sup> and experiment between  $2200$  and  $2300 \text{ cm}^{-1}$ .<sup>81</sup> These  $\nu^{OH}$  could be associated with the H-bond protons in the  $H_3O^+ \cdots H_2O$  contact structure. For larger protonated water clusters, the structures with the Zundel complex as the central charged species exhibit higher tendencies of proton transfers, with  $1000 < \nu^{OH} < 1450 \text{ cm}^{-1}$ , whereas the structures with  $H_3O^+$  as the central charged species possess  $1900 < \nu^{OH} < 2760 \text{ cm}^{-1}$ .

Due to the asymptotic behavior at large  $R_{O-O}$ , the relationships between  $\nu^{OH}$  and  $R_{O-O}$  in Fig. 2b cannot be approximated by

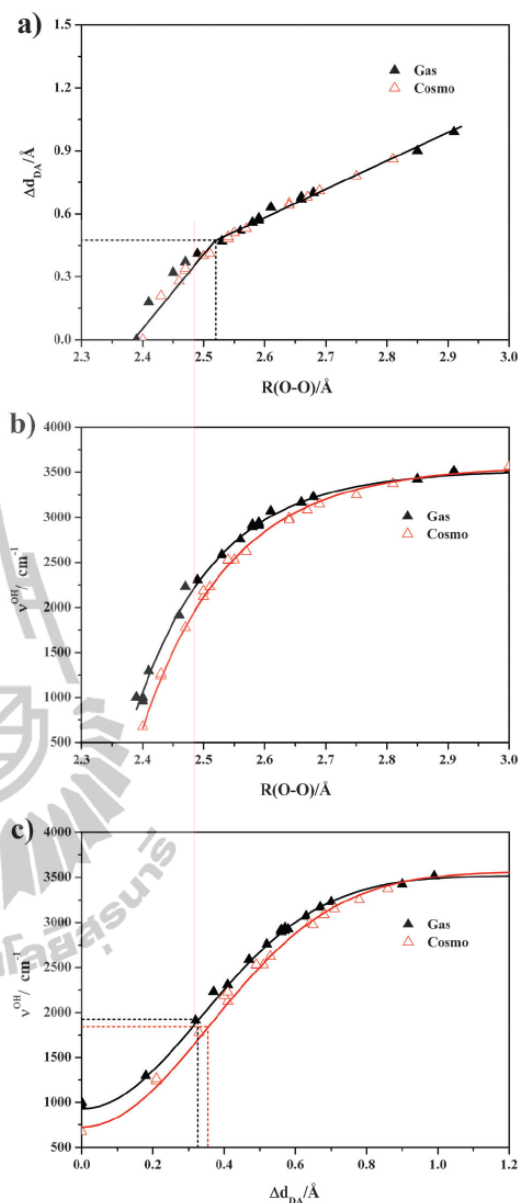


**Fig. 2** (a) Plot of the asymmetric stretching coordinates ( $\Delta d_{DA}$ ) and the O-H...O H-bond distances ( $R_{O-O}$ ), obtained from B3LYP/TZVP calculations. (b) Plot of the asymmetric O-H stretching frequencies ( $\nu^{OH}$ ) and the O-H...O H-bond distances ( $R_{O-O}$ ), obtained from B3LYP/TZVP calculations. (c) Plot of the asymmetric O-H stretching frequencies ( $\nu^{OH}$ ) and the asymmetric stretching coordinates ( $\Delta d_{DA}$ ), obtained from B3LYP/TZVP calculations.

linear functions; at large  $R_{O-O}$ ,  $\nu^{OH}$  converges to the asymmetric O-H stretching frequency of the free or non-H-bonded proton in  $H_3O^+$ . After several trial fittings, an exponential function similar to the integrated rate expression for the first order



reaction was found to be the most appropriate, with the asymptotic values in the gas phase and continuum aqueous solution fixed at  $\nu^{\text{OH}} = 3521$  and  $3566 \text{ cm}^{-1}$ , respectively. The agreements between  $\nu^{\text{OH}}$  obtained from B3LYP/TZVP calculations and the fitted values are included in Fig. 2b. The fitted functions in the gas phase and continuum aqueous solution are given in eqn (3) and (4), respectively.

$$\text{Gas phase: } \nu^{\text{OH}} = -1.67 \times 10^{11} e^{-R_{\text{O-O}}/0.1331} + 3521 \quad (3)$$

$$\text{COSMO: } \nu^{\text{OH}} = -5.15 \times 10^{10} e^{-R_{\text{O-O}}/0.1438} + 3566 \quad (4)$$

An attempt has been made to distinguish between normal and strong H-bonds, however without a concrete result. It was found in general that, when the H-bond is shorter, it becomes stronger, with the strongest attractive interaction at the shortest H-bond distance.<sup>28,82</sup> According to the analyses of the H-bond energies with the H-bond distances in crystal structures, Hibbert and Emsley revealed that the experimental H-bond energies change dramatically at the H-bond distance of 2.45 Å.<sup>82</sup> They concluded that 2.45 Å is the threshold distance for very strong H-bonds. Theoretical studies, on the other hand, revealed smooth linear relationships between the H-bond energies and the H-bond distances, with no dramatic change when the H-bond distance is between 2.45 and 2.80 Å, a reflection of similar electronic structures of the H-bond complexes within this range.<sup>28</sup> A similar linear correlation was

obtained when the differences between the proton affinities of donor–acceptor pairs ( $\Delta\text{PA}$ ) and the H-bond energies were plotted, with no significant deviation in the H-bond energy at  $\Delta\text{PA} = 0$ , at which a low-barrier proton transfer potential was anticipated.<sup>28</sup>

Since strong H-bonds are susceptible to proton transfers, normal and strong H-bonds could be distinguished using IR frequencies of the transferring protons. In the present work,  $\nu^{\text{OH}}$  and  $\Delta d_{\text{DA}}$  are plotted and illustrated in Fig. 2c, in which an interesting correlation was observed;  $\nu^{\text{OH}}$  could be expressed in terms of  $\Delta d_{\text{DA}}$  using an exponential function resembling the normal distribution function. The fitted functions for the protonated water clusters in the gas phase and continuum aqueous solution are given in eqn (5) and (6), respectively.

$$\text{Gas phase: } \nu^{\text{OH}} = 3521 - \frac{6354}{\sqrt{2\pi}} e^{-4.5\Delta d_{\text{DA}}^2} \quad (5)$$

$$\text{COSMO: } \nu^{\text{OH}} = 3566 - \frac{6964}{\sqrt{2\pi}} e^{-3.9\Delta d_{\text{DA}}^2} \quad (6)$$

The agreements between  $\nu^{\text{OH}}$  obtained from B3LYP/TZVP calculations and the fitted values are also included in Fig. 2c. Two inflection points are seen in Fig. 2c, in the gas phase at  $\Delta d_{\text{DA}} = 0.33$  and in continuum aqueous solution at  $\Delta d_{\text{DA}} = 0.36$  Å. These correspond to  $\nu^{\text{OH}} = 1984$  and  $1881 \text{ cm}^{-1}$ , respectively. It should be mentioned that, for the Zundel

**Table 2** Dynamic results of the shared-proton complexes obtained from BOMD simulations at 350 K. Distances, energies and IR frequencies are in Å, kJ/mol and  $\text{cm}^{-1}$ , respectively. Proton diffusion coefficient (D) is in  $\text{cm}^2 \text{ s}^{-1}$ ,<sup>a</sup>

Structure		$\langle R_{\text{O-O}} \rangle$	$\langle \Delta d_{\text{DA}} \rangle$	$\nu^{\text{OH,MD}}$		$I_{\text{A}}/I_{\text{O-O}}$	$I_{\text{B}}/I_{\text{A}}$	D ( $10^{-5}$ )	
				A	B				
a		Gas	2.42	0.18	1127.8	1851.7	0.57	0.51	10.26
		Cosmo	2.43	0.20	942.7	1750.7	0.69	0.09	9.16
d		Gas	2.42	0.21	1178.3	1767.5	0.48	0.19	10.89
		Cosmo	2.48	0.35	1447.7	2003.3	0.14	0.55	10.54
e		Gas	2.43	0.19	1262.5	1784.4	— <sup>b</sup>	0.45	11.09
		Cosmo	2.44	0.22	1178.3	1649.7	0.29	0.23	12.95
f		Gas	2.46	0.32	1515.0	2053.2	0.28	0.63	8.89
		Cosmo	2.47	0.44	1733.9	2592.4	0.17	0.79	8.20

<sup>a</sup>  $\langle R_{\text{O-O}} \rangle$  = average H-bond distance;  $\langle \Delta d_{\text{DA}} \rangle$  = average asymmetric stretching coordinate;  $\nu^{\text{OH,MD}}$  = asymmetric O–H stretching frequency;  $I_{\text{A}}$  = intensity of the oscillatory shuttling band;  $I_{\text{B}}$  = intensity of the structural diffusion band;  $I_{\text{O-O}}$  = intensity of the O–O stretching band; D = proton diffusion coefficient. <sup>b</sup> Not obtainable due to H-bond structure reorganization in the course of BOMD simulations.

complex in the gas phase, the term “critical distance” was used to describe  $R_{O-O}$  at which symmetric double-well potential with high barrier at the center is transformed into single-well potential without barrier.<sup>55,83</sup> In Fig. 2a,  $\Delta d_{DA} = 0.33$  and  $0.36$  Å correspond to  $R_{O-O} = 2.47$  and  $2.48$  Å, respectively, slightly longer than the critical distance of  $R_{O-O} = 2.43$  Å.<sup>55</sup> Therefore, the inflection points in Fig. 2c could be associated with the “threshold” asymmetric stretching coordinates ( $\Delta d_{DA}^*$ ) and frequencies ( $\nu^{OH*}$ ) for proton transfer, and could be used to distinguish between normal and strong H-bonds in the protonated water clusters.

### Dynamic results

All the shared-proton complexes obtained in the previous subsection were investigated in BOMD simulations at 350 K; except structure **h**, for which the cyclic H-bonds were transformed into linear (similar to structure **f**) in the course of BOMD simulations. As pointed out in the previous subsection, the stabilities of the protonated water clusters are substantially decreased in continuum aqueous solution. This and the fact that our model systems did not take into account the H-bond networks of water in the vicinities of the protonated water clusters, especially in the presence of strong thermal energy fluctuations in BOMD simulations, made it difficult to discuss the energetic results. Therefore, the focuses are on the H-bond structures and IR spectra, from which the characteristic IR frequencies were used to explain the vibrational behaviors and dynamics of the proton transfer processes.

**Average H-bond structures of shared-proton complexes.** The average H-bond distances ( $\langle R_{O-O} \rangle$ ) and asymmetric stretching coordinates ( $\langle \Delta d_{DA} \rangle$ ) of the shared-proton complexes obtained from BOMD simulations are listed in Table 2. Linear relationships between  $\langle \Delta d_{DA} \rangle$  and  $\langle R_{O-O} \rangle$  were also obtained from BOMD simulations. They are illustrated in Fig. 3a. The fitted functions for the internal and external H-bonds are represented by eqn (7) and (8), respectively.

$$\text{Internal H-bonds: } \langle \Delta d_{DA} \rangle = 2.74 \times \langle R_{O-O} \rangle - 6.47 \quad (7)$$

$$\text{External H-bonds: } \langle \Delta d_{DA} \rangle = 1.59 \times \langle R_{O-O} \rangle - 3.57 \quad (8)$$

BOMD simulations at 350 K predicted the separation between the internal and external H-bonds at  $\langle R_{O-O} \rangle = 2.5$  Å, the same as that from B3LYP/TZVP calculations.

**Asymmetric O–H stretching frequencies and proton transfer pathways.** The characteristic asymmetric O–H stretching frequencies ( $\nu^{OH,MD}$ ) of the protons in the shared-proton complexes are included in Table 2. Examples of symmetric and asymmetric O–H stretching bands, as well as the O–O vibration band, are shown in Fig. 4.

In order to discuss the dynamics of the structural diffusion mechanism, the IR spectra of the transferring protons were analyzed in details, using the Zundel complex as an example. The IR spectra of the transferring protons are broad in general, especially in continuum aqueous solution. The BOMD results in Fig. 4 show two characteristic asymmetric O–H stretching bands, labeled with **A** and **B**; for the Zundel complex in the gas phase (in Fig. 4a) at  $\nu^{OH,MD} = 1128$  and  $1852$   $\text{cm}^{-1}$ , respectively, and in continuum aqueous solution

(in Fig. 4b) at  $\nu^{OH,MD} = 943$  and  $1751$   $\text{cm}^{-1}$ , respectively. The low-frequency bands at **A**, appearing at  $\nu^{OH,MD}$  slightly higher than those from B3LYP/TZVP calculations, are associated with the asymmetric O–H stretching mode, for which proton shuttles back and forth at the center of the H-bond.  $\nu^{OH,MD}$  at **A** agree well with the IRMPD experiment<sup>24</sup> and BOMD simulations at 80 and 270 K.<sup>20</sup> The higher-frequency bands at **B**, not obtainable from single-well static proton transfer potentials with harmonic approximation, represent the vibrational mode with the center of vibration slightly shifted towards an oxygen atom.<sup>26</sup> Both characteristic IR bands could be regarded as spectral signatures of proton transfer reactions;<sup>26,27</sup> the former reflects the extent of the shared-proton complex formation and the latter the product formation. They are comparable with the “oscillatory shuttling motion” and the “Grotthuss shuttling motion” (or “structural diffusion motion”), respectively.<sup>79</sup>

A review on state-of-the-art methods for the calculations of vibrational energies of polyatomic molecules using quantum mechanical, variationally-based approaches was presented,<sup>84</sup> in which accurate IR spectra of ionic species in the gas phase were discussed in comparison with experiment.<sup>80</sup> One of the emphases was on the analyses of the middle spectral region ( $800$ – $2000$   $\text{cm}^{-1}$ ) which can be directly related to the proton transfer in the Zundel complex; the experiment<sup>80</sup> showed a doublet centered at  $1000$   $\text{cm}^{-1}$  as the most characteristic feature, with the low-energy component at  $928$   $\text{cm}^{-1}$  and the high-energy component at  $1047$   $\text{cm}^{-1}$ . Based on the multi-configuration time-dependent Hartree (MCTDH) method, the most intense band was concluded to be the proton transfer fundamental band (asymmetric O–H stretching mode) and the doublet was attributed to the coupling among the low-frequency water-wagging modes, water-water stretching motion and the proton transfer motion. Additionally, the MCTDH method predicted a water bending state which couples strongly with the proton transfer motion at  $1741$   $\text{cm}^{-1}$ , compared with the experiment at  $1763$   $\text{cm}^{-1}$ .<sup>80</sup> The present BOMD simulations predicted the proton transfer fundamental frequency in the gas phase close to the MCTDH method and the experiment<sup>80</sup> ( $1128$   $\text{cm}^{-1}$  at 350 K, compared with  $1047$   $\text{cm}^{-1}$  at 275 K). Since one of the main objectives of the present work is to search for an appropriate theoretical method to monitor proton transfer processes in BOMD simulations on larger H-bond systems and it is sufficient to employ the fundamental asymmetric O–H stretching frequencies, the low-frequency band of the doublet was not investigated in details.

As the proton transfer in H-bond depends strongly on the O–O vibration,<sup>27</sup> the relative probability or the extent of the shared-proton complex formation in BOMD simulations could be approximated from the ratio between the intensity of  $\nu^{OH,MD}$  at **A** ( $I_A$ ) and the intensity of the O–O vibration ( $I_{O-O}$ ).<sup>26</sup> In Table 2,  $I_A/I_{O-O}$  for the Zundel complex in the gas phase and continuum aqueous solution are 0.6 and 0.7, respectively, indicating that, in BOMD simulations in the gas phase, about 60% of the  $\text{H}_3\text{O}^+ - \text{H}_2\text{O}$  1:1 complex are in the form of the Zundel complex, whereas in continuum aqueous solution about 70%. The values of  $I_A/I_{O-O}$  in Table 2 also suggest that the extent of the oscillatory shuttling motion is decreased when the number of water molecule increased;

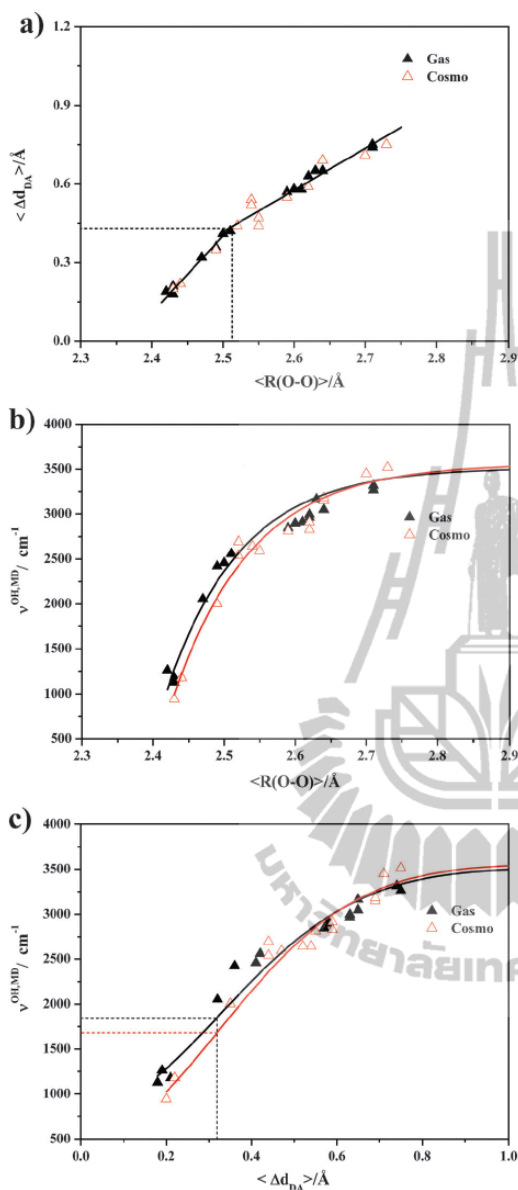


**Fig. 3** (a) Plot of the average asymmetric stretching coordinates ( $\langle \Delta d_{DA} \rangle$ ) and the average O-H...O H-bond distances ( $\langle R_{O-O} \rangle$ ), obtained from BOMD simulations at 350 K. (b) Plot of the asymmetric O-H stretching frequencies ( $\nu^{\text{OH,MD}}$ ) and the average O-H...O H-bond distances ( $\langle R_{O-O} \rangle$ ), obtained from BOMD simulations at 350 K. (c) Plot of the asymmetric O-H stretching frequencies ( $\nu^{\text{OH,MD}}$ ) and the asymmetric stretching coordinates ( $\langle \Delta d_{DA} \rangle$ ), obtained from BOMD simulations at 350 K.

indicating a higher efficiency of proton transfer in extended H-bond network.

The observation that the proton transfer process in the  $\text{H}_3\text{O}^+ - \text{H}_2\text{O}$  1:1 complex consists of two consecutive steps

namely, a quasi-dynamic equilibrium between the precursor (the  $\text{H}_3\text{O}^+ - \text{H}_2\text{O}$  1:1 complex) and the shared-proton complex (the Zundel complex), followed by the actual proton transfer,<sup>27</sup> made it possible to establish a criterion to measure the extent or the efficiency of proton transfer from IR spectra; the quasi-dynamic equilibrium prevents proton transfer reaction from being concerted and is considered to be the rate-determining step.<sup>26,27</sup> Hence, an effective proton transfer process should take the reaction path with the shortest lifetime of the quasi-dynamic equilibrium. Therefore, in order to achieve an “ideal” maximum efficiency, according to the transition-state theory, the populations of the shared-proton complex and the product must be the same. In other words, every shared-proton complex formation should lead to the actual proton transfer. This is possible only when the O–O distance undergoes large-amplitude vibration, for which the O–H and O–O vibrations are coherent.<sup>27</sup> It should be emphasized that, since the present model systems involved only the O...H<sup>+</sup>...O H-bonds, the product becomes precursor for the successive proton transfer event.

As the populations of the shared-proton complex and the precursor in BOMD simulations could be approximated from the intensities of the oscillatory shuttling band (A) and the structural diffusion band (B), the efficiency of proton transfer could be approximated from the ratio between  $I_B/I_A$  ( $I_B/I_A = 1$  for the ideal maximum efficiency). Table 2 reveals that, for the Zundel complex in the gas phase,  $I_B/I_A$  is about 0.5 (half of the ideal maximum efficiency), whereas in continuum aqueous solution  $I_B/I_A < 0.1$ , a dominance of the oscillatory shuttling motion (shared-proton complex). It turned out that, based on this criterion, the most extended H-bond structure with incomplete hydration at  $\text{H}_3\text{O}^+$  (structure f) possesses the highest efficiency for proton transfer.

Fig. 3b shows the relationships between  $\nu^{\text{OH,MD}}$  at A (the oscillatory shuttling frequencies) and  $\langle R_{O-O} \rangle$ . Similar to B3LYP/TZVP calculations, the exponential functions in eqn (9) and (10) can well represent  $\nu^{\text{OH,MD}}$  in the gas phase and continuum aqueous solution, respectively.

$$\text{Gas phase: } \nu^{\text{OH,MD}} = -2.47 \times 10^{13} e^{-(R_{O-O})/0.1051} + 3521 \quad (9)$$

$$\text{COSMO: } \nu^{\text{OH,MD}} = -9.14 \times 10^{12} e^{-(R_{O-O})/0.1105} + 3566 \quad (10)$$

As in the case of the B3LYP/TZVP calculations, the relationships between  $\nu^{\text{OH,MD}}$  and  $\langle \Delta d_{DA} \rangle$  in Fig. 3c were used to approximate the threshold frequencies for proton transfers in BOMD simulations. They are represented by eqn (11) and (12), in the gas phase and continuum aqueous solution, respectively.

$$\text{Gas phase: } \nu^{\text{OH,MD}} = 3521 - \frac{6630}{\sqrt{2\pi}} e^{-4.7(\Delta d_{DA})^2} \quad (11)$$

$$\text{COSMO: } \nu^{\text{OH,MD}} = 3566 - \frac{7563}{\sqrt{2\pi}} e^{-4.9(\Delta d_{DA})^2} \quad (12)$$

The calculations of the second derivatives of the functions in eqn (11) and (12) yielded two inflection points at  $\langle \Delta d_{DA} \rangle = 0.32 \text{ \AA}$ , corresponding to the threshold frequencies at  $\nu^{\text{OH,MD}*} = 1917$  and  $1736 \text{ cm}^{-1}$ , in the gas phase and continuum aqueous solution, respectively. The values are slightly

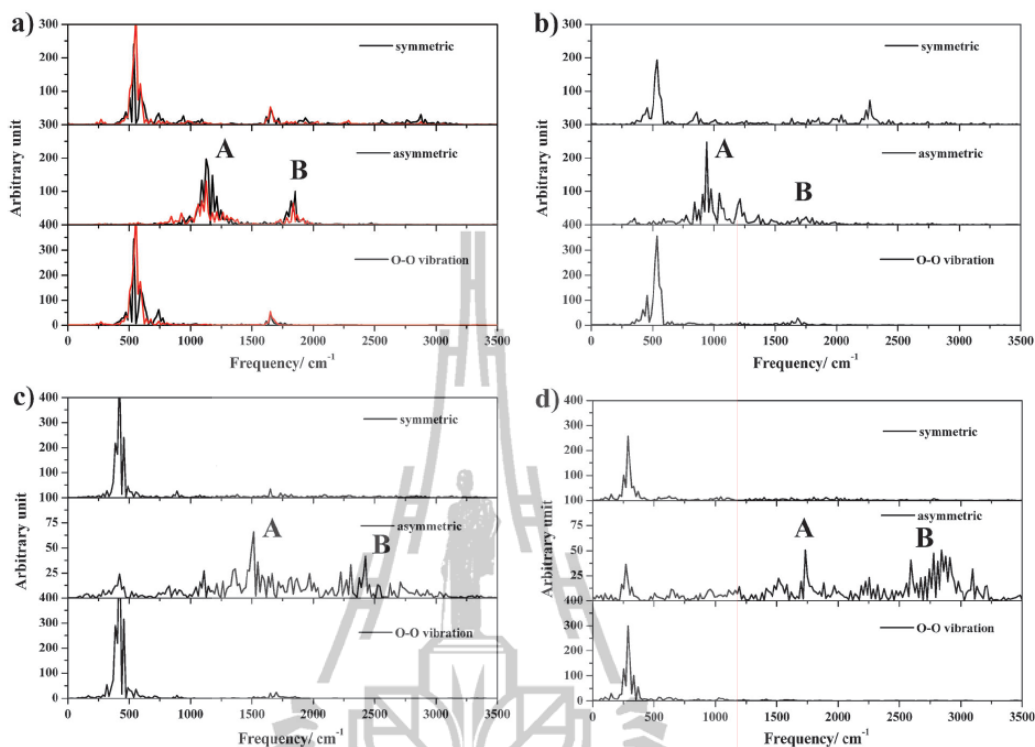


Fig. 4 Symmetric and asymmetric O-H stretching bands of the transferring protons in the shared-proton complexes, together with the O-O vibration band, obtained from BOMD simulations at 350 K. (a) The Zundel complex (structure a) in the gas phase; — = BOMD simulations with the simulation length of 5 ps. (b) The Zundel complex (structure a) in continuum aqueous solution. (c) The H<sub>3</sub>O<sup>+</sup>-H<sub>2</sub>O 1:4 complex (structure f) in the gas phase. (d) The H<sub>3</sub>O<sup>+</sup>-H<sub>2</sub>O 1:4 complex (structure f) in continuum aqueous solution.

lower than those obtained from B3LYP/TZVP calculations, due to the inclusion of the thermal energy fluctuations and dynamics in BOMD simulations.

**Dynamics of structural diffusion.** The diffusion coefficients (*D*) of the transferring protons in the shared-proton complexes are listed in Table 2. The diffusion coefficients of the Zundel complex in the gas phase and continuum aqueous solution, obtained from BOMD simulations at 350 K, are  $10.3 \times 10^{-5}$  and  $9.2 \times 10^{-5} \text{ cm}^2 \text{ s}^{-1}$ , respectively. Based on the same approach, BOMD simulations predicted the diffusion coefficient at 298 K to be  $5.0 \times 10^{-5} \text{ cm}^2 \text{ s}^{-1}$ ,<sup>26</sup> slightly lower than the NMR result;<sup>10</sup> in NMR experiments, the diffusion coefficient of a proton moving across a single water molecule was estimated from the NMR hopping time ( $\tau_p$ ) and the Einstein relation ( $D = l^2/6\tau_p$ ) to be  $7.0 \times 10^{-5} \text{ cm}^2 \text{ s}^{-1}$ ; where *l* is the hopping length or the H-bond distance (2.5 Å) and  $\tau_p = 1.5$  ps. It should be added that, the diffusion coefficient reported in ref. 10 was derived by subtracting the water self-diffusion coefficient ( $2.3 \times 10^{-5} \text{ cm}^2 \text{ s}^{-1}$ ) from the proton diffusion coefficient ( $9.3 \times 10^{-5} \text{ cm}^2 \text{ s}^{-1}$ ). The deviation of about 28% from the experimental value<sup>10</sup> could be attributed to the neglect of the H-bond networks connecting the hydration shells of the Zundel complex.<sup>26</sup> For larger protonated water clusters, the shared-proton complex with an extended H-bond

network, structure f, possesses  $D = 8.9 \times 10^{-5}$  and  $8.2 \times 10^{-5} \text{ cm}^2 \text{ s}^{-1}$ , in the gas phase and continuum aqueous solution, respectively. The values are lower than those of the Zundel complex. These support the conclusion that the oscillatory shuttling motion is slightly more important in the H<sub>3</sub>O<sup>+</sup>-H<sub>2</sub>O 1:1 complex, compared to the extended H-bond structures.

In order to further assess the reliability of the dynamic results obtained from BOMD simulations, the lifetimes ( $\tau$ ) of the shared-proton structures were computed from VACF of the O-O vibrations.<sup>73</sup> VACF of the O-O vibrations in the Zundel complex and structure f, the structure with the highest efficiency of proton transfer in this series, are shown as examples in Fig. 5. It appeared that an asymptotic exponential relaxation behavior of the envelope of VACF could be approximated, except for the Zundel complex in continuum aqueous solution (Fig. 5b), for which the envelope of the O-O vibration at short time cannot fit an exponential function. For the Zundel complex in the gas phase, BOMD simulations at 350 K predicted  $\tau$  to be 270 fs, corresponding to the classical first-order rate constant (*k*) for the interconversion between the shared-proton structure (H<sub>5</sub>O<sup>+</sup>) and the H<sub>3</sub>O<sup>+</sup>-H<sub>2</sub>O contact structure of  $5.1 \text{ ps}^{-1}$ . The shared-proton structure in structure f possesses shorter lifetimes,  $\tau = 241$  and 233 fs, in the gas phase and continuum aqueous solution, respectively.

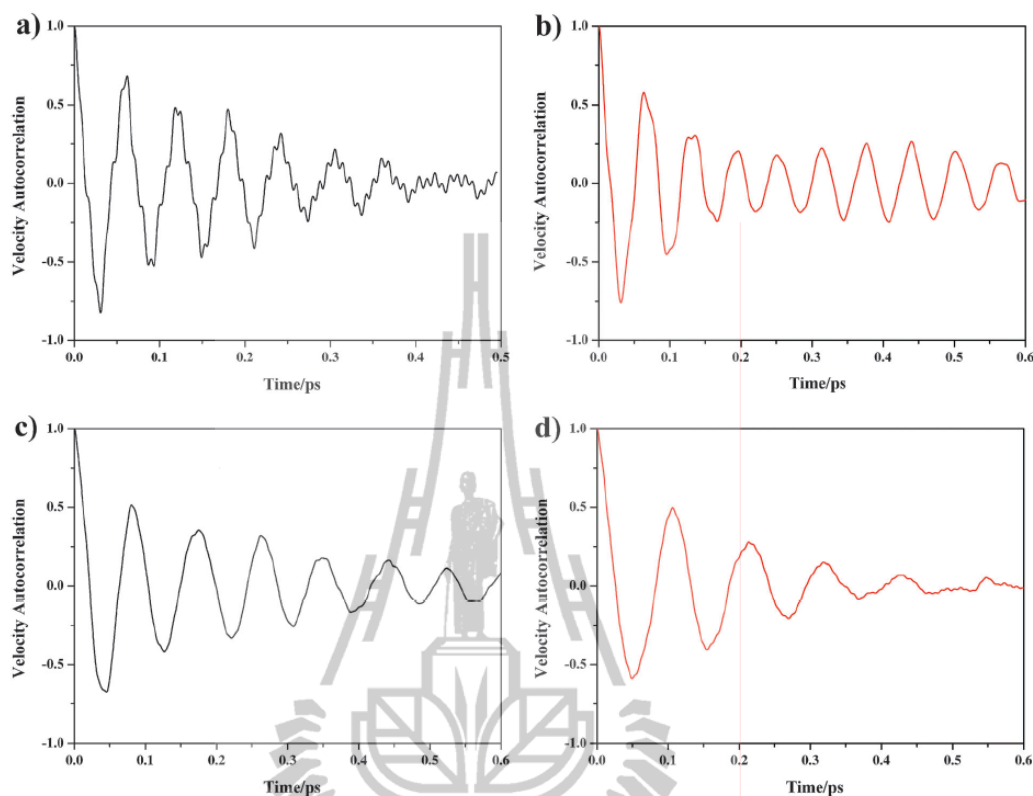


Fig. 5 Examples of velocity autocorrelation functions (VACF) of the O–O vibrations in the shared-proton structures, obtained from BOMD simulations at 350 K. (a) The Zundel complex in the gas phase. (b) The Zundel complex in continuum aqueous solution. (c) The  $\text{H}_3\text{O}^+ - \text{H}_2\text{O}$  1 : 4 complex (structure f) in the gas phase. (d) The  $\text{H}_3\text{O}^+ - \text{H}_2\text{O}$  1 : 4 complex (structure f) in continuum aqueous solution.

The values correspond to  $k = 5.8$  and  $6.0 \text{ ps}^{-1}$ , respectively. The latter reflect higher efficiencies of proton transfer in an extended H-bond network. The lifetimes of the shared-proton structures are in reasonable agreement with the result obtained from the multistate empirical valence bond (MS-EVB) calculations at 280 K,  $\tau = 370 \text{ fs}$ ,<sup>85</sup> whereas the rate constants are in accordance with the O–O vibration rate, obtained from quantum MD simulations at 300 K,  $k = 5.0 \text{ ps}^{-1}$ .<sup>12</sup>

Finally, in order to ensure that the dynamics and IR results discussed above are reliable, an attempt was made to perform NVT BOMD simulations with longer simulation times. This was successful only for the Zundel complex in the gas phase, and not longer than 5 ps; all the other shared-proton complexes became fragmented after 2.5 ps. It appeared that, for the IR spectra, the oscillatory shuttling and structural diffusion frequencies remain the same (see Fig. 4a), with slight decreases of the intensities,  $I_B/I_A = 0.49$  compared with 0.51. The diffusion coefficient in the gas phase is slightly decreased, from  $10.3 \times 10^{-5}$  to  $9.5 \times 10^{-5} \text{ cm}^2 \text{ s}^{-1}$ . This leads to a conclusion that, although for small H-bond complexes, the IR spectra obtained from short BOMD simulations show some fine structures, meaningful and reasonable interpretations could be made, especially for all the H-bond complexes investigated

here; a similar conclusion was presented by Termath and Sauer<sup>20</sup> based on a series of BOMD simulations on  $\text{H}_3\text{O}_2^+$  and  $\text{H}_7\text{O}_3^+$ , from which insights into fast dynamic processes in H-bonds (e.g. H-bond structures and IR spectra) were obtained from relatively short BOMD trajectories (about 2 ps).

## Conclusion

Proton transfer reactions and dynamics in protonated water clusters were systematically studied using the H-bond complexes formed from  $\text{H}_3\text{O}^+$  and  $n\text{H}_2\text{O}$ ,  $n = 1-4$ , as model systems. The theoretical investigations began with searching for the H-bond complexes which could be important in the dynamic proton transfer pathways, as well as characteristic H-bond structures and IR spectra of the transferring protons, both in the gas phase and continuum aqueous solution. DFT calculations at the B3LYP/TZVP level revealed that the potential H-bond structures consist of the Zundel complex, with the characteristic asymmetric O–H stretching frequencies ( $\nu^{\text{OH}}$ )  $< 1000 \text{ cm}^{-1}$  and the threshold frequencies for proton transfers in the gas phase and continuum aqueous solution at  $\nu^{\text{OH}*} = 1984$  and  $1881 \text{ cm}^{-1}$ , respectively. According to the results obtained from the static proton transfer potentials, the

trends of the interaction energies with respect to the number of water molecules in the gas phase and continuum aqueous solution are quite similar. The destabilization effects caused by the continuum aqueous solvent bring about smaller variation of the interaction energies with respect to the number of water molecules compared to the gas phase. The destabilization effects also lead to shifts of the transferring protons away from the centers, especially for the H-bond complexes with the Zundel complex as the central charged species. The trend of the solvation energies revealed that, when the number of water molecules is the same, the H-bonds inside the protonated water clusters experience comparable uniform electric field.

BOMD simulations at 350 K predicted the characteristic asymmetric O–H stretching frequencies in a quite wide range, from 940 to 1740  $\text{cm}^{-1}$ . Most importantly, BOMD simulations suggested additional characteristic asymmetric O–H stretching bands at higher frequencies. They are in the range of 1640 and 2600  $\text{cm}^{-1}$ . The low-frequency bands are regarded as the “oscillatory shuttling band” and the high-frequency bands the “structural diffusion band”. The latter cannot be determined easily from static proton transfer potentials, due to the anharmonic and dynamic behaviors of the vibrational motions of the transferring protons. The oscillatory shuttling and structural diffusion bands could be considered as the spectroscopic evidences for the shared-proton complex and product (or precursor) formations, respectively.

The analyses of the H-bond structures and  $\nu_{\text{OH,MD}}$  yielded the threshold frequencies ( $\nu_{\text{OH,MD}}^*$ ) for the proton transfers in the gas phase and continuum aqueous solution at  $\nu_{\text{OH,MD}}^* = 1917$  and 1736  $\text{cm}^{-1}$ , respectively. Because the quasi-dynamic equilibrium between the Zundel and Eigen complexes was suggested to be the rate-determining step, in order to achieve an “ideal” maximum efficiency, a concerted proton transfer pathway should be taken. The present results anticipated that the effective interconversion between the two proton states, the Zundel-like and hydronium-like structures, could be reflected from comparable intensities of the oscillatory shuttling and structural diffusion bands. These pieces of information could provide an appropriate IR spectroscopic method to investigate proton transfer reactions in larger model systems, and iterated the necessity to incorporate the thermal energy fluctuations and dynamics in the model calculations.

### Acknowledgements

The authors would like to acknowledge the financial supports from the Thailand Research Fund (TRF): the Advanced Research Scholarship, Grant No. BRG5180022 to Prof. Kritsana Sagarik; the Royal Golden Jubilee (RGJ) Ph.D. Program, Grant No. PHD/0121/2549 to Charoensak Lao-ngam and Prof. Kritsana Sagarik. Linux clusters provided by the following organizations are also gratefully acknowledged: School of Mathematics and School of Chemistry, SUT; National Electronics and Computer Technology Center (NECTEC), National Science and Technology Development Agency (NSTDA); the Thai National Grid Center (THAIGRID), Ministry of Information and Communication Technology.

### References

- 1 T. Koppel, *Powering the Future: The Ballard Fuel Cell and the Race to Change the World*, John Wiley & Sons Ltd., New York, 1999.
- 2 J. Larminie and A. Dicks, *Fuel Cell Systems*, John Wiley & Sons Ltd., Chichester, 2001.
- 3 C. A. Vincent and B. Scrosati, *Modern Batteries: An Introduction to Electrochemical Power Sources*, John Wiley & Sons Ltd., New York, 1997.
- 4 K. D. Kreuer, *Chem. Mater.*, 1996, **8**, 610.
- 5 K. D. Kreuer, S. J. Paddison, E. Spohr and M. Schuster, *Chem. Rev.*, 2004, **104**, 4637.
- 6 K. A. Mauritz and R. B. Moore, *Chem. Rev.*, 2004, **104**, 4535.
- 7 S. J. Paddison, *Annu. Rev. Mater. Res.*, 2003, **33**, 289.
- 8 A. Botti, F. Bruni, S. Imberti, M. A. Ricci and A. K. Soper, *J. Mol. Liquid*, in press.
- 9 J. M. Hermida-Ramon and G. Karlstroem, *J. Mol. Struct. (Theochem)*, 2004, **712**, 167.
- 10 N. Agmon, *Chem. Phys. Lett.*, 1995, **244**, 456.
- 11 M. Eigen and L. D. Maeyer, *Proc. Roy. Soc.*, 1958, **A247**, 505.
- 12 M. E. Tuckerman, K. Laasonen, M. Sprik and M. Parrinello, *J. Chem. Phys.*, 1995, **103**, 150.
- 13 M. E. Tuckerman, D. Marx, M. L. Klein and M. Parrinello, *Science*, 1997, **275**, 817.
- 14 J. B. Asbury, T. Steinel and M. D. Fayer, *J. Lumin.*, 2004, **107**, 271.
- 15 J. C. Jiang, C. Chaudhuri, Y. T. Lee and H. C. Chang, *J. Phys. Chem. A*, 2002, **106**, 10937.
- 16 C. C. Wu, C. Chaudhuri, J. C. Jiang, Y. T. Lee and H. C. Chang, *J. Phys. Chem. A*, 2004, **108**, 2859.
- 17 R. Ifimie, V. Thomas, S. Plessis, P. Marchand and P. Ayotte, *J. Am. Chem. Soc.*, 2008, **130**, 5901.
- 18 R. Buzzoni, S. Bordiga, G. Ricchiardi, G. Spoto and A. Zecchina, *J. Phys. Chem.*, 1995, **99**, 11937.
- 19 M. Okumura, L. I. Yeh, J. D. Myers and Y. T. Lee, *J. Phys. Chem.*, 1990, **94**, 3416.
- 20 V. Termath and J. Sauer, *Mol. Phys.*, 1977, **91**, 963.
- 21 C.-C. Wu, J. C. Jiang, D. W. Boo, S. H. Lin, Y. T. Lee and H.-C. Chang, *J. Chem. Phys.*, 2000, **112**, 176.
- 22 K. R. Asmis, N. L. Pivonka, G. Santambrogio, M. Bruemmer, C. Kaposta, D. M. Neumark and L. Woeste, *Science*, 2003, **299**, 1375.
- 23 H.-P. Cheng and J. L. Krause, *J. Chem. Phys.*, 1997, **107**, 8461.
- 24 T. D. Fridgen, T. B. McMahon, L. MacAleese, J. Lemaire and M. Maitre, *J. Phys. Chem. A*, 2004, **108**, 9008.
- 25 U. W. Schmitt and G. A. Voth, *J. Chem. Phys.*, 1999, **111**, 9361.
- 26 K. Sagarik, S. Chaiwongwattana, V. Vchirawongkwin and S. Pruksaaron, *Phys. Chem. Chem. Phys.*, 2010, **12**, 918.
- 27 K. Sagarik, M. Phonyiem, C. Lao-Ngam and S. Chaiwongwattana, *Phys. Chem. Chem. Phys.*, 2008, **10**, 2098.
- 28 J. Chen, M. A. McAllister, J. K. Lee and K. N. Houk, *J. Org. Chem.*, 1998, **63**, 4611.
- 29 J. Fritsch and G. Zundel, *J. Phys. Chem.*, 1981, **85**, 556.
- 30 M. Rospenk, J. Fritsch and G. Zundel, *J. Phys. Chem.*, 1984, **88**, 321.
- 31 G. Zundel and J. Fritsch, *J. Phys. Chem.*, 1984, **88**, 6295.
- 32 J. Rejnek, M. Hanus, M. Kabelá, F. Ryjáek and P. Hobza, *Phys. Chem. Chem. Phys.*, 2005, **7**, 2006.
- 33 K. Sagarik and S. Chaiyapongs, *Biophys. Chem.*, 2005, **117**, 18.
- 34 K. P. Sagarik, *J. Mol. Struct. (Theochem)*, 1999, **465**, 141.
- 35 K. P. Sagarik and R. Ahlrichs, *J. Chem. Phys.*, 1987, **86**, 5117.
- 36 K. P. Sagarik and P. Asawakun, *Chem. Phys.*, 1997, **219**, 173.
- 37 K. P. Sagarik, S. Chaiwongwattana and P. Sisot, *Chem. Phys.*, 2004, **1**.
- 38 K. P. Sagarik and S. Dokmaisrijan, *J. Mol. Struct. (Theochem)*, 2005, **718**, 31.
- 39 K. P. Sagarik, V. Pongpituk, S. Chiyapongs and P. Sisot, *Chem. Phys.*, 1991, **156**, 439.
- 40 K. P. Sagarik and B. M. Rode, *Chem. Phys.*, 2000, **260**, 159.
- 41 K. P. Sagarik and E. Spohr, *Chem. Phys.*, 1995, **199**, 73.
- 42 P. A. Giguere, *J. Chem. Educ.*, 1979, **56**, 571.
- 43 S. J. Paddison, *J. New Mater. Electrochem. Syst.*, 2001, **4**, 197.
- 44 S. J. Paddison and J. A. Elliott, *J. Phys. Chem. A*, 2005, **109**, 7583.
- 45 S. J. Paddison, L. R. Pratt and T. A. Z. Jr., *J. New Mater. Electrochem. Syst.*, 1999, **2**, 183.

- 46 S. J. Paddison, L. R. Pratt and T. Z. Jr., *J. Phys. Chem. A*, 2001, **105**, 6266.
- 47 S. J. Paddison and J. T. Zawodzinski, *Solid State Ionics*, 1998, **115**, 333.
- 48 A. D. Becke, *J. Chem. Phys.*, 1993, **98**, 5648.
- 49 C. Lee, W. Yang and R. G. Parr, *Phys. Rev. B*, 1988, **37**, 785.
- 50 A. Schaefer, C. Huber and R. Ahlrichs, *J. Chem. Phys.*, 1994, **100**, 5829.
- 51 G. Santambrogio, M. Bruemmer, L. Woeste, J. Doebler, M. Sierka, J. Sauer, G. Meijer and K. R. Asmis, *Phys. Chem. Chem. Phys.*, 2008, **10**, 3992.
- 52 R. Ahlrichs, M. Baer, M. Haeser, H. Horn and C. Koelmel, *Chem. Phys. Lett.*, 1989, **162**, 165.
- 53 O. Treutler and R. Ahlrichs, *J. Chem. Phys.*, 1995, **102**, 346.
- 54 S. F. Boys and F. Bernardi, *Mol. Phys.*, 1970, **19**, 553.
- 55 M. Benoit and D. Marx, *ChemPhysChem*, 2005, **6**, 1738.
- 56 D. Marx, M. E. Tuckerman, J. Hutter and M. Parrinello, *Nature*, 1999, **367**, 101.
- 57 J. A. Morrone, K. E. Haslinger and M. E. Tuckerman, *J. Phys. Chem. B*, 2006, **110**, 3712.
- 58 A. P. Scott and L. Radom, *J. Phys. Chem.*, 1996, **100**, 16502.
- 59 D. Xenides, B. R. Randolph and B. M. Rode, *J. Chem. Phys.*, 2005, **122**, 174506.
- 60 P. B. Balbuena and J. M. Seminario, *Theoretical and Computational Chemistry 7*, Elsevier, Amsterdam, 1999.
- 61 R. N. Barnett and U. Landman, *Phys. Rev.*, 1993, **B48**, 2081.
- 62 C. J. Cramer, *Essentials of Computational Chemistry: Theory and Models*, John Wiley & Sons, Ltd., 2002.
- 63 F. Huisken, S. Mohammad-Pooran and O. Werhahn, *Chem. Phys.*, 1998, **239**, 11.
- 64 E. P. L. Hunter and S. G. Lias, *J. Phys. Chem. Ref. Data*, 1998, **27**, 413.
- 65 X. Jing, N. Troullier, D. Dean, N. Binggeli, J. R. Chelikowsky, K. Wu and Y. Saad, *Phys. Rev.*, 1994, **B50**, 122.
- 66 J. Lobaugh and G. A. Voth, *J. Chem. Phys.*, 1996, **104**, 2056.
- 67 A. R. Leach, *Molecular Modelling: Principles and Applications*, Longman, Edinburgh, 1996.
- 68 B. E. Conway, J. O. M. Bockris and H. Linton, *J. Chem. Phys.*, 1956, **24**, 834.
- 69 K. D. Kreuer, *Solid State Ionics*, 2000, **136**, 149.
- 70 R. R. Sadeghi and H.-P. Cheng, *J. Chem. Phys.*, 1999, **111**, 2086.
- 71 D. Sheppard, R. Terrell and G. Henkelman, *J. Chem. Phys.*, 2008, **128**, 134106.
- 72 D. J. Wales, *Mol. Phys.*, 2002, **100**, 3285–3305.
- 73 P. Bopp, *Chem. Phys.*, 1986, **106**, 205.
- 74 M. P. Allen and D. J. Tildesley, *Computer Simulation of Liquids*, Oxford University Press, New York, 1987.
- 75 J. M. Haile, *Molecular Dynamics Simulations*, John Wiley & Sons Ltd, New York, 1997.
- 76 D. C. Rapaport, *The Art of Molecular Dynamics Simulation*, Cambridge University Press, London, 1995.
- 77 M. Park, I. Shin, N. J. Singh and K. S. Kim, *J. Phys. Chem. A*, 2007, **111**, 10692.
- 78 R. Parthasarathi, V. Subramanian and N. Sathyamurthy, *J. Phys. Chem. A, Lett.*, 2007, **111**, 13287.
- 79 Y. Wu, H. Chen, F. Wang, F. Paesani and G. A. Voth, *J. Phys. Chem. B*, 2008, **112**, 467.
- 80 N. I. Hammer, E. G. Diken, J. R. Roscioli, M. A. Johnson, Evgeniy M. Myshakin, K. D. Jordan, A. B. McCoy, X. Huang, J. M. Bowman and S. Carter, *J. Chem. Phys.*, 2005, **122**, 244301.
- 81 H. A. Schwarz, *J. Chem. Phys.*, 1977, **67**, 5525.
- 82 F. Hibbert and J. Emsley, *Adv. Phys. Org. Chem.*, 1990, **26**, 255.
- 83 T. Komatsuzaki and I. Ohmine, *Chem. Phys.*, 1994, **180**, 239.
- 84 J. M. Bowman, T. Carrington and H. Meyer, *Mol. Phys.*, 2008, **106**, 2145–2182.
- 85 H. Lapid, N. Agmon, M. K. Petersen and G. A. Voth, *J. Chem. Phys.*, 2005, **122**, 014506.



# CURRICULUM VITAE

**MR. CHAROENSAK LAO-NGAM**

**Date of Birth:** January 19, 1982 in Ubon Ratchathani province, Thailand

**Educations:**

2002-2005 B.Sc. in Chemistry, Ramkhamhaeng University, Thailand

2005-2011 Ph.D. in Chemistry, Suranaree University of Technology, Thailand

**Experiences:**

May, 2011-August, 2011 Scholar Visitor, Institute for Materials Research (IMR),  
Tohoku University, Sendai, Japan

**Grants and Fellowships:**

2005-2007 Royal Golden Jubilee (RGJ) Ph.D research scholarship  
from Thailand Research Fund (TRF)

2007-2011 SUT Teaching Assistantship